from *The Porphyrin Handbook*, Kadish, K.; Smith, K.; Guilard, R., ed.; Academic Press: New York, 2000; vol. 6, ch. 41, pp. 43-131.

Applications of Porphyrins and Metalloporphyrins to Materials Chemistry

Jun-Hong Chou[†], Margaret E. Kosal[†], Hari Singh Nalwa[‡], Neal A. Rakow[†], and Kenneth S. Suslick[†]

School of Chemical Sciences
University of Illinois at Urbana-Champaign
600 S. Goodwin Av.
Urbana, IL 61801

and

Hitachi Research Laboratory,
Hitachi Ltd.
7-1-1 Ohmika-cho,
Hitachi City, Ibaraki 319-1292
JAPAN

[†] University of Illinois
[‡] Hitachi

I. Introduction

Porphyrins and related macrocycles provide an extremely versatile synthetic base for a variety of materials applications. The exploration of metalloporphyrin assemblies as building blocks for tailored materials properties has found rapid growth during the past decade [1]. In this chapter, we shall review the rather diverse applications of porphyrins to materials chemistry and try to draw the common threads between these topics as possible.

Porphyrins and metalloporphyrins have found broad applications as field-responsive materials, particularly for optoelectronic applications. For example, the facile substitution of the periphery of various porphyrins has generated a series of unusual liquid crystalline materials. The porphyrin ligand serves as a platform on which one can erect desirable molecular and materials properties, including very large dipole moments, polarizabilities, and hyperpolarizabilities. The nonlinear optical properties of these materials are of special interest, in part for energy transfer with molecular control, and in part for potential applications in optical communications, data storage, and electrooptical signal processing. The stability of mono- and di-cation porphyrin π-radicals makes these systems especially interesting for photoionization processes, closely related to the so-called special-pair reaction center of photosynthesis and the photogeneration of electron transfer. As another example, various polymeric porphyrins have been examined for their unusual low-dimensional conductivity.

In contrast to their interaction with applied electric, magnetic or electromagnetic fields, porphyrins and metalloporphyrins can also interact with other chemical species. One might view such interactions as chemo-responsive rather than field-responsive. The development of chemo-responsive materials based on porphyrins, however, has seen somewhat less development. As an example of such applications, porphyrin solids are often highly porous and the intentional development of molecularly-based molecular sieves or shape-selective solid catalysts is currently under development. Porphyrins and metalloporphyrins have also been examined for a variety of sensor applications, which clearly represent an important class of chemo-responsive materials.

II. Photonic Materials

A. Mesogenic Porphyrins

Appending long alkyl chains to the periphery of a rigid tetrapyrrolic core has proved to be a general methodology for the synthesis of liquid crystalline materials. Liquid crystals possess properties of both the liquid and solid phases, possessing order over intermediate distances, but retaining many of the rheological properties of liquids. Phthalocyanine derivatives have been widely investigated as thermotropic mesogenic materials,[2,3] whereas porphyrins and metalloporphyrins have received only cursory examination. The larger phthalocyanines tend to have high melting points; porphyrins offer a similar geometrical structure and a greater ease of functionalization, while

having a smaller inner core and therefore lower, more useable melting points. The majority of porphyrin mesogenic materials have a discotic columnar nature in which the porphyrins stack like saucers along their short axis.

1. Octa-substituted Porphyrins

The first reported porphyrin exhibiting mesophasic behavior was an octa-β-substituted *uro*-porphyrin I octa-*n*-dodecyl ester (Figure 1).[4] The investigation was modeled on the observation that similarly-shaped flat, hexagonal molecules had previously displayed discotic liquid crystal phases. Upon heating the porphyrin compound melted directly from a crystal to an isotropic liquid. During cooling, a mesomorphic phase of 0.1°C was noted between 96.8 °C and 96.7 °C. This phase was characterized as having discotic order via microscopic texture analysis and miscibility experiments in comparison to known discotic materials.

[Figure 1]

Fox and co-workers have synthesized and investigated the physical properties of a series of octyl-ether and octyl-ester porphyrin materials. The free base and metalated derivatives of 2,3,7,8,12,13,17,18-octakis(β-*n*-alkoxy)ethylporphyrin, $H_2((OC_nH_{2n+1})OEP)$ (abbreviations given in Table 1), were examined as possible liquid crystalline porphyrin materials (Figure 1). Of the free base species examined, only the *n*-octyl porphyrin displayed a narrow five degree liquid crystalline phase (Table 2). The metalated (M = Zn, Cu, Pd, Cd) porphyrins demonstrated discotic mesomorphism. The lowest melting point (61 °C) was observed for an equimolar mixture of the *n*-octyl and *n*-decyl zinc octaether porphyrin materials. Appendage of a single electron donating cyano group to the 5-position of *n*-octyl octaether porphyrin ($H_2((OC_nH_{2n+1})OECNP)$) resulted in depression of the melting point and the clearing point. Substitution of an electron accepting nitro group in the same position ($H_2((OC_nH_{2n+1})OENO_2P)$) produced a depression of the clearing point without affecting the melting transition, thereby reducing the total range of liquid crystalline behavior. The authors attribute this to distortion of the planar macrocyclic ring by the large nitro group.[5] The free base and zinc(II) derivatives of three similar octaester porphyrins ($H_2((O_2C_nH_{2n+1})OEP)$) were found to exhibit discotic columnar mesophases (Figure 2). The *n*-hexyl ester exhibited lower melting points than either the *n*-butyl or *n*-octyl species (Table 2).[6] It was noted that in both the octa-ether and octa-ester porphyrin materials metallation contributed a stabilizing factor inducing wider mesomorphic temperature regimes.

[Table 1]
[Figure 2]
[Table 2]

The orientation of *n*-nonoxyethyl octa-substituted liquid crystalline material was explored by X-ray diffraction. The molecules were found to structurally order in columns such that the macrocyclic planes tilt at an angle of 46° to the columns (Figure 2).[7] The intricacies of the structure was further elaborated for the *n*-decoxyl derivative. The interfacial porphyrin-porphyrin distance was found to be 3.98Å, and the inter-column separation was 23.59Å (Figure 3). This structure has been suggested as a one-dimensional "molecular wire" motif for electronic conduction.[8]

[Figure 3]

Thin films of the zinc-octakis(β-decoxyethyl)porphyrin material included in indium-tin-oxide (ITO) electrodes were explored as an electrooptical data storage system. Capillary filling of the porphyrin into the ITO cell provided the physical construction of the photoconductive system. A scanning tunneling microscope (STM) was used to initiate charge trapping ("writing") and measurement ("reading"). A storage density of ~3 gigabits per cm^2 was maintained over 2000 hours of continual subjection to charge, and greater than 60% of the current signal was still "readable" after ~1500 readings. Subsequent work demonstrated 1.5 billion "writing" and "reading" sequences of the material without substantial change in output signal (Figure 4).[9-11]

[Figure 4]

Motivated by interest in exploring stronger intermolecular interactions than those of previously described porphyrin or phthalocyanine mesophasic materials, Doppelt and Huille reported the mesogenic behavior of sulfur-substituted azaporphyrin species (Figure 5). Mesogenic phases were not observed in the free base 2,3,7,8,12,13,17,18-octakis(octylthio)tetraazaporphyrin, whereas the Co(II/III), Ni(II), Cu(II), and Zn(II) complexes revealed a discotic hexagonal columnar liquid crystal (D_h). By optical microscopy and differential scanning calorimetry (DSC), the cobalt material was found to exhibit the largest mesophasic range between 48 and 206 °C. The copper(II) and the nickel(II) species manifested liquid crystalline behavior from 71.5 °C to 120 °C and 65 °C to 154.5 °C, respectively. The zinc(II) complex underwent a crystal to crystal phase transition at 44 °C, followed by an observed melting point at 55.5 °C and a clearing point at 125.5 °C. X-ray diffraction experiments furnished an inter-columnar distance of 23.6Å for the Zn, Ni, and Cu materials. A slightly small inter-columnar distance of 22.8Å was observed for the cobalt complex.[12]

[Figure 5]

2. Tetra-substituted Porphyrins

An investigation of the photophysics of 5,10,15,20-tetrakis(4-*n*-pentadecylphenyl)porphyrin, H_2(T(4-*n*-$C_{15}H_{31}$)PP), produced the second porphyrin liquid crystal material to be well-documented in the literature and the first to utilize a tetraphenylporphyrin core (Figure 6).[13] Three mesogenic phases were reported; melting of the crystalline phase was observed upon heating at 27 °C, a second mesomorphic transition followed at 56 °C, onset of the third mesophase was noted at 65.5 °C and the material cleared to an isotropic liquid at 134.5 °C. A correlation between the photoconductive properties of the material as part of an electrochemical cell and the phase transitions of free base porphyrin (H_2(T(4-*n*-$C_{15}H_{31}$)PP)) was found. Discontinuities in the photocurrent and dark-current were observed at the phase transitions (Figures 7 and 8). The third-order nonlinear susceptibilities of benzene solutions of M(T(4-*n*-$C_{15}H_{31}$)PP), where M = H_2, Co, Ni, Cu, Zn or V=O, were studied using the degenerate four-wave mixing (DFWM) technique. The $\chi^{(3)}$ value for all samples was determined to be on the order of ~10^{-11} esu calculated at 532 nm.[14] Two mesomorphic phases were observed for a similar species 5,10,15,20-tetrakis(4-*n*-dodecylphenyl)porphyrin. Phase transitions were observed at 31.0 °C, 52.0 °C and 155.0 °C. This material was determined to be a discotic lamellar (D_L) liquid crystal via X-ray diffraction studies.[15] Novel ferromagnetic materials were prepared by mixing two different paramagnetic M(T(4-*n*-$C_{12}H_{25}$)PP) materials (M = Cu(II), V(IV), Co(II), Mo(V), Ag(II) or Fe(II)).[16]

[Figure 6]
[Figure 7]
[Figure 8]

The mesogenic behavior of 5,10,15,20-tetrakis(4-*n*-alkyloxyphenol)porphyrins, (H_2(T(*p*-*n*-$OC_{10}H_{21}$)PP) and H_2(T(*p*-*n*-$OC_{12}H_{25}$)PP)), was explored by Kugimiya and Takemura. Two liquid crystalline phases were attributed to each the free base and cobalt(II) derivatives of T(*p*-*n*-$OC_{10}H_{21}$)PP. A large temperature regime for mesomorphism was found for Co^{II}(T(*p*-*n*-$OC_{10}H_{21}$)PP). The zinc(II) complex featured three liquid crystal phases between –16 °C and 170 °C. The first two phases were not observed during repeated melting cycles of the material.[17]

Ohta and coworkers presented a number of porphyrins synthesized specifically in order to examine their liquid crystalline characteristics. The highly substituted 5,10,15,20-tetrakis(3,4,3”,4”-tetradodecyloxy-*o*-terphenyl)porphyrins (H_2(T($C_{12}H_{25}O)_{16}$TP)), although possessing core tetra-substituted porphyrin rings, have sixteen long alkyl chains for inducing mesogenic behavior (Figure 9). The di-substituted dodecyl ether porphyrin, H_2(T($C_{12}H_{25}O)_{16}$TP), displayed an extremely complicated DSC trace — at least four different mesophases were noted. By X-ray diffraction, a discotic hexagonal ordered columnar material (D_{ho}) was identified which melted at –80 °C and cleared at 39 °C. A second mesophase that cleared at 59°C was determined to be discotic hexagonal disordered columnar (D_{hd}). Upon cooling, two other phases that could not be identified were observed. The similar di-substituted dodecyl ether copper complex, Cu(T($C_{12}H_{25}O)_{16}$TP), exhibited one D_{hd} mesophase that melted at –37 °C and cleared at 57 °C. The authors credit steric influences of the sixteen long alkoxyl chains to the formation of a columnar assembly (versus lamellar which was observed for by Shimizu.[15]). When one of the alkoxyl groups on

each of the eight pendant phenyl groups was replaced with a proton, $H_2(T(C_{12}H_{25}O)_8TP)$, a high-melting (202.2 °C), non-liquid crystalline material resulted.[18] Di-substituted *o*-terphenyl mesogenic porphyrins materials were also studied and are reviewed subsequently.

[Figure 9]

Controlled orientation of the porphyrin macrocycle in a liquid solution for use in electron pair resonance (EPR) experiments was the motivation for the synthesis of an *ortho*-amino-tetraphenylporphyrin based liquid crystalline material. Appending biphenyl long chain alkoxyl groups to the *ortho*-amino substituents generated a mesogenic material in which the porphyrin macrocyclic plane was orthogonal relative to the director *L* in a nematic phase matrix. Unaltered tetraphenylporphyrin aligns such that the macrocyclic ring is parallel to *L* (Figure 10).[19,20]

[Figure 10]

Griesar et al. synthesized a material that had both liquid crystal and ferrimagnetic properties. A discotic mesophase was observed between 108 °C and 155 °C for $Mn^{III}(T(p\text{-}n\text{-}OC_{12}H_{25})PP)(TCNE)\bullet 2$ toluene (TCNE = tetracyanoethylene). The X-ray diffraction pattern revealed that the material possessed a hexagonal columnar lattice with a characteristic inter-columnar spacing of 30Å. The system was also found to display ferrimagnetic behavior below 25.0 K [21]

Liquid crystalline behavior can also be induced in some hydroxy-substituted porphyrins by incorporating them as "guest" molecules in a mesogenic matrix of "clipper" host molecules (Figures 11). Two smectic phases were observed between 15 °C and 150 °C for the 5,10,15,20-tetrakis(3,5-dihydroxyphenyl)porphyrin complex. Mesomorphic behavior was not observed for 2,6-substituted-dihydroxyphenylporphyrins due to steric restrictions which prevented the "host" complex from binding the in the *ortho*-positions.[22]

[Figure 11]

Patel and Suslick recently reported the synthesis and properties of a series of mesogenic porphyrins with liquid crystal phases stable over an extremely wide temperature range, which greatly increases their potential utility. In addition, they isolated novel metalloporphyrin mesogens that permitted axial ligation to the metal, including one novel phase possessing a permanent dipole moment. Hexagonal columnar discotic liquids crystals of the *n*-alkyl esters of free base 5,10,15,20-tetrakis(3,5-dicarboxyphenyl)porphyrin ($H_2(T(3,5\text{-}CO_2R)PP)$, R = $n\text{-}C_nH_{2n+1}$, n = 10,12,14,16,18,20,22) displayed a narrowing range of mesogenic behavior as the alkyl chain length increased (Figure 12). These porphyrins feature pocketed sites on both faces of the porphyrin macrocyclic ring due to the relative rotation of the phenyl groups (Figure 13). The presence of these protected pockets for axial ligation was utilized to construct a unique five-coordinate vanadyl derivative with dodecyloxyl chains. This approach produced both a liquid crystalline range of over 246°C and a substantial dipole moment perpendicular to the porphyrin plane.[23]

[Figure 12]
[Figure 13]

An early report of mesogenic behavior in a porphyrin species was originally presented by Gaspard in 1984. In an attempt to discover the minimum number of pendant long alkyl chains need to induce a liquid crystalline phase in a porphyrin system, derivatives of 5-phenalkoxy-10,15,20-tritolylporphyrin and 5,15-di(phenalkoxy)-2,3,7,8,12,13,17,18-octamethylporphyrin were explored. The free base compounds proved to not be mesogenic. This was attributed to the non-planar orientation of the tolyl and phenoxyl groups relative to the porphyrin macrocyclic ring. However, mixtures of the copper(II) derivatives of 5-phenyl-*n*-dodecyloxy-10,15,20-tritolylporphyrin with one single long alkoxyl chain were reported to display metastable mesophases in combination with paraffin or halogenated long alkyl chains.[24]

3. Di-substituted Porphyrins

Due to the disc-like geometry of the porphyrin macrocycle, discotic mesophases have generally been the most common for porphyrin liquid crystalline materials. The first porphyrin liquid crystals featuring "rod-like"

calamitic mesophases were described by Bruce and coworkers using substituted 5,15-di(phenyl) zinc porphyrin complexes as the basic molecular building block.[25-29] The first materials studied were derivatives of 5,15-(4-*n*-alkoxyphenyl)porphyrins ($H_2((OC_nH_{2n+1})DPP$), n = 8, 10, 12, 14, 16) which feature long alkoxyl chains directly attached in the *para*-phenyl position (Figure 14).[25] Mesogenic compounds of the *n*-octyloxy and *n*-decyloxy porphyrin systems have relatively high melting points. Liquid crystalline materials with shorter alkoxyl chains (R = R' = C_nH_{2n+1}, n = 8, 10) were characterized as having smectic B phases; whereas, the less ordered smectic E or smectic E' phases were observed in the longer chain materials (R = R' = C_nH_{2n+1}, n = 12, 14, 16).[25]

[Figure 14]

Subsequent extensions of this motif incorporated a cyclohexane ester or phenyl ester spacer between the *n*-alkoxyl groups and the *meso*-phenyl group on a single or both sides of the core diphenylporphyrin (Figure 15, R = C_6H_{10}-C_7H_{15}, R' = H; or R = C_6H_4-OC_7H_{15}, R' = H; or R = R' = C_6H_{10}-C_7H_{15}; or R = R' = C_6H_4-OC_7H_{15}).[26] The observed mesophase transition type and temperatures as determined by polarizing microscopy and differential scanning calorimetry are delineated below (Table 3). The melting points remained high with the addition of ester groups, and the observed mesophases were of the more disordered nematic and smectic A variety. Although the melting temperatures were similar, the substitution of a second phenyl or spacer group raised the clearing temperature. In the case of di-substituted cyclohexyl spacer, the clearing temperature was increased by 31 °C; a second phenyl spacer more dramatically produced an clearing temperature elevated 113 °C compared to that observed for the mono-substituted material.[26]

[Figure 15]
[Table 3]

In order to depress the melting points of the diphenyl porphyrin materials, synthetic modifications were employed to limit intermolecular π–π attractions between macrocyclic rings. Long lateral alkoxyl chains were attached to the *ortho*-position of the phenyl ester (Figure 15) or in the *ortho*-position of the 5,15-diphenyl groups (Figures 16 and 17) as an attempt to restrict attractive electrostatic interactions. This approach proved less successful than that of Patel and Suslick. While the melting points of these materials were significantly lowered in comparison to the previously studied materials, some of the compounds no longer displayed liquid crystalline phases. The materials with lateral alkoxyl substituents appended to the 5,10,15,20-phenyl ring manifested both decreased melting points and mesomorphic behavior (Figures 16 and 17). It was noted that two of the compounds with phenyl spacers (Figure 15, R = (2',4'-OC_8H_{17})C_6H_4, and Figure 17, R = C_6H_4-O-C_8H_{17}) are structural isomers – illustrating the dependence of specific orientation of the lateral alkoxyl chain in affording liquid crystalline properties to otherwise similar porphyrin systems. A material with a single lateral chain substituent (Figure 16) displayed a smaller temperature range for mesophasic behavior (~20 °C) than those with two lateral chains (Figure 17). Nematic mesophases, more disordered than the smectic type, were observed for these materials. This is also attributed to the presence of the lateral chains.[27]

[Figure 16]
[Figure 17]

Further attempts to restrict porphyrin to porphyrin interactions culminated in the synthesis of novel "donor-acceptor" and "strapped" porphyrin compounds. Instead of alkoxyl chains, lateral *p*-nitrophenylsulfonyl groups were substituted on the 5,10,15,20-phenyl ring (Figure 18). The phenyl ester species (R = C_6H_4-O-*n*C_7H_{15}) displayed a high melting point and a small nematic mesomorphic range (28 °C) before decomposing. The cyclohexane ester (R = C_6H_{10}-*n*C_7H_{15}) decomposed directly from the melt. Significant distortion of the macrocyclic ring in the xylene "strapped" porphyrin complex (R = C_6H_4-O-*n*C_7H_{15}), was cited for the lack of mesogenic behavior (Figure 19).[28]

[Figure 18]
[Figure 19]

Efforts have been directed to increasing the "rod-like" geometry of the zinc porphyrin systems by extending the linear expanse through additional phenyl ester groups (Figures 20 and 21). This approach generally resulted in

lower temperatures for the onset of the first phase transition, however, in the some cases, this was a crystalline to crystalline phase change. At high temperatures, both a smectic C and a nematic phase were observed in the 3,4-*n*-dodecyloxyphenyl compound. One system that featured eight linear phenyl ester moieties but no lateral chains dangling over the porphyrin macrocyclic ring (Figure 20. Y = $OC_{12}H_{25}$; *n* = 12, *m* = 2) manifested a columnar mesophase. A relatively low phase transition (50 °C) to a nematic phase was seen in the material with both lateral chains and eight linear phenyl ester groups (Figure 21. Y = $OC_{12}H_{25}$; *m* = 2). The material cleared to an isotropic fluid at 153°C.[29]

[Figure 20]
[Figure 21]

Ohta and coworkers studied the liquid crystalline behavior of a series of disubstituted phenyl porphyrins. Similar to the highly substituted tetraphenyl species, 5,15-bis(3,4,3",4"-tetra(alkoxy-*o*-terphenyl))porphyrins, $H_2(B(C_nH_{2n+1}O)_mTP)$ where n = 12 or 16 and m = 4 or 8, were prepared with as many as eight long alkoxyl chains (Figure 22). A discotic, rectangular disordered columnar (D_{rd}), arrangement was observed for $H_2(B(C_{12}H_{25}O)_8TP)$. Increasing the alkyl chain length (e.g., $H_2(B(C_{16}H_{33}O)_8TP)$) produced a material that also exhibited a D_{rd} columnar mesophase, which cleared to an isotropic liquid at nearly the same temperature as the dodecyloxy compound. Substitution of one of the dodecyloxyl chains on each porphyrin with a proton, generated a material with two discotic lamellar mesophases. The clearing point of this compound (228.6°C) was approximately 100° higher than that of either di-substituted compounds (136.7 °C and 132.9 °C, respectively).[18]

[Figure 22]

Two other di-substituted species were examined by Ohta and coworkers. The tetra alkoxyl-containing 5,15-bis(3,4-didodecyloxyphenyl)porphyrin displayed a discotic lamellar mesophase with a melting pointing of 60.4 °C and clearing point of 200.7 °C (Figure 23). Four crystalline phases and one undetermined mesophase were delineated for 5,15-bis(4-didodecyloxybiphenyl)porphyrin between initial crystalline phase transitions at 40.1 °C to melting to the mesomorphic material at 430.9 °C (Figure 24). The material was observed to decompose at 450.5 °C.[18]

[Figure 23]
[Figure 24]

B. Porphyrins as Nonlinear Optical Materials

The synthesis and chemistry of nonlinear optical (NLO) porphyrin-based materials has been examined in some detail. Porphyrins have several desirable properties for use in optoelectronics: they have greater thermal stability (compared to typical organic chromophores); their extended π-conjugated macrocyclic ring gives large NLO effects; and subtle variation in their physical properties can be made easily through chemical modification of their periphery. Here we highlight progress in the development of NLO porphyrinic materials describing their second-, and third-order nonlinear optical properties. Due to space limitations, we provide only the most cursory introduction to the physics of nonlinear optical phenomena; several excellent references are available for further details.[30-37]

The optical properties of a medium are characterized by the optical susceptibility, χ. This optical susceptibility is closely related to the refractive index and the dielectric constant. In an isotropic medium at optical frequencies (ω), the relationship between the linear susceptibility, the refractive index (n), and the dielectric constant (ε) can be expressed as:

$$1 + 4\pi\chi(\omega) = n^2(\omega) = \varepsilon(\omega) \quad (1)$$

The microscopic polarization (p) induced in an isolated molecule under the applied electric field (E) of an incident electromagnetic wave can be expressed by the following equation:

$$p = \alpha E + \beta EE + \gamma EEE \quad (2)$$

where p and E are related to the tensor quantities α, β, γ, which are referred to as the polarizability, first hyperpolarizability and second hyperpolarizability, respectively. Similarly, the macroscopic polarization induced in the bulk media can also be expanded in the external field power series:

$$P = \chi^{(1)} E + \chi^{(2)} EE + \chi^{(3)} EEE + \ldots \quad (3)$$

where $\chi^{(1)}$ is the linear optical susceptibility, and $\chi^{(2)}$ and $\chi^{(3)}$ are the second and third-order nonlinear optical susceptibilities; these physical meanings similar to their microscopic counterparts α, β, and γ, respectively. The even-order tensor $\chi^{(2)}$ is zero in a centrosymmetric environment, whereas the odd-order tensor $\chi^{(3)}$ does not have any symmetry restrictions and produces a non-vanishing higher order optical susceptibility. Therefore, $\chi^{(n)}$ are (n+1) rank tensor associated with the nonlinear optical response of the medium. Both the field E and the polarization P are vectors, while the nonlinear optical coefficients are tensors. The $\chi^{(n)}$ is frequency dependent, and as a result, resonant and non-resonant parameters can differ significantly depending upon frequencies used. There are 9 elements of $\chi^{(1)}$, 27 elements of $\chi^{(2)}$, and 81 elements of $\chi^{(3)}$; the number of independent elements, however, is usually much smaller. For example, in liquids, gasses and isotropic solids, there are only three independent elements for $\chi^{(3)}$: $\chi^{(3)}_{xxxx}$, $\chi^{(3)}_{xyyx}$, and $\chi^{(3)}_{xyxy}$.

1. Second-Order NLO Systems

Suslick et al.[38] measured the first hyperpolarizabilities (β) of porphyrins having electron donor (amino) and acceptor (nitro) groups in the *para*-position of 5,10,15,20-substituted tetraphenylporphyrins (Figure 25) using electric field induced second harmonic generation (EFISH) technique at 1.19 μm with chloroform solutions. The dipole moment (μ) and β values were affected by the position of donor and acceptor groups. A β value of 30 x 10^{-30} esu and dipole moment of 7 x 10^{-18} esu were measured for the porphyrin having $R^1=R^2=NO_2$, $R^3=R^4=NH_2$; and the porphyrin with $R^1=NO_2$, $R^2=R^3=R^4=NH_2$ exhibited a β value of 20 x 10^{-30} esu and dipole moment of 5 x 10^{-18} esu (1 au = 1.48176 x 10^{-25} esu = 1.64877 x 10^{-41} $C^2m^2J^{-1}$). In these cases, the amino group "pushes" electron density macrocycle while the nitro groups "pull," increasing the hyperpolarizability substantially. The β value of a porphyrin with $R^1=R^2=R^3=NO_2$, $R^4=NH_2$ was found to be $\geq$10 x 10^{-30} esu. The well-aligned charge transfer gives rise to large β values.

[Figure 25]

Since second order NLO response occurs only in a non-centrosymmetric environment, the incorporation of porphyrins into a polar (in the sense of poled or asymmetric) array is mandatory for most optoelectronic applications. The importance of the organizational structure is shown in Figure 26. Langmuir-Blodgett (LB) films are an extremely effective means of providing the necessary asymmetric environment for good NLO response. Suslick and coworkers incorporated similar "push-pull" porphyrins derivatives into Langmuir-Blodgett films in order evaluate bulk response of the material.[39] They found that good films could be created from these push-pull porphyrins, simply by conjugating a long chain fatty acid to the free phenylamine functionalities. The mean molecular area of these LB films depended strongly on the number of alkyl chains, as shown in the LB isotherms (Figure 27). The number of alkyl chains did not change the porphyrin orientation, but rather altered the packing density of the porphyrins.

[Figure 26]
[Figure 27]

Sen et al.[40,41] measured β values of a series of donor-acceptor substituted fluoroarylporphyrins by using hyper-Rayleigh scattering (HRS) at 1064 nm (Table 5). The first hyperpolarizabilities are influenced by the nature and position of donor and acceptor groups. An increase in β values was observed when a β-pyrrole position of the TPP chromophores was substituted with an electron accepting nitro group. The open-shell Cu(II) (d^9) porphyrins show larger β values than closed-shell Zn(II) (d^{10}) porphyrins. The high observed β values in Zn(II) porphyrins are due to the large change in dipole moment upon excitation. The highest β values were obtained for porphyrins having N,N'-dimethylamino and nitro substituents. These porphyrins absorb at 532 nm; two-photon resonance enhancement contributes to large β values but the effect of metal d-electrons is more pronounced.

[Table 4]

Priyadarshy et al.[42] calculated the first hyperpolarizabilities of porphyrin-bridged donor-acceptor molecules using semi-empirical INDO/SCI-SOS method. The chemical structures and calculated β values are shown

below (Table 6). The β values of 5-((4'-dimethylaminophenyl)ethynyl)-15-((4''-nitrophenyl)ethynyl)-10,20-diphenylporphyrinatozinc(II) (D-Zn(DPP)-A) (4) calculated at 830 and 1064 nm were 8152 x 10^{-30} and 477 x 10^{-30} cm^5/esu, respectively. From such calculations, it is clear that resonant enhancements of hyperpolarizabilities can be extremely important. This makes comparison between experiments difficult unless the wavelengths used are far removed from the intense porphyrin absorbance bands. The calculated μβ value at 1907 nm was 2548 x 10^{-48} cm^5/esu. The first hyperpolarizabilities are one order of magnitude larger than other porphyrin-bridged donor-acceptor molecules. The dimethylamino donor - nitro acceptor zinc species was determined to have a β value four times greater than that a similar compound lacking the nitro acceptor substituent. This indicates that extended π-conjugation length and strength of donor and acceptor groups significantly increase the β value. The β value varied slightly as a function of aryl group composition for a series of compounds with phenylamine donors and nitrophenyl or nitrophenylethynyl acceptor groups.

[Table 5]

LeCoers et al.[43] synthesized "push-pull" arylethynyl porphyrins and measured their β values by hyper-Rayleigh scattering (HRS) in chloroform solutions. The donor-acceptor compound (D-Zn(DPP))-A) produced approximately frequency independent β values: 5142 x 10^{-30} esu at 830 nm and 4933 x 10^{-30} esu at 1064 nm. The copper analogue (D-Cu(DPP))-A) exhibited frequency-dependent β values of 4374 x 10^{-30} esu at 830 nm and 1501 x 10^{-30} esu at 1064 nm. Significant shifts in molecular dipole moment were observed for the "push-pull" arylethynyl porphyrins by electroabsorption or Stark effect spectroscopy.[44] The β value of the zinc porphyrin dimer (D-Zn(DPP))-Zn(DPP))-A) calculated at 1064 nm was 742 x 10^{-30} cm^5/esu (Figure 28). The calculated μβ value at 1907 nm was 3299 x 10^{-48} cm^5/esu. The β value of D-Zn(DPP))-Zn(DPP))-A is 1.6 times larger than that of D-Zn(DPP))-A. The larger β value is associated with two Zn(DPP)) units linked together by an ethynyl bridge connecting the chromophores at their 5- and 5'-positions.

[Figure 28]

The first nickel "push-pull" 5,15-diphenylporphyrin derivatives were recently synthesized by Yeung.[45] Using an amino arylethynyl group as the donor substituent and a formyl or a dicyanoethynyl group as the acceptor group on the porphyrin, the nickel-containing species exhibited significant first hyperpolarizability. Using EFISH at 1907 μm, the first hyperpolarizabilities were determined as 124 x 10^{-30} esu and 66 x 10^{-30} esu for the formyl and dicyanoethynyl species, respectively. The larger β value for dicyanoethynyl compound is attributed to its higher relative electronic acceptor strength.

Albert et al.[46] calculated β values of "push-pull" porphyrins using semi-empirical INDO/S Hamiltonian and singles-only CI (Table 6). The calculated optimized β values and chemical structures are therein. The β value increased as the benzene ring was replaced by an electron-deficient moiety such as diazene or tetra-azine or by an electron-rich ring such as thiophene or pyrrole. The β_{vec} and μβ increased by a factor of two by replacing the benzene rings at the donor end by electron-donating pyrrole rings. A series of porphyrins with reduced dihedral twist of the phenyl rings were synthesized and present very large β values. Small dihedral angles were observed for the alkyne bridged (7°) and for the azo-bridged species (0.5°).

[Table 6]

A multifunctional polyimide consisting of a free base porphyrin and a NLO chromophore side chain was synthesized by Peng and associates (Figure 29).[47] This photorefractive molecular system was modeled on the charge transfer properties observed in porphyrin electron acceptors of photosynthetic processes. The polyimide exhibited a T_g of 250 °C. Absorption peaks at 510, 540 and 630 nm from the porphyrin rings and at 458 nm from the NLO-chromophore were observed. This multifunctional polyimide system is photoconductive as well as SHG active. The photoconductivity was determined to be 1.1 x 10^{-12} S/cm under an external field of 1500 kV/cm at 690 nm. The polymer film showed a NLO coefficient d_{33} of 110 pm/V at 1.064 μm after corona poling. Interestingly, the NLO coefficient d_{33} showed no decay at 90 and 150 ^oC, and the d_{33} of 80% was retained even at 170 ^oC after 120 hours. This porphyrin containing polyimide displayed both higher NLO coefficient as well as stability of second

harmonic generation at high temperature. Additional photorefractive effects were also observed in the two beam coupling experiment. An optical gain coefficient of 22.2 cm^{-1} under zero-field condition was noted.

[Figure 29]

Another new photorefractive polyimide (Figure 30) with a main-chain zinc porphyrin (m=0.005) and a NLO-chromophore side chain (n=0.995) was reported by Peng et al.[48] This porphyrin-containing fluorinated polyimide displayed a T_g of 228 °C and maintained thermal stability to 350 °C. The photoconductivity was found to be electric field dependent. The SHG remained unchanged to 180 °C.

[Figure 30]

Li et al.[49] looked at the SHG properties of self-assembled monolayer thin films of tetra-para-pyridylporphyrin (H_2(TPyP)) and some derivatives on fused quartz and silicon surfaces. By covalently bonding the TPyP molecules to an alkyl- or phenyl- siloxy group, the centrosymmetric nature of the porphyrin is nullified. The SHG response at 532 nm was observed ($\chi_{zzz} \sim 2 \times 10^{-8}$ esu). This relatively large value was attributed to a completely delocalized π-electron system in the in the porphyrin monolayer.

2. Third-Order NLO Systems

As with phthalocyanines, the third order nonlinear optical susceptibility, $\chi^{(3)}$, of porphyrins can be manipulated by chemical substitution. The third-order NLO properties of several tetraphenylporphyrin compounds were first reported by Meloney et al.[50] The $\chi^{(3)}$ was measured by the degenerate four-wave mixing (DFWM) technique from toluene solutions of free base, zinc, and cobalt-containing TPPs. The effective $\chi^{(3)}$ values of these materials were estimated from the thermally induced refractive index changes. All porphyrin derivatives showed $\chi^{(3)}$ values on the order of 10^{-11} esu. Sakaguchi et al.[51] also used DFWM for determining the $\chi^{(3)}$ values of cobalt, nickel, zinc, copper, and oxovanadium complexes of 5,10,15,20-tetrakis(4-n-pentadecylphenyl)porphyrins, H_2(T(4-n-$C_{15}H_{31}$)PP). The measurements were made in a benzene solution with concentrations of 0.02-0.05%. The $\chi^{(3)}$ values were found to be in the range of 10^{-11} esu, however, these values are influenced by concentration. The Cu(T(4-n-$C_{15}H_{31}$)PP) having a 0.05% weight dissolved in benzene showed $\chi^{(3)}$ of 1.8×10^{-11} esu whereas the Ni(T(4-n-$C_{15}H_{31}$)PP) accorded $\chi^{(3)}$ of 10^{-10} esu at a concentration of 0.5 g/L. The $\chi^{(3)}$ values did not exhibit any significant effect of the metal atom.

Rao et al.[52] measured $\chi^{(3)}$ values of a series of metal containing tetrabenzoporphyrin derivatives in tetrahydrofuran employing the DFWM technique at 532 nm. The chemical structures of these porphyrins and their abbreviated names are listed below (Figure 31, Table 1). These benzoporphyrins were substituted at the 5,10,15,20-positions with a variety of functional groups such as *m*-fluorophenyl, *p*-methoxyphenyl and *p*-methylphenyl. Values as high as 2.8×10^{-8} esu for $\chi^{(3)}$ were observed for zinc 5,10,15,20-tetrakis(*p*-dimethylaminophenyl)tetrabenzoporphyrin, H_2(TMAPTBP). In particular, large $\chi^{(3)}$values were recorded for benzoporphyrins containing electron donating 5,10,15,20-phenyl groups. Guha et al.[53] evaluated imaginary and real parts of $\chi^{(3)}$ for the zinc tetraphenyl benzoporphyrin species [Zn(TPTBP)] and the *p*-methoxyphenyl substituted version [Zn(TMOPTBP)] in THF by using picosecond and nanosecond laser pulses. The imaginary parts of $\chi^{(3)}$ and γ (second hyperpolarizability) of these two porphyrins at 532 nm were found to be five to ten times larger than the real parts measured at 1.064 μm. The Zn(TMOPTBP) showed an imaginary $\chi^{(3)}$ of 9×10^{-13} esu and γ of 8.0×10^{-31} esu whereas a $\chi^{(3)}$ of approximately 1.8×10^{-13} esu and γ of 1.6×10^{-31} esu was observed for Zn(TPTBP) at a concentration of 0.46 g/L. Nonlinear refractive index values (n_2) of 7.8×10^{-10} and 9.1×10^{-10} cm^2/MW were estimated for Zn(TMOPTBP) and Zn(TPTBP), respectively.

[Figure 31]

Hosada et al.[54] measured $\chi^{(3)}$ of spin-coated films of free base and manganese chloride derivatives of octaethylporphyrin (OEP) and N,N',N'',N'''-tetramethyl-octaethylporphyrin(+2) bis(trifluoroacetate) [$Me^{+}_4(OEP)^{-2}$)] by third harmonic generation (THG) at 1.907 μm to investigate the effect of increasing ring size on third-order optical nonlinearity (Figure 32). The $\chi^{(3)}$ of $Me^{+}_4(OEP)^{-2}$, with an extended π-conjugation, was about five times

larger than that of H_2(OEP), illustrating the increase in $\chi^{(3)}$ as the number of π-electrons in the conjugated ring increases. A similar effect is observed in one-dimensional π-conjugated polymers such as polyacetylenes. The Mn(OEP)Cl showed slightly larger $\chi^{(3)}$ than H_2(OEP) presumably due to the inclusion of a metal atom.

[Figure 32]

Norwood and Sounik[55] measured $\chi^{(3)}$ values of magnesium octaphenyltetrazaporphyrin (Mg(OPTAP)) (Figure 33) as a 5% weight incorporation in poly(methyl methacrylate) (PMMA). The thin films showed $\chi_{xxxx}^{(3)}$ and $\chi_{xyyx}^{(3)}$ values of the order of 1.17 x 10^{-11} and 3.03 x 10^{-12} esu, respectively from DFWM at 598 nm. The ratio of $\chi_{xxxx}^{(3)}$ to $\chi_{xyyx}^{(3)}$ was three, implying that the optical nonlinearity is predominantly electronic. The Mg(OPTAP) showed a response time of 44 ps.

[Figure 33]

Anderson et al.[56] synthesized the soluble conjugated porphyrin polymer of 5,10,15,20-diethylnyl zinc porphyrin ($(DEtyP)_n$) using Glaser-Hay coupling (Figure 34). The real and imaginary components of $\chi^{(3)}(-\omega;0,0,\omega)$ of these polymers were calculated from the electroabsorption spectra. The $\chi^{(3)}(-\omega;0,0,\omega)$ on the order of 7.3 x 10^{-8} esu was obtained at the peak resonance due to resonance enhancement.

[Figure 34]

Bao and Yu[57] synthesized free base and Zn-metalloporphyrin-containing polymers (Figure 35) and measured their $\chi^{(3)}$ values by DFWM technique at 532 nm. These polymers possess photoconductive and photovoltaic properties. Notable $\chi^{(3)}$ values were obtained for the polymeric materials. The $\chi^{(3)}$ value found for Zn(TPP) was twice as large as the free base porphyrin. The $\chi^{(3)}$ values were on the order of 10^{-10} esu for thin films. Polymer solutions showed $\chi^{(3)}$ values of 1 x 10^{-12} and 1.9 x 10^{-12} esu for the Zn and free base porphyrin polymer materials, respectively, which was more than two orders of magnitude smaller than those obtained for thin films. These $\chi^{(3)}$ values were enhanced due to the resonant contributions.

[Figure 35]

Kandasamy et al.[Kandsamy, 1997 #20] measured second hyperpolarizabilities of six tetraphenylporphyrin derivatives using the Z-scan technique at 784 nm. The γ value grew with increasing negative value of the Hammett constant. All porphyrins showed negative γ values both in neutral and acidic media. The γ value of porphyrins increased three to five times in an acidic medium compared to neutral. One species, H_2(T(*o*-$OCH_2CO_2C_2H_5$)PP), showed γ values of -273.5 x 10^{-30} esu in acidic medium, about 5 times larger than in the neutral medium. The H_2(T(*o*-$OCH_2CO_2C_2H_5$)PP)material also accorded a γ value 36 times larger than H_2(TPP) in an acidic medium. The NLO properties of H_2(T(*o*-$OCH_2CO_2C_2H_5$)PP)were significantly higher than the other materials because of the substituted electron donor groups at the *ortho* phenyl positions.

Kandasamy et al.[58] measured second hyperpolarizabilities of divalent M(TPP) derivatives using the Z-scan technique at 802 nm. The γ value was enhanced by metal substitution, and it increased from the completely filled d-shell of Zn to the partially filled d-shell of Cu and Ni. The γ value of Ni(TPP) was more than three times that of Zn(TPP). The γ value of Sn(IV) substituted 5,10,15,20-tetrakis((4-carboethoxymethyleneoxy)phenyl] porphyrins [Sn(TCEMPP)X_2; X=I^-, N_3^-, Br^-, Cl^- or OH^-] was determined by the same method at 802 nm in order to investigate the effect of axial ligand substitution on γ values. The γ value increased when a strongly electronegative axial ligand such as iodine was substituted. The high charge density at the core gives rise to larger γ values. The large γ value observed for the azido axial ligand porphyrin originates from its strong electron donor activity. These porphyrins produced negative γ values confirming their self-defocusing optical nonlinearity.

Kumar et al.[59] reported third-order optical nonlinearities in basket handle porphyrins (PSI) using DFWM technique at 532 nm (Figure 36). The planar Cu(TPP) porphyrin showed $\chi^{(3)}(-\omega;\omega.\omega,-\omega)$ of 1.03 x 10^{-12} esu, while the value for the ruffled PSI molecules was found to be approximately 10^{-13} esu.

[Figure 36]

The $\chi^{(3)}$ of thin films of C_{60} and H_2(TPP) composites were measured by a research team at Naval Research Laboratory using DFWM and nonlinear transmission at 590.5 nm.[60,61] Kajzar and associates.[62] measured $\chi^{(3)}$ values in multilayer and composite C_{60}-based thin films with tetraphenylporphyrin, H_2(TPP), and tetraphenylnaphthacene, H_2(TPN), using THG at 1.907 μm. Lower $\chi^{(3)}$ values were observed for both composite films and multilayered structures compared to C_{60} films.

Third order nonlinearity of solution-state and thin films of triethoxysilane-substituted Zn(TPP) polymers were examined by Sinha et al.[63] Using DFWM, $\chi^{(3)}$ was measured in solution at 3.06 x 10^{-10} esu at 532 nm and 0.36 x 10^{-10} esu at 1064 nm, demonstrating resonance enhancement at the higher frequency. A cured polysiloxane film containing the same porphyrin provided a $\chi^{(3)}$ of 3.25 x 10^{-10} esu at 532 nm. The corresponding γ values were determined to be 24.49 x 10^{-32} and 2.81 x 10^{-32} esu, in solution at 532 and 1064 nm, respectively, and 60.10 x 10^{-32} esu for the thin film at 532 nm. Additionally, the polymer film was determined to be thermally stable in excess of 500°C by thermogravimetric analysis.

A comparison of the third-order optical nonlinearity on various metalloporphyrins results is summarized below (Table 7). The $\chi^{(3)}$ values vary as much as seven orders of magnitude depending upon chemical structures, measurement technique, wavelength, state of matter, and resonant contributions.

[Table 7]

3. Optical Limiting Systems

Optical limiting properties of fullerenes, porphyrins and phthalocyanines have attracted much attention since they have applications in passive solid-state sensors and the human eye protection from high-intensity visible light sources.[64,65]

Although metallophthalocyanines have been studied in detail, there are few reports on optical limiting properties of porphyrins. Blau et al.[66] showed reverse saturable absorption (RSA) by cobalt and zinc TPP complexes. Fei et al.[67] reported RSA in Fe(TPP). Nonlinear excited state absorption in a series of metallo-texaphyrin compounds (Figure 37) in acetonitrile solutions using 8 ns and 23 ps optical pulses at 532 nm was noted by Shi et al.[68,69] The texaphyrin compounds show reverse saturable absorption at weakly fluorescent bands for nanosecond pulses, while saturable absorption occurs for highly fluorescent bands only for picosecond pulses. A six level model was presented to explain the nonlinear absorption effects. Cadmium texaphyrin showed strong RSA and nonlinear absorption while it was very weak in the other metallo-texaphyrin derivatives.

[Figure 37]

Su and Cooper.[70] reported optical limiting properties of free base octabromo-tetraphenylporphyrin ($H_2(Br_8TPP)$) and its metal-containing derivatives (Figure 38). Nonlinear optical absorption efficiency was measured at 532 nm. The efficiency data showed a trend as $Zn(Br_8TPP) > Cd(Br_8TPP) > H_2(Br_8TPP) > Pb(Br_8TPP) > Cu(Br_8TPP) \approx Cd(Br_8TPP)$ which was related to the spin state of the central metal atom. Comparable to phthalocyanines, $Zn(Br_8TPP)$ showed the strongest nonlinear absorption efficiency observed among porphyrins.

[Figure 38]

C. Porphyrins and Metalloporphyrins as Opto-materials

In photosynthesis, the chlorophylls and pheophytins (close cousins of metalloporphyrins and porphyrins, respectively) play key roles in adsorbing light energy over a wide spectral range and converting it into the highly directional transfer of electrons.[71-76] It is a marvelous but highly complex process that has inspired considerable interest in the synthesis of porphyrin arrays. A biomimetic approach to the photosynthetic apparatus may also lead to applications of similar systems as opto-electronic devices. After brief overviews of artificial photosynthetic models and light harvesting antennae to set the stage, this section will focus predominantly on porphyrinic materials in applications to optoelectronics.

The remarkable efficiency of reaction center photochemistry has encouraged the design and the study of synthetic models. Most research on artificial photosynthesis has been directed toward mimicry of the natural

reaction center (RC). The center functions as a molecular-scale solar photovoltaic device that converts light energy into chemical energy that can be transported and stored for maintenance, growth, and reproduction of the organism. Green plants employ chlorophyll, a magnesium-chlorin, as the chromophore to harvest light. The trapped light energy is used to promote electrons into high-energy excited states. However, these excited states tend to decay to their ground states within nanoseconds, wasting the harvested energy as heat. Chromophores in green plants prevent this from happening by extremely rapid electron transfer. The acceptors are chlorophyll and pheophytin molecules initially, and quinones eventually. The resulting separation of negative and positive charges at the reaction center preserves a substantial fraction of the photon energy as chemical potential energy by generating a potential across the organelle membrane. At the minimum, then, an artificial reaction center requires some kind of chromophore that can absorb light and act as electron donor, an electron acceptor, and an organized superstructure that controls the electronic interaction between the donor and the acceptor. Initial work on model systems involved simple mixing of donor pigment molecules with acceptor molecules in solution. The electron transfer events were monitored by observing ion pairs that were the result of donor/acceptor collisions. Flash photolysis, nanosecond, and picosecond emission spectroscopy were used to characterize transient intermediates to better understand electron transfer kinetics.

1. Artificial Photosynthetic Systems

Achieving a long-lived charge separation after photoinduced electron transfer is the key to realizing artificial photosynthesis. This section will focus on molecules designed to maximize the lifetime of a charge-separated state. The ultimate goal here is to create a sufficiently long-lived excited state that chemical reactions can compete with the back reaction and convert the excited state free energy into a less volatile form. The first such systems, developed in the 1970s, were molecules consisting of synthetic porphyrins covalently linked to quinones. The porphyrin first excited singlet state is a strong reductant and is easily observed by flash kinetics. Simple porphyrin-quinone complexes are relatively easy to synthesize. The use of porphyrin pairs (as in the reaction center itself) is rather a more difficult challenge, however [77]. Following absorption of light, the porphyrin (P) transfers an electron to the quinone (Q) resulting a charge-separated state consisting of a cationic radical $P^{\bullet+}$ and an anionic $Q^{\bullet-}$. The lifetime of $P^{\bullet+}$–$Q^{\bullet-}$ is usually very short because of the back-reaction. The electron rapidly returns to the porphyrin molecule, losing energy as heat, and the ground state of the molecule is restored.

Kong and Loach described the first reaction center mimic to have a covalently-bound porphyrin-quinone linkage.[78,79] Shortly thereafter, Tabushi and coworkers designed a porphyrin-quinone molecule in which the quinone is bound to the porphyrin *via* an amide linkage.[80] These early systems outlined the basic conditions upon which future systems have dramatically improved. An extensive collection of porphyrin-quinone model compounds have been generated for the purpose of investigating long-lived charge-separated states. This overview will not be comprehensive, but instead will discuss a few illustrative examples. Interested readers are encouraged to consult an excellent review by Wasielewski on this subject.[81]

Substantial success has been made in using these complexes for biomimetic studies. In the 1980s, Gust and Moore have shown that the back reaction could be slowed substantially using a “triad” molecule composed of a tetraphenylporphyrin covalently linked to both a carotenoid and a quinone.[82-86] The slowing results from the formation of the charge-separated state in which the two radical ions are separated by a neutral porphyrin (Figure 39). Carotenoporphyrin-quinone molecules possess a long-lived ion-pair lifetime on the microsecond timescale. For comparison, a typical donor-acceptor excited state lives for only several hundred picoseconds due to efficient charge recombination. Wasielewski and coworkers designed an octaethylporphyrin triad to effect a long-lived charge-separated state also based on the multistep principles found in carotenoid systems. The donor and acceptor distance was controlled by triptycene-derived quinone and amine groups. Electron transfer from N, N-dimethylaniline (D) to P^+ was competitive with charge recombination in the $D\text{-}P^+\text{-}Q^-$ state; therefore, a long-lived charge-separated state was observed. Gust and Moore incorporated the successful multistep strategy in a pentad comprised of carotenoid-diporphyrin-diquinone subunits. The pentad adopted an extended linear shape about 80Å in length. Irradiation at 650 nm produced the porphyrin first excited singlet state, which underwent a series of complex electron transfer events. The final charge-separated state $D^{\bullet+}\text{-}P^+\text{-}Q^{\bullet-}$ was long-lived and formed with a quantum yield that approach unity.

[Figure 39]

In the early 1990s, Osuka developed elaborate covalently-linked porphyrin dimers bound to a quinone electron acceptor, tethered via an aromatic hydrocarbon linkage.[87,88] The structural and functional aspects found in reaction center chromophores were modeled using stacked porphyrins that roughly mimic special pair, at least in general structure (Figure 40). Because Osuka's system featured octa-alkylated porphyrins as the primary donor, the optically well-defined P^+ cation intermediate absorption at 670 nm provided a suitable marker to monitor transients. The anthracene-pillared coplanar system had charge-separated state lifetimes that survived for only several hundred picoseconds. One failing of this system is the large separation between the porphyrin faces in the porphyrin pair relative to that found in photosynthetic reaction center special pair.

[Figure 40]

Osuka has also designed a system comprised of a zinc porphyrin dimer (DP), a zinc porphyrin monomer (ZnP), and a pyromellitimide (pm) in place of the quinone.[89] The pyromellitimide anion absorbs at 715 nm, which is spectrally resolved from the porphyrin absorption bands. Upon photoexcitation in THF at 532 nm, these triads give DP^+—ZnP—pm^- ion pairs with lifetime of 2.4 μs in relatively low quantum yield. By replacing the intermediate Zn porphyrin with the non-metalated free base (Figure 41),[90] reasonable functional similarity to the photosynthetic reaction center was obtained. An efficient electron transfer relay, $^1DP^*$—P—pm → DP^+—P^-—pm → DP^+—P—pm^-, was observed, similar to the primary electron transfer events in the reaction centers.

[Figure 41]

A spectacular example of a long-lived, charge-separated donor–acceptor triad was demonstrated by Gust and Moore.[91] The Arizona researchers reported a molecular triad consisting of a diarylporphyrin (P) covalently linked to a carotenoid polyene (C) and a fullerene (C_{60}) (Figure 42). In 2-methyltetrahydrofuran solution, the triad undergoes photoinduced electron transfer to yield C—$P^{\bullet+}$—$C_{60}^{\bullet-}$, which evolves into $C^{\bullet+}$—P—$C_{60}^{\bullet-}$ with an overall quantum yield of 0.14. This state decays by charge recombination to yield the carotenoid triplet state with a time constant of 170 ns. The results demonstrate that fullerenes can act as effective primary electron acceptors in multicomponent systems that generate long-lived charge-separated states. The $C^{\bullet+}$—P—$C_{60}^{\bullet-}$ charge-separated state recombines to yield the carotenoid triplet state, rather than the molecular ground state, as in photosynthetic reaction centers.

[Figure 42]

Finally it should be mentioned that among the numerous synthetic analogs made for the photosynthetic reaction center[81], nearly all utilize only a single porphyrin as the initial photoelectron donor, rather than a porphyrinic dimer as in the reaction center. The use of face-to-face bisporphyrin complexes linked to a quinone is perhaps the most sophisticated of these and provides a starting point for combination of synthetic light harvesting systems with synthetic electron donor-acceptor complexes.[77,92]

2. Porphyrins for Optoelectronics

An ultimate goal in microelectronics is the design of electronic switches, wires, transistors, and gates made of single molecules. Approaches to this goal borrow heavily from the photosynthetic reaction center, both in their physics and in their chemistry. In principle, porphyrin arrays connected with conducting or insulting molecular wires could be converted into such molecular photo-electronic devices. In practice, however, the majority of the models have yet to function as electronic switching devices or molecular wires.

Toward that goal, Wasielewski et al. have designed a molecule (Figure 43) consisting of two porphyrin donors rigidly attached to the two-electron acceptor N N'-diphenyl-3,4,9,10-perylenebis(dicarboximide) (PBDCI), that acts as a picosecond electron switch when exposed to short pulse of light.[93] Excitation of the porphyrins within this molecule with subpicosecond laser pulses results in single or double reduction of the acceptor depending on the light intensity. The singly and doubly reduced electron acceptors absorb light strongly at 713 and 546 nm respectively.

[Figure 43]

More recently, the same research group reported a prototype molecular switch by utilizing photoinduced electron transfer in a donor-acceptor (D–A) system.[94] The underlying principle is that the local electric field produced by a photogenerated donor-acceptor (D_1^+–A_1^-) ion pairs in the first unit can be used to control the photoinduced electron transfer reaction in a second donor-acceptor (D_2^+–A_2^-) ion pair. They constructed a donor1-acceptor1-acceptor2-donor2 molecule (D^1–A^1–A^2– D^2) (Figure 43), in which they selectively excite the second donor. Zinc 5-phenyl-10,15,20-tri(*n*-pentyl)porphyrin (D^1) and phenyldimethylpyrromethene dye (D^2) were chosen because they can be independently excited at 416 and 512 nm, respectively. The two acceptors were chosen because their ground states absorb only weakly at 416 and 512 nm and their radical anion absorption bands are well separated. Two ultrafast (150 fs) laser pulses were used to control the rate of a photoinduced electron transfer within the molecule. The results suggest that this type of molecule may lead to the realization of molecular electronic devices.

Lindsey and Wagner have investigated a variety of multi-porphyrin arrays that are connected by diarylethyne bridges for studies of artificial photosynthesis and molecular photonics. They have synthesized a "molecular photonic wire" consisting of array of metalloporphyrins 90Å in length.[95] The difference between a molecular electronic wire and molecular photonic wire is that latter supports excited-state energy transfer rather than electron/hole transfer process. The wire consists of a boron-dipyrromethene dye as an input chromophore at one end, a linear array of three zinc porphyrins as a signal transmission element, and a free base porphyrin as an optical output element at the other end (Figure 44). Absorption of a photon by the input chromophore at one end causes the emission of a photon as the optical output at the other end. The overall yield of energy transmission from input to output is 76%.

[Figure 44]

Crossley and Burn also reported a molecular wire based on a more conjugated backbone.[96] The tetrakis(porphyrin) is about 65Å in length and possesses a number of *tert*-butylporphyrin groups along the backbone that provide the molecule with good solubility in a number of organic solvent systems. Individual porphyrins are either directly fused or are linked by a coplanar aromatic system and are expected to be reasonably conductive. (Figure 45)

[Figure 45]

The synthesis of this extended porphyrin system involved a seven-step procedure. The final porphyrin tetramer was obtained by the condensation of porphyrin-α-dione with a bis-α-diamine. "Molecular optoelectronic gates" were also prepared by the same research group to see if the emission signal at the output chromophore in the photonic wire could be turned on/off in a controlled manner.[97] In order to achieve this goal a different metalloporphyrin was inserted into the molecular wire as a redox switch. To serve as a redox switch, this metalloporphyrin must meet four design conditions: (1) It must have a higher absorption energy, in the neutral state, so that the energy transfer does not occur between the free base and the metalloporphyrin. (2) When oxidized, the

metalloporphyrin should not fluoresce upon excitation. (3) It must have reversible redox properties. (4) It should possess the highest HOMO of all pigments in the assembly to ensure that oxidation takes place at the designated site. Mg-porphyrins seem to meet all the criteria. A schematic of the two designed gates is shown in Figure 46. The linear design has the switch attached to the end of the wire while the T-shape gate has the redox switch attached to the Zn-porphyrin. Oxidation was achieved by either chemical method or electrochemical method. In both cases the fluorescence of the free base porphyrin decreased significantly. Addition of triethylamine causes reduction of the Mg-porphyrin radical cation and recovery of the fluorescence.

[Figure 46]

Shimidsu et al. have obtained both one-dimensional and two-dimensional porphyrin polymers with oligothienyl molecular wires.[98-101] The electron conductivity of the 1-D polymers with conjugating oligothiophene was strongly enhanced by irradiation of light and was dependent on the light intensity. The 1-D porphyrin array with insulating wire was prepared by condensing the dichloro-P-porphyrin and the corresponding diol. The 2-D porphyrin network was synthesized by electropolymerization of the corresponding phosphorus-porphyrin with four oligothienyl groups at the *meso* positions. The 2-D porphyrin arrays showed similar functions as the 1-D porphyrin arrays with conjugating wires (Figure 47).

[Figure 47]

3. Synthetic Light-Harvesting Antenna

Photosynthetic microorganisms use light-harvesting antenna to trap solar energy and funnel it to the reaction centers.[102-105] The energy conversion and migration can involve hundreds of pigments. A light-harvesting antenna should be a multicomponent assembly including chromophores that can absorb strongly in the blue and red regions of the solar spectrum and an energy-acceptor component to accept it. Synthetic porphyrins arrays are obvious candidates for the design of artificial antenna since chlorophylls are the main natural chromophores. Such exploration, however, has been limited by a lack of appropriate synthetic methodology for the preparation of large porphyrin arrays. Conventional synthetic strategies frequently involve a large number of sequential steps and extensive chromatographic purification. Consequently, the majority of the research done in this area focus on the synthesis of multi-porphyrin networks. Viable syntheses of suitable large arrays have only recently become available with the development of building-block methodologies.

In this section, we will concentrate on synthetic methods since the materials synthesized are potential light-harvesting antennas. Burrell and coworkers described the synthesis of functionalized TPPs building blocks that have been successfully used to prepare a variety of porphyrin arrays including trimers, pentamers, and nonamers (Figures 48 and 49).

[Figure 48]
[Figure 49]

In the early 1990s, Osuka et al. reported the synthesis of linear and stacked trimeric and pentameric porphyrins bridged by rigid aromatic spacers.[106] When the number of porphyrin rings increased, serious solubility problems occurred which prevented study of higher homologs. To circumvent this difficulty, peripheral substituents were placed on the porphyrin in hopes of increasing the solubility so that larger porphyrin arrays could be manipulated in common organic solvents. Using this strategy, they reported linear 1,4-phenylene-bridged porphyrin arrays including the dimer, trimer, pentamer, heptamer, and nonamer by acid-catalyzed condensation of formyl-substituted porphyrins with di(3-ethyl-4-methylpyrrol-2-yl)methane.[107] The molecular length of the nonamer is estimated upwards of 122Å (Figure 50).

[Figure 50]

The same research group also reported the first bridgeless 5,10,15,20-linked porphyrin arrays which were synthesized by direct oxidative coupling of zinc porphyrins.[108] Treatment of zinc(II) 5,15-di(-3,5-di-*tert*-butylphenyl)porphyrin with $AgPF_6$ in acetonitrile for 5 h produced the dimer and the trimer in low yield. The

proposed mechanism is an initial one-electron oxidation of the zinc porphyrin by the Ag(I) follow by the nucleophilic attack of the neutral zinc porphyrin. The dimer and the trimer were separated by size exclusion chromatography. Reaction of the dimer under similar conditions afforded the tetramer in modest yield (Figure 51).

[Figure 51]

An extension of this work was reported for orthogonally-arranged, windmill-like porphyrin arrays, involving a 5,10,15,20-linked porphyrin dimer unit.[109] The synthesis involved the preparation of a symmetric, linear 1,4-phenylene-bridged porphyrin trimer. The reaction of the trimer with two equivalents of $AgPF_6$ produced windmill-like porphyrin hexamer and nonamer systems. (Figure 52)

[Figure 52]

Other groups are also pursuing light-harvesting porphyrin arrays. In 1993, Lindsey et al. reported a convergent strategy for the synthesis of soluble covalently-linked porphyrin arrays.[110,111] The porphyrins are linked together via homogeneous Pd-catalyzed couplings of iodo- and ethyne-substituted tetraarylporphyrins (Figure 53). Reaction of the iodo-porphyrin and the ethyne-porphyrin in pyridine/triethylamine at 100ºC for 12 h afforded a mixture of products including higher molecular weight material, the pentamer, dimer, and unreacted starting materials. Chromatography on silica gel yielded the pentamer in 50% yield. The absorption spectrum of the pentamer is similar to the monomers with a slight red-shift of the Soret band. Arrays with various metallation states are readily available. The fluorescence spectrum of the system with a central free base porphyrin and peripheral zinc porphyrins is dominated by the emission of the free base porphyrin. The yield of energy transfer from the zinc to free base porphyrin is estimated to be ~ 90%.

[Figure 53]

An excellent example of employing secondary pigment to enhance the absorption properties of the porphyrin was reported by Lindsey, Holten, Bocian, Birge and coworkers. They designed and synthesized light-harvesting arrays comprised of a central porphyrin with one, two, or eight boron-dipyrrin (BDPY) pigments (Figure 54).[112] In order to connect as many as eight boron-dipyrrin pigments around a central porphyrin, the *meta*-position of the 5,10,15,20-aryl rings on the porphyrin was utilized. Instead of the "porphyrin first, coupling second" approach, they decided to build the BDPY unit into the aryl aldehyde unit at the 4- or 3,5- positions using a Pd-catalyzed coupling reaction. The BDPY-incorporated aldehyde is then condensed with pyrrole to afford the desired BDPY-substituted porphyrin arrays. This strategy eliminated successive Pd-catalyzed coupling reactions and relied on the robust Lindsey porphyrin condensation. The synthetic routes of 4-(BDPY)benzaldehyde and 3,5-bis(BDPY)benzaldehyde are shown in Figure 54. Porphyrin arrays containing one, two, and eight PDPY dyes were prepared by mixed-aldehyde condensation reactions. These arrays are soluble in common organic solvents and can be easily metalated by treating the corresponding arrays with $Zn(O_2CCH_3)_2$ in methanol. Two important results with regard to the photophysical properties of the BDPY-porphyrin arrays are: (1) The intense blue-green absorption bands of the BDPY dyes complement the porphyrin Soret bands. (2) The energy transfer efficiency between the BDPY dyes and the central porphyrin is nearly quantitative in the arrays with one or two BDPY units, but drops (to 80–90%) in the arrays with eight BDPY units. The authors suggest that " the BDPY-porphyrin arrays are excellent candidates for inclusion in light-harvesting model system and as input elements of prototypical molecular photoic devices."

[Figure 54]

Another popular approach in the construction of suprarmolecular porphyrin arrays uses metal-ligand interactions.[113-120] Most of this work has concentrated on 5,10,15,20-pyridylporphyrin (TpyP) and the porphyrin arrays prepared from TpyP range from dimeric molecule through polymeric networks. This synthetic strategy was adopted by Lehn and Drain for the preparation of multi-porphyrin arrays with square architecture (Figure 55).[113] There most impressive assembly is a 21-component structure consisting of nine porphyrins linked together by 12 palladium cations (Figure 56).[121] It is composed of three different kinds of porphyrins: a tetrapyridylporphyrin

coordinated to four metal ions forms the center of the array; tripyridylporphyrins coordinated to three metal ions constitutes the sides of the array; and the dipyridyl porphyrins form the corners. The synthesis involved placing these components in solution with the correct ratio at room temperature. The product was isolated in an amazing yield of 90%.

[Figure 55]
[Figure 56]

In an effort to prepare new biomimetic light-harvesting systems, Therien and coworkers have adopted recently developed metal-mediated cross-coupling methodologies and synthesized a new class of porphyrin arrays.[122] The porphyrins are linked together by yne and polyynyl units (Figure 57). They believe that ethyne, oligoethyne, and multiethyne linkages between the porphyrins will produce multichromophoric systems with unusually strong excitonic and electronic coupling. The most important feature of these porphyrin arrays is that their spectroscopic data bear strong similarity to that of the purple bacterial light-harvesting complexes as well as to the light-harvesting structures in green photosynthetic bacteria.

[Figure 57]

III. Porphyrinic Solids

A. Microporous Solids

A number of researchers have explored synthetic strategies for the construction of porphyrinic solids that contain molecularly sized cavities or channels. Porphyrin macrocycles can be envisioned as flat, rigid, geometrically square building blocks approximately 1 nm wide. Out-of-plane twisting by the 5,10,15,20-substituted phenyl rings (as necessitated by steric constraints) provides a route to construct structures extending beyond the porphyrin macrocycle plane. Chemical modification of the perimeter is facile in many cases. Additionally the thermal stability makes them an attractive precursor for potential use at elevated temperatures. Furthermore, metalloporphyrins have demonstrated catalytic ability in a wide variety of reactions;[123,124] thus, porous metalloporphyrin networks have the potential to act as shape- and size-selective catalysts.

1. Porous Molecular Porphyrin Stuctures

Strouse and coworkers.[125-127] examined the extensive crystal structure library of free base and metalated porphyrin lattice clathrates in which the predominant intermolecular bonding interactions were of a very weak nature. In addition to H_2(TPP), their database included simple substituted porphyrins such as *o*-amino- (H_2(T(*o*-NH_2)PP)), *p*-methoxy- (H_2(T(p-OCH_3)PP)) and *p*-bromo- (H_2(T(p-Br)PP)) tetraphenylporphyrins. While the most commonly metalloporphyrin studied was the Zn(II) species, at least eleven other metalloporphyrins were examined. They realized that the large majority of these structures contained a high concentration of solvates and were in effect "porphyrin sponges."

These TPP derivative materials were held together by van der Waals forces and found to exhibit a comparable packing modes generalized as the simple body-centered-cubic (BCC) arrangement. The driving force for clathrate formation was identified as the efficient packing of the porphyrin moieties in two dimensions. A third dimension is accessible for inclusion of guest molecules. The dominant interaction is described as "porphyrin-porphyrin interactions" between perpendicularly oriented phenyl groups on adjacent molecules. Similar packing modes were observed for over sixty-five different TPP species.[125]

Channels of solvate molecules exist between chains of parallel porphyrin molecules (Figure 58). Estimates of the size of channel width were based on the *d*(002) lattice parameter essentially corresponding to half of the face to face porphyrin separation. The axial coordination sites or faces of the porphyrin macrocyclic ring line the edge of the channels. In the free base and 4-coordinate metalloporphyrin materials, the most commonly observed ratio was two guest molecules per porphyrin host molecule (Figure 59); notable exceptions were in cases of large solvate molecules (i.e. *p*-xylene, phenathracene or napthracenequinone) (Figure 60). Two axial ligands occupy the channels in six-coordinate metalloporphyrins; and, in the 5-coordinate materials, a single axial ligand and a single guest molecule were observed to alternately fill the voids (Figure 61). This is cited as an example of "programmability" in design of the clathrate materials. Porphyrin to guest ratios as high as 1:5 were observed for Fe^{III}(TPP)(*tert*-

$MeUro)_2(SbF_6^-)(THF)_2$ and $Mn^{III}(TPP)$ $(MeOH)_2(SbCl_6^-)(CH_2Cl_4H_2)_2$. The latter compound was also characterized as having multiple channels (Figure 62).[126]

[Figure 58]
[Figure 59]
[Figure 60]
[Figure 61]
[Figure 62]

Channel width was generally observed to be on the order of 3.4-6.6Å. Some of the smallest guest filled channels were observed in the Zn(TPP)(*m*-fluoronitrobenzene)$_2$, Zn(TPP)(2,4-dinitrobenzene)$_2$ and Zn(TPP)(acridine)$_2$ systems – all which had channel widths calculated at less than 4Å. The largest spacing for a "normal" clathrate material was observed for $Ru^{II}(TPP)((Ph_2P)_2Me)_2(CH_2Cl_2)$.[126] Layered materials with *d*(002) spacing of 6.8Å were observed for $Rh^{III}(TPP)(benzylisocyano)(PF_6^-)_2$ in which a single layer of guest molecules is located between a double layer of the host porphyrin species, and an even larger *d*(002) spacing of 7.8Å was noted for a material with a double layer of host $Ce^{IV}(TPP)^{+2}$ separated by another double layer of phthalocyanine molecules and $SbCl_6^-$ anions (Figure 63).[127]

[Figure 63]

Pursued applications of these clathrate "porphyrin sponges" include as materials to selectively "immobilize and isolate molecular species" and as intercalation compounds. The forces holding these solids together, however, are very weak. Consequently, upon removal of solvent, rapid structural changes to a different crystalline phase or to an amorphous material typically occur. In some cases, reintroduction of a vapor phase guest to the desolvated materials can produce a powder pattern that matched that of the crystalline clathrate materials grown in solution.[128] One specific application mentioned incorporating insect attractants as guest species into the lattice clathrate materials.[127]

Goldberg and coworkers have synthesized porphyrinic solids that utilize other weak intermolecular interactions between porphyrin building blocks. The structures of inclusion compounds formed from halogen substituted tetraphenylporphyrins displayed three general motifs. The most commonly observed patterns involve halogen-halogen attractions between the halo-substituted phenyl groups and attractions between halogen atoms and β-pyrrole hydrogen atoms; these can lead to both one- and two-dimensional arrays (Figure 64). Inclusion compounds of this variety were observed for Zn(T(p-Cl)PP) species with guests: guaiacol, nitrobenzene, DMSO, methyl salicylate,[129] methyl phenylacetate, mesitylene, ethyl benzoate and acetophenone.[130] and Zn(T(p-Br)PP) species with guests: benzylacetate, methyl salicylate, ethyl benzoate, bromobenzene or *p*-xylene.[131] The intermolecular Cl•••Cl distance defines the width of the guest cavities. The Cl•••Cl separation of 3.63Å reported for Zn(T(p-Cl)PP)•$C_7H_8O_2$ (Figure 65) is typical of the 1:1 inclusion complexes; values for 1:2 inclusion compounds such as Zn(T(p-Cl)PP)•$2C_2H_6OS$ (3.90Å) were higher.[129] Slightly offset stacking of the porphyrin macrocycles in subsequent layers defined the depth of the cavities. The intermolecular Br•••Br contact distances were reported as 3.837Å for a 1:2 Zn(T(p-Br)PP)•$2C_8H_8O_3$ (methyl salicylate) inclusion material. Thermal gravimetric analysis (TGA) was reported for Zn(T(p-Br)PP)•$2C_8H_8O_3$, showing a 21% weight loss for loss of solvent (theoretical 23%) at ~125°C without further loss to 350°C.[131] In the case of the 1:1 Zn(T(p-Cl)PP):nitrobenzene inclusion compound, the observed helical arrangement of the porphyrin backbone produced a polarized cavity environment (Figure 66). Guest molecules were observed to order in response.[130] The *p*-xylene clathrate of Zn(T(p-F)PP) featured a linear chain structure similar to that noted in the chloro- and bromo-derivatives. However, the non-bonding F•••F contact distances have increased to 4.1Å and 4.2Å. characteristic of a repulsive interaction rather than attractive force as observed in other halogenated porphyrin materials.[129]

[Figure 64]
[Figure 65]
[Figure 66]

A second motif observed by Strouse and coworkers is characterized by tightly packed herringbone-like layers (Figure 67). Structures of this type were observed for Zn(T(p-Cl)PP)•C_7H_7Cl (*o*-chlorotoluene),[129] Zn(T(p-Br)PP)•$3C_5H_5N$ and Zn(T(p-Br)PP)•$4C_9H_{12}$ (mesitylene).[131] In the *p*-bromo compounds, ligation of two pyridines to the Zn(II) ion was observed. The remaining uncoordinated guest molecules were observed to occupy voids between the porphyrin moieties.

[Figure 67]

A third motif, also observed in Strouse's TPP materials, is characterized by tightly packed corrugated layers in which the guest molecules intercalate between the layers: Zn(T(p-Br)PP)•$4C_6H_7N$ (aniline) and Zn(T(p-Br)PP)•$2C_8H_{11}N$ (methylbenzylamine) (Figure 68).[131]

[Figure 68]

2. Hydrogen-Bonded Network Materials

In an effort to synthesize more robust frameworks, hydrogen-bond interactions have been explored as basis for linking porphyrin molecules. Hydrogen bonds offer the additional advantages of directionality and selectivity.[132] While hydrogen bonding is certainly a stronger interaction than the van der Waals interactions that hold the "porphyrin sponge" solids together, even multiple hydrogen bonds per porphyrin still provide only modest stabilization of the solids in the absence of their solvates.

Goldberg and co-workers have explored a number of substituted tetraphenylporphyrins as building blocks for porous solids. Some of the inclusion compounds of 5,10,15,20-tetra(4-hydroxy)phenyl porphyrins (H_2(T(p-OH)PP))featured structures similar to those observed in halogenated species.[130] In a motif similar to the previously observed linear polymeric chains, the Zn(T(p-OH)PP)•$2C_6H_6O$•$2H_2O$ (phenol), Zn(T(p-OH)PP)•$2C_9H_{10}O$•H_2O (benzyl acetate) and Zn(T(p-OH)PP)•$2C_7H_6O$•H_2O (benzaldehyde) clathrate materials are characterized by dual *cis*-side OH•OH intermolecular attractions. There are no intermolecular interactions between *para*-substituted hydroxyl groups and β-pyrrole hydrogen atoms of adjacent linear chains (as observed in the halogenated materials). Instead, *para*-substituted hydroxyl groups hydrogen bond with hydroxyl groups on adjacent linear chains, forming a two-dimensional porphyrin network. A guest water molecule participates in this interchain bonding arrangement (Figure 69). In this manner, two different guest cavities are formed – voids between porphyrins in a polymeric chain and between chains in the two-dimensional array. Layers are stacked in an offset manner, therefore forming pores instead of channels in which axially coordinated ligands partially occupy the voids in successive layers.

[Figure 69]

Similar *cis*-side OH•••OH interactions are observed in the Cu(T(p-OH)PP)•$4C_8H_8O$ (acetophenone), Zn(T(p-OH)PP)•$2C_8H_{10}$•$4CH_3OH$ (*o*-xylene and methanol) and Zn(T(p-OH)PP)•$5C_7H_8O_2$ (guaiacol) materials. The linear porphyrinic chains are separated by guest molecules which hydrogen bond to the hydroxyl groups (Figure 70). In the acetophenone and *o*-xylene included materials, porphyrin macrocyclic planes of successive layers are offset preventing the formation of distinct channels. The parallel porphyrin macrocycles of successive layers are directly aligned in the guaiacol-included material generating ~9Å cavities. Between layers of porphyrin macrocycles is located, "sandwiched", a single parallel-orientated guest molecule (Figure 71). There is another guest guaiacol molecule situated below the area of hydrogen-bonding between porphyrin molecules.[130]

[Figure 70]
[Figure 71]

For the toluene inclusion solid, Zn(T(p-OH)PP)•$3C_7H_8$, a three-dimensional framework is observed (Figure 72). Hydrogen bonding between *trans*-orientated porphyrin hydroxyl groups and parallel chains form a geometry approximating a body-centered cubic arrangement. Porphyrins within successive layers of *trans*-hydrogen bonded chains have a interlayer separation of 6.5Å in which a guest molecule resides. Channels perpendicular to the layers of porphyrin chains are observed. The significant translational and rotational disorder of guest species in the crystal

structure supports the presence of channels. *Trans*-OH•••OH interactions define the framework of the Zn(T(*p*-OH)PP)•2C_7H_8O•2H_2O (*p*-cresol) inclusion solid. One dimensional hydrogen-bonded chains between *trans*-hydroxyl groups on porphyrins which are stacked partly overlapping the porphyrin macrocyclic ring resulting in a layered material with intercalated guest species (Figure 73).[130]

[Figure 72]
[Figure 73]

The clathrate of equimolar 5,10,15,20-tetra(4-methoxy)phenylporphyrinatozinc(II), phenol and water, Zn(T(p-OCH_3)PP)•C_6H_6O•H_2O, exhibits intermolecular hydrogen-bonding between methoxy substituents and axially coordinated water molecules in successive porphyrin layers (Figure 74). This arrangement generates a three-dimensional cross-linked framework in which phenol molecules occupy cavities between layers of porphyrin molecules similar to results reported for tetraphenylporphyrin inclusion solids by Strouse with *m*-xylene guest molecules.[125] A corrugated sheet-like geometry is observed in the Zn(T(*p*-CH_2OH)PP)•2$C_8H_8O_2$ (*o*-hydroxyacetophenone) material (Figure 75).[130]

[Figure 74]
[Figure 75]

For clathrates of 5,10,15,20-tetra(4-cyano)phenyl porphyrin, H_2(T(p-CN)PP), four structural motifs were encountered by Goldberg et al.[133] The first hydrogen-bonding motif involves open two-dimensional networks in which a cyano group hydrogen bonds to β-hydrogen atoms on an adjacent porphyrin pyrrole rings in a dimeric fashion (Figure 76). The individual [-C≡N ••• H-(β-pyrrole)] interactions are described as short (3.41-3.59Å) and linear, although the two H-bond interactions of the dimer are not parallel to each other. The 1:2 inclusion compound of Cu(T(p-CN)PP) with chloroform produced a framework with elliptical interporphyrin cavities (6.4Å x 11Å) (Figure 77) whereas larger square-shaped cavities (10Å x 10Å) were observed for Zn(T(p-CN)PP) with two ethyl benzoate molecules – one axially ligated to the central Zn(II) ion and the other located within the interporphyrin void (Figure 78).

[Figure 76]
[Figure 77]
[Figure 78]

One dimensional chains utilizing similar dimeric interactions were observed for the inclusion solids Zn(T(p-CN)PP)•3$C_7H_8O_2$ (where the solvate is guaiacol) and Zn(T(p-CN)PP)•2.5C_7H_8O (anisole) (Figure 79). In the guaiacol-included material, a 20.06Å x 4.1Å cavity is noted. A similar structure is observed for Zn(T(*p*-NO_2)PP)•3$C_{10}H_{12}O_2$ (eugenol) with a large cavity of dimensions 23.34Å x 4.19Å (Figure 80). Herringbone-type interchain interaction between a single cyano substituent and a β-pyrrole hydrogen atom is characteristic of the third type of pattern observed for *para*-cyanophenyl porphyrin materials (Figure 81). Interlayer spacing of 4.3Å was observed for Zn(T(p-CN)PP)•$CHCl_3$•C_6H_6. In the Cu(II) porphyrin species, Cu(T(p-CN)PP)•2$C_6H_5NO_2$, cross-linking between adjacent chains is observed (Figure 82). The fourth bonding pattern utilizes ligand to metal coordination and is addressed subsequently.[133]

[Figure 79]
[Figure 80]
[Figure 81]
[Figure 82]

Two clathrates of 5,10,15,20-tetra(4-carboxy)phenylporphyrin have been reported by Dasitidar et al.[134] Interpenetrating networks in the 1:1 Zn(T*p*CPP) : *sec*-phenethyl alcohol included material are formed when a porphyrin molecule hydrogen bonds to four other porphyrins via 'typical' carboxylic acid dimer aggregation. A planar two-dimensional array is formed in this manner (Figure 83). The *sec*-phenethyl alcohol is axially bound to the central zinc ion. Porphyrin macrocycles of parallel layers overlap and are interpenetrated by layers approximately

perpendicular (a dihedral angle of ~70° is reported). Observation of "a large central cavity of a rhombic shape" with dimensions 18Å x 16Å x 21Å is reported. However, in reality this "cavity" is nonexistent: it is actually fully filled by two metalloporphyrins from perpendicular arrays.

[Figure 83]

Construction of Zn(TpCPP)•$3C_2H_6SO$ (DMSO) porous material is based on *cis*-side interaction of carboxylic acid groups with hydrogen bonding to a bridging DMSO molecule resulting in generation of a one-dimensional polymer chain. Additional DMSO molecules bridge parallel polymeric chains creating a two-dimensional array. Each layer is intersected by an approximately perpendicular network. There are no H-bonds between perpendicular layers (Figure 84). A cavity of 6.5 x 10Å is reported, and TGA results suggests loss of solvents in two steps (axially-coordinated versus guest DMSO molecules).[134]

[Figure 84]

Supramolecular networks based on hydrogen bonding between symmetrically substituted octahydroxyporphyrins were explored by Suslick and coworkers.[135,136] Both *ortho*- and *meta*-dihydroxyphenylporphyrins (Figure 85) and their Zn(II) and Mn(III) derivatives were developed as molecular building blocks for nanoporous materials. The position of the peripheral hydroxyl groups, the choice of metalated or free base porphyrin, and the nature of the solvate dramatically influence structural features. These materials featured significant void volumes, as high as 67% calculated channel volume from x-ray crystal structures (Table 8).

[Figure 85]
[Table 8]

A one-dimensional hydrogen-bonding structure was found for H_2(T(3',5'-DHP)P)•5EtOAc in which porphyrin macrocycles stack in a columnar fashion. These columns of porphyrins align parallel to one another, forming a porous three-dimensional network with channels of 6.5Å x 6.5Å between them and 3.4Å x 3.4Å running perpendicular to the columns (Figure 86). These columns are held together by weak van der Waals interactions. When benzonitrile is used as the solvent species, the structure of H_2(T(3',5'-DHP)P)•$7C_6H_5CN$ changes substantially to a two dimensional array of porphyrins interconnecting via hydrogen bonds generating a three-dimensional corrugated-sheet configuration. The observed variation in solid-state structure is credited to steric requirements necessitated by the larger benzonitrile guest molecules. Channels parallel to the corrugated layers with dimensions 5.5Å x 6.0Å and another set approximately perpendicular calculated to be 4.0Å x 5.0Å were identified (Figure 87).

[Figure 86]
[Figure 87]

Both the Zn(II) and Mn(II) derivatives of the *meta*-hydroxyl species featured three-dimensional hydrogen-bonded networks. Zn(T(3',5'-DHP)P)$(THF)_2$•2THF•$3CH_2Cl_2$ has an interconnected layer motif in which the metalloporphyrins are arranged in a "slipped stack" orientation (Figure 88). In the structure of Mn(T(3',5'-DHP)P)-(Cl)•2EtOAc, the chloride anion bridges four hydroxyl groups from four separate porphyrins in a square planar arrangement with an average Cl•••O distance of 3.01Å creating a two-dimensional array (Figure 89). Hydrogen bonding between layers generates a three-dimensional network with 4.6Å x 3.4Å wide channels (Figure 90).

[Figure 88]
[Figure 89]
[Figure 90]

When the hydroxyl substituents are simply changed from the *meta*- to the *ortho*-phenyl positions, an essentially two-dimensional layered material results. The peripheral hydroxyl groups of H_2(T(2',6'-DHP)P)•4EtOAc induce a slight ruffling of the porphyrin macrocyclic rings and show strong directional hydrogen

bonding (Figure 91). Channels 3.0Å x 3.6Å wide were formed by the packing of the layers (Figure 92). A similar packing motif was observed for the Zn(II) metalloporphyrin species.[135]

[Figure 91]
[Figure 92]

3. Metal Ion Coordination Network Materials

In the last decade significant progress toward the rational construction of three-dimensional solids constructed from metal cations and organic molecules has been described.[137,138] Of particular interest have been metal-organic coordination networks possessing nanoscale pores.[139] Metal-ligand interactions are often quite strong and should therefore provide a more robust framework than those based on van der Waals, hydrogen-bonds or π–π interactions.

Goldberg and coworkers have reported a number of inclusion compounds utilizing coordination of substituted tetraphenylporphyrins. Porphyrinic inclusion compounds of 5,10,15,20-tetra(4-pyridyl)porphyrin, H_2(TPyP), exhibited two general motifs.[140] Crystallization of the Zn(TPyP) complex resulted in a geometry featuring "zigzag" polymer chains in which the central Zn(II) ion is axially ligated by pyridyl substituent from an adjacent porphyrin (Figure 93). A similar arrangement was observed for inclusion compounds of aromatic solvents such as aniline (Figure 94) Only one pyridyl moiety per porphyrin building block coordinates to another porphyrin, thereby limiting ligand-metal interactions to one-dimensional polymeric chains. The guest species is located in a cavity adjacent to the pyridyl substituent *trans*- to the pyridyl axially ligating the metal center of an adjacent porphyrin in the zigzag chain.

[Figure 93]
[Figure 94]

A second motif encountered in tetrapyridylporphyrin systems is typified by inclusion compounds with wet methanol and water that produce three-dimensional coordination polymers. *Trans*-pyridyl substituents on a Zn(TPyP) were observed to axially ligate the metal centers of adjacent porphyrin moieties generating a polymeric chain in one dimension. Cross-linking in a second dimension occurs when the original porphyrin molecule is coordinated by two pyridyl moieties from two additional porphyrin molecules (Figure 95). The two remaining pyridyl groups participate in hydrogen-bonding with included water molecules. An intricate three dimensional framework results (Figure 96).

[Figure 95]
[Figure 96]

For inclusion solids of 5,10,15,20-tetra(4-cyano)phenylporphyrin, H_2(T(p-CN)PP), one of the four structural motifs encountered by Goldberg involved ligand to metal interactions.[133] Two-dimensional coordination networks similar to those observed for Zn(TPyP) materials were found in Zn(T(p-CN)PP)•$2C_6H_5NO_2$ (nitrobenzene), Zn(T(p-CN)PP)•$CHCl_3$ (chloroform) and Zn(T(p-CN)PP)•C_7H_8O (anisole) materials (Figure 97). The guest species intercalate between the porphyrin layers (Figure 98).

[Figure 97]
[Figure 98]

Attempting to mimic the topology of the PtS structure, Robson and coworkers explored metal to ligand coordinative bonding as means to build more robust porphyrinic materials. They reported a structure in which Pd(TPyP) molecules are interconnected by Cd(II) centers.[141] Each porphyrin is coordinated by two *trans* pyridyl donor porphyrin molecules and by two *cis* donor porphyrin molecules (Figure 99). The overall neutral framework [Pd(TPyP)•$Cd(NO_3)_2$•$8.6H_2O$] features infinite interwoven layers of the porphyrin network.

[Figure 99]

In subsequent work, Robson and coworkers.[142] reported three-dimensional network solids using the copper porphyrin complexes of 5,10,15,20-tetra-4'-pyridylporphyrin, Cu(TPyP), and 5,10,15,20-tetra-4'-cyanophenylporphyrin, Cu(TCNPP). Large extended channels (10-20Å) were observed in which tetrahedral Cu(I) ions (as opposed to the square planar Cu(II) ions bound to the center of the porphyrin ring) coordinate to pyridyl or cyano groups on the periphery of four porphyrin molecules. While the cationic frameworks were reported to occupy less than half the volume of the crystal, the void spaces were occupied by non-coordinating anions (BF_4^-) and highly disordered solvent molecules (acetonitrile/nitrobenzene); upon removal of the anions, crystallinity was lost. In the tetrapyridyl system, a single infinite PtS-like network was revealed (Figure 100). In contrast, in the tetracyano system, two independent, interpenetrating networks were delineated (Figure 101). The tetrahedral Cu(I) ions in the tetrapyridyl system are located closer to the large pyridyl ring, which sterically restricts the inclusion of another independent network.

[Figure 100]
[Figure 101]

Anionic functional groups on the organic molecules circumvent the problems of a charged framework. Suslick and coworkers have explored the use of carboxylic acid-substituted porphyrins for building microporous porphyrinic solids. Tetraphenylporphyrins with carboxylate functionalities, i.e., 5,10,15,20-*tetra*-(4-carboxy)phenylporphyrin, H_2(TpCPP), and 5,10,15,20-*tetra*-(3,5-dicarboxy)phenylporphyrin, H_2(DiCarPP),[143] were selected as organic precursors. The carboxylic acids serve to solubilize of the large porphyrin molecules and, when deprotonated, to provide an anionic site for coordination of cationic metal atoms. A tightly packed and interpenetrated linear polymeric array was observed in the solid-state structure of the free base *p*-carboxylate porphyrin with Ca(II) bridging centers (Figure 102). Hydrogen-bonding between coordinated water molecules in the calcium layers was observed to stabilize the 3-dimensional structure.[144] Porous network material of the Co(III) and Mn(III) derivatives of *p*-carboxylate porphyrin have been characterized by X-ray crystallography and gas adsorption studies (Figures 103 and 104).[145] The tetrakis(di-*meta*-carboxyphenyl)porphyrin, H_2(DiCarPP), is anticipated to have a greater possibility of producing an intricate 3-dimensional structure due to the geometrical orientation of the carboxylic acid groups. In the crystal structure of the free base porphyrin, channels were observed to form in the packing of the discrete porphyrin molecules (Figure 105).[143]

[Figure 102]
[Figure 103]
[Figure 104]
[Figure 105]

4. Porphyrin-Incorporated Zeolites

Zeolites are crystalline alumina-silica based open anionic framework structures with uniformly sized, rigid pores and channels. Incorporation of porphyrins into zeolites has been explored as means to biomimetic oxidation catalysts.[146]

The initial efforts to combine porphyrins with zeolites resulted in materials in which the porphyrins were supported on the external zeolite surfaces rather than encapsulated inside the pores. The first of this type of material was reported by Bedioui and coworkers [147,148] in which the Mn(III), Co(III) and Fe(III) metalated species of multi-charged 5,10,15,20-tetra(4-*N*-methylpyridinium)porphyrins, H_2(TMPyP), were adsorbed onto zeolite Y (faujasite) surfaces. The electrochemical behavior of these electrocatalytic surface materials was studied by cyclic voltammetry. Subsequent work extended the inorganic supports to include ZSM-5 and EMC-2 zeolites and the VPI-5 molecular seize.[149] A significant positive shift of the electrochemical potential value of Mn^{III}/Mn^{II} redox pair was noted for the porphyrins adsorbed on zeolite surfaces (up to +380 mV in DMSO/H_2O). The effect of the interaction of the negatively charged zeolite surface with the metal ion is credited for this result.

Mallouk and co-workers explored the electrochemistry and photochemical evolution of hydrogen from water using a zeolite modified electrode. Methylviologen (MV^{2+}) was encapsulated in platinized zeolite L powder onto which Zn(TMPyP^{4+}) was externally adsorbed (Figure 106).[150] Taking advantage of the zeolite microstructure in an attempt to construct an artificial photosynthetic system, addition of EDTA as an electron donor resulted in

production of hydrogen from aqueous solutions. Substitution of the larger tetra(trimethylamino)-4-phenyl)porphyrin Zn(II) derivative, inhibited evolution of hydrogen gas from a similar system. Examining the electrochemistry of adsorbed Zn(TMPyP)Cl and Zn(TMPyP)Cl on zeolite Y, a positive shift of the reduction potential by 200 mV was reported versus aqueous solution.[151]

[Figure 106]

Other zeolitic materials with adsorbed porphyrins on external surface include the immobilization of $Sn(TMPyP)Cl_2$ and $Sn(TPyP)Cl_2$ on zeolite Y for use as a solid photosensitizer material in the photodegradation of organic substrates.[152] Zeolite supported Fe(T(*n*-MPy)P) (*n* = 2, 3 or 4) was explored in heterogeneous catalytic autoxidations of sulfite. It was observed that the *ortho*- methyl pyridyl substituted porphyrinic materials demonstrated approximately twice the catalytic activity of the *meta*- and *para*- substituted systems.[153] A Cu(TPP)/zeolite Y material was coated onto an electrode as part of a carbon paste to be used as an electrochemical sensor. No catalytic activity was noted when glutathione was used as a substrate for electroxidation, cysteine was observed to block electroxidation, and efficient activity for the electrocatalytic oxidation of hydrazine was observed. The authors cited this as an example of conferred selectivity due to the presence of the Cu(TPP)/zeolite material (Figure 107).[154]

[Figure 107]

The first of the so-called "ship-in-bottle" porphyrin systems in which the porphyrin macrocycle is synthesized from molecular precursors inside the zeolite cavities was reported by Tatsumi and coworkers.[155] Refluxing pyrrole and acetaldehyde under Rothmund conditions in the presence of ion-exchanged zeolite Y led to the formation of metalated 5,10,15,20-tetramethylporphyrin, H_2(TMP) within the zeolitic pore structure. H_2(TMP) is cited as being sterically amenable to the internal zeolite pores. Diffuse reflectance UV-Vis spectroscopy was used to characterize the materials (Figure 108). Significantly increased yields of cyclohexanol and cyclohexane from the oxidative conversion of cyclohexane were reported for the ion-exchanged xeolite complexes of Mn(II) and Fe(II) complexes of TMP versus the free metalloporphyrins.

[Figure 108]

The dioxygen affinity of Co(TMP) encapsulated in zeolite Y by similar "ship-in-bottle" methodology was studied by Govind et al.[156] The porphyrin-free zeolite exhibits quantitatively similar absorption isotherms for both oxygen and argon. In comparison, the Co(TMP) encapsulated zeolite compound was observed to absorb eight times the amount of oxygen to argon (Figure 109).

[Figure 109]

A larger pore zeolite, MCM-41, was used for the first reported encapsulation of a tetraphenylporphyrin and the first porphyrin-ligated second row transition metal. Surface modification of the zeolite with 3-aminopropyltriethoxysilane (APTES) was necessary to achieve encapsulation of ruthenium (II) 5,10,15,20-tetra(4-chlorophenyl)porphyrin, Ru(T(p-Cl)PP)(CO)(EtOH). The encapsulated porphyrin/zeolite material was characterized by vibrational and diffuse reflectance spectroscopy and powder x-ray diffraction (Figure 110). Twenty to forty times higher product turnovers were reported for oxidative catalysis of alkene substrates by *tert*-butylhydroperoxide with the porphyrin/MCM-41 material versus free Ru(T(p-Cl)PP)(CO)(EtOH).[157]

[Figure 110]

Kevan and coworkers synthesized, via physisorption, H_2(TPP) encapsulated within mesoporous MCM-41 hosts. Generated by photoinduced electron transfer, the long-lived $H_2(TPP^{\bullet+})$ cation was characterized by electron spin resonance (ESR) and diffuse reflectance electronic spectroscopy (Figure 111). For a series of (H_2(TPP)/C_n-MCM-41, C_n = C_{10}, C_{12}, C_{14} and C_{16}) materials, an increase in photoyield was observed to correspond with an

increase in alkyl chain length (causing increased pore size). The photoionization efficiency was observed to increase along the series AlMCM-41 < MCM-41 < TiMCM-41.[158]

[Figure 111]

The first inverse of the "ship-in-bottle" synthesis, in which the zeolite cage is constructed around a porphyrin template, was reported by Li and Zhan.[159] The Fe(II) and Mn(II) derivatives of tetra(*N,N,N*-trimethylanilinium)porphyrin and H_2(TMPyP) were used as cationic templates in zeolite hydrothermal synthesis. Attempts to incorporate an anionic porphyrin species, metallo-tetra(4-sulfunatophenyl)porphyrin, were unsuccessful; and trials with neutral TPP species resulted in trace encapsulation. High activity for the catalytic oxidation of cyclohexene by *tert*-butyl hydroperoxide was reported.

Using similar methodology, encapsulation of the positively charged species 5,10,15,20-tetra(5-trimethylaminopentyl)porphyrin, H_2(TMAP), in MCM-41 was reported by Stein and coworkers (Figure 112). Free base porphyrins were metalated with Cu(II), Ni(II) or Fe(II) ions subsequent to zeolite incorporation. For comparison, H_2(TMAP) was also encapsulated by ion-exchange. It was cited by comparison of UV-Vis spectral intensities that porphyrins incorporated via ion-exchange did not remain isolated from other porphyrin species and the surrounding zeolite framework. The opposite was observed in the material encapsulated as a template during hydrothermal preparation of the zeolite. The catalytic activity of the Cu(TMAP)/MCM-41 material was explored.[160]

[Figure 112]

5. Clays and Layered Materials Incorporating Porphyrins

Metalloporphyrins catalyze a large number of reactions including important biological oxidations.[Suslick, 1996 #4; Collman, 1993 #67; Sheldon, 1994 #69; Groves, 1997 #68] There has been increased interest in supported catalysts based on such metalloporphyrins absorbs or covalently linked to polymer systems. Organic polymers,[161] and inorganic supports such as silica,[162] and zeolites,[163-165] have been to capture these catalysts. Layered materials that are able to intercalate neutral or ionic guests into the interlayer spaces offer unique opportunity into this research area. Through the incorporation of a guest species into a layered host, novel solids may be engineered with desirable physical and chemical properties. Many layered materials such as clays, metal dichalcogenides, metal phosphate and phosphonates have been studied as potential catalysts. The synthetic methods of these intercalated materials involved co-precipitation or ion-exchange and are straightforward.

Clays are colloidal layered hydrous aluminosilicates. There are relatively few examples of porphyrin intercalation into clays reported, mostly with either smectite clays or layered double hydroxides (LDH). Smectite clays consist of negatively charged layered aluminosilicate sheets. These sheets are separated by cations and water molecules. The layers are constructed from tetrahedral SiO_4 and octahedral AlO_6. The layer charge originates from the substitution of Al(III) by Mg(II). The clay layers are held together through weak dipole and van der Waals forces and can be easily separated by insertion of charged-balanced cations. LDHs are available as naturally occurring minerals and as synthetic materials, and consist of positively charged mixed metal hydroxide layers that are charge-balanced by interlayered anions.

a. Smectite clays

Porphyrins were first introduced into clays in 1977 by the physical absorption of porphyrin molecules into montmorillonite in aqueous solutions.[166] The most common examples are the binding of tetra-cationic M(TMPyP) porphyrins (M = Co(II), Mn(III), Fe(III)) into montmorillonite clays. $Co(TMPyP)^{+4}$ was the first porphyrin to be intercalated into montmorillonite by ion exchange in acid solution.[167] The interlayer distance expanded from 27Å to 37Å upon intercalation. UV-visible studies revealed the retention of cobalt ions in the porphyrin molecules. Mansuy and coworkers have extended this approach and prepared the Mn-porphyrins intercalated materials and found it to be an efficient alkene epoxidation and alkane hydroxylation catalyst.[168] Additionally, the catalyst exhibited a marked shape selectivity in favor of small linear alkanes when compared to a more bulky substrates. It was also shown that the intercalated solid obtained did not release its porphyrin even after week-long extraction with CH_3CN. Recently, Carrado, and Wasserman examined the complexation chemistry of Cu(II) and Fe(III) with

TMPyP within the interlayers of smectite clays.[169] They demonstrated that Cu(II) porphyrins are stable within the slightly acidic clay environments and that the free base porphyrin can be metalated inside a Cu(II)-exchanged clay. Unlike the copper moieties, Fe(III) ions do not complex the free base porphyrin inside the clays.

Another method for the intercalation of metalloporphyrins into clays has been explored using porphyrins and metalloporphyrins as organic templates in the hydrothermal synthesis of layered silicates.[170] X-ray powder diffraction data indicated that the porphyrins are intercalated parallel between the silicate layers. Microanalysis and UV-visible diffuse reflectance spectra indicated that the porphyrins are incorporated intact.

b. Layered Double Hydroxides and Other Layered Materials

Anionic porphyrins and metalloporphyrins can be ion-exchanged into layered double hydroxide (LDH) materials (Figure 113). The first example of an LDH-porphyrin composite material was reported by Kato and coworkers in 1989.[171] The X-ray powder diffraction pattern of the intercalated material showed the d-spacing increased to 22.4Å from 8.0Å upon intercalation. This increase in the gallery height strongly indicated that the porphyrin were arranged perpendicular to the LDH layers.

[Figure 113]

Tetra-anionic Mn^{III}(TSPP)-LDH was prepared by anion-exchange.[172] The resulting LDH material contained 2.5 to 4.5% of Mn-porphyrin; even after prolong soaking in methanol and water, the metalloporphyrin was not extracted.. More recently, Besse and coworkers reported the intercalation of carboxylate (H_2(TpCPP)) and sulfonate (H_2(TSPP)) porphyrins in LDH systems by coprecipitation and anionic exchange.[173] Powder X-ray diffraction data and UV-visible diffuse reflectance absorption spectra of the intercalated LDH show complete intercalation. Interlayer d-spacing increased from 18.5Å for H_2(ToCPP)-LDH to 22.9Å for H_2(*p*TSPP)-LDH and 22.7Å for H_2(TpCPP)-LDH. Several orientations of the porphyrin molecules between the LDH were proposed (Figure 114). The authors suggest that the interlayer arrangement is determined by both the layer charge density of the host materials and the isomeric position of the anionic groups substituted on the guest molecules.

[Figure 114]

Binding of tetracationic porphyrins on layered antimony hydrogen phosphate and zirconium hydrogen phosphate (α-ZrP) have been reported by Thompson and coworkers.[174] Both monolayer and bilayer guest structures have been prepared with the heme guests adopting parallel or tilted orientation relative to the host layers. The authors argue that the orientation results from maximization of electrostatic and hydrogen-bonding interactions between the host and the guest.

From the work mentioned above, it is clear that clay-intercalation of porphyrins can be done efficiently. The rapid development of materials such as larger-pore pillared clays should lead to more intense exploration of this area.

B. Conductive Polymers and Ferroelectrics

Studies in the areas of conductive polymers and ferroelectric materials constitute a relatively small subset of porphyrin materials research. Nonetheless, the versatility of porphyrins has allowed for some interesting and useful results in these areas. We will examine the variety of approaches toward the creation of porphyrin-based conductive polymers and the potential applicability of porphyrinic polymers as ferroelectric materials.

1. Conductive Porphyrin Polymers

Electrical conductivity of polymers continues to be one of the most important research areas for materials science. The conductivity of metals (typically $10^2 \sim 10^3\ \Omega^{-1}cm^{-1}$ at room temperature) is generally higher than for semiconductors, but it is the temperature dependence that truly defines the difference: electrical conductivity of metallic substances increases with decreasing temperature, while that of a semiconductor decreases.[175] The interest in superconducting materials parallels the interest in synthetic metals. In a sense, the copper oxide high temperature superconductors (e.g., $YBa_2Cu_3O_{7-x}$ with $T_c \sim 95$ K) are two dimensional coordination polymers, but we will not discuss them further here.[176-178]

Porphyrins constitute a versatile building block for the preparation of conductive polymers. The large π system of porphyrins and metalloporphyrins yields a HOMO and LUMO which are generally separated by only 2 eV.[179] This gap can be narrowed via polymerization or additional conjugation, leading to interesting conductivity possibilities. In addition to conduction through the π system, metal-metal conductivity is possible within a chain of metalloporphyrins. Because porphyrins are able to coordinate a wide range of metals, conductivity is readily tunable in these cases.

a. Shish Kebab Porphyrin Polymers

The "shish kebab" approach[180-182] yields a class of coordination polymers based on stacked macrocyclic metal complexes (Figure 115). Here, macrocyclic complexes are linked together by axial coordination of bridging ligands. Until recently, "shish kebab" polymers with bridging ligands larger than a single atom were rare. $[Sn^{IV}(OEP))(pimelate)]_\infty$) and $[Zr(OEP))(succinate)]_\infty$ were two early examples.[183] In the late seventies, Hanack et al. started to prepare a large family of such polymers employing phthalocyanines of the type $[M(Pc)(L\text{-}L)]_\infty$.[181]

[Figure 115]

Collman and coworkers have reported similar "shish-kebab" polymers of the type $[M(OEP))(L\text{-}L)]_\infty$ (M = Fe, Ru, Os, and L-L = pyz, bpy, dabco) and examined their conductivities.[182,184,185] Many of the these "shish kebab" coordination polymers can be doped with iodine, which drastically increases their conductivity (e.g., $\sigma_{300K} = 1 \times 10^{-6}\ \Omega^{-1}cm^{-1}$ for $[Fe^{II}(Pc)(pyz)]_\infty$; $\sigma_{300K} = 2 \times 10^{-1}\ \Omega^{-1}cm^{-1}$ for $[Fe^{II}(Pc)(pyz)I_{2.54}]_\infty$). The conductivity of these doped "shish kebab" polymers depends on the interaction of the metal d_π orbitals with the π^* level of the bridging ligand. Collman et al. found that the metal-metal communication is greater for the better π-bonding metals (e.g., Os > Ru > Fe) and the more π-acidic bridging ligand (e.g., pyz > bpy >> dabco). The X-ray single crystal structure of the related non-macrocyclic metal complex $[Co^{II}(dmgH)_2(pyz)]_\infty$ confirmed that the polymeric "shish kebab" type structure can be formed with symmetric multi-atom bridges.[186]

b. Covalent, Conjugated Porphyrin Polymers

Porphyrins linked with conjugated organic bridges form another subclass of conductive porphyrin materials. Work toward such polymers was done by Crossley and coworkers, who synthesized linearly conjugated porphyrin systems.[179] Seen in Figure 116 is their conjugated tetrakis(porphyrin) system. Preliminary spectroscopic data on this system indicated a significant decrease in the HOMO-LUMO gap (by *ca*. 0.8 eV) compared with the porphyrin monomer. In related studies, Yu et al. used the Heck coupling reaction to synthesize conjugated porphyrinic polymers.[187] A series of polymers (Figure 117) were generated with M_w values of 5,000 to 46,000. The polymers were soluble in a range of organic solvents and were cast as optical films onto glass slides. Their conductivities were studied, showing a steady increase in current upon photo-irradiation.

[Figure 116]
[Figure 117]

Recent studies by Jones and coworkers have produced conjugated porphyrin polymers with oligophenylenevinylene bridges.[188,189] Using the Wittig reaction, as illustrated in Figure 118, a series of polymers were synthesized, labeled PP1 through PP3. The molecular weights, as determined by GPC, were inversely proportional to bridge length, ranging from M_n = 6692 (PP3) to 12230 (PP1). To increase solubility of the polymers in organic solvents, long alkoxy groups were appended to the bridges, which allowed casting of porphyrin films from toluene solution. Preliminary results showed that the non-doped polymers had conductivities of less than $10^{-12}\ \Omega^{-1}cm^{-1}$. Doping with nitromethane solutions of anhydrous $FeCl_3$ increased conductivities to approximately $10^{-6}\ \Omega^{-1}cm^{-1}$. The visible spectrum of the doped polymer, which showed red shifting of the absorption bands relative to the porphyrin monomer, was indicative of the narrowed HOMO-LUMO gap.

[Figure 118]

c. Conductive Porphyrin-Linked Polymers and Porphyrin Arrays

Another approach taken toward the creation of porphyrin-containing conductive polymers has been to incorporate porphyrins into the backbone of traditional conductive polymers. This approach has been studied extensively by Shimidzu and coworkers.[190,191] As shown in Figure 119, $P(TPP)(Cl)_2$ can react with thienyl or oligothienyl alcohols to generate the corresponding polymer precursors. Electrochemical oxidation of the thiophene-containing precursor gives the polymer. These types of polymers have also been built two dimensionally via electrochemical polymerization of 5,10,15,20-oligothienyl substituted porphyrins. The 1-D polymers are particularly interesting in that their conductivities are enhanced by photoirradiation. The conductivities of poly-2 and poly-3 were $1.2 \times 10^{-9}\ \Omega^{-1}cm^{-1}$ and $5.1 \times 10^{-8}\ \Omega^{-1}cm^{-1}$, respectively, under dark conditions. When irradiated with photons from a 500 W Xe lamp, conductivity enhancements of greater than threefold were seen.

[Figure 119]

2. Ferroelectric Porphyrin Materials

Very little work has been done in the development of coordination polymers as molecular-based ferroelectric materials. Ferroelectrics carry a permanent, macroscopic electric dipole moment (*i.e.*, polarization) in the absence of electric field. Furthermore, the polarization of ferroelectric materials can be switched with the application of an external electric field. Ferroelectrics have unusual electro-optical, photorefractive and pyroelectric properties. They can be fabricated into electronic oscillators, high frequency filters, electroacoustic converters, pyroelectric radiant-energy receivers, and nonlinear capacitive elements. Most ferroelectrics are metal oxides.[192-194] (such as $BaTiO_3$ and $LiNbO_3$); a few are liquid crystal materials.[195-198]

In a further development of the "shish-kabob" class of polymers, metalloporphyrin coordination polymers have been suggested as possible ferroelectric materials.[180,199,200] Coordination polymers of non-planar metalloporphyrins with *non-symmetrical* bridging ligands carry an aligned dipole moment along the stacking axis (Figure 120). The dipole moment originates from the charge separation between the bowl-shaped porphyrinato core and the metal atom (Figure 121). The metal atom tends to be pulled out of the porphyrin plane by strong axial ligands. If the metalloporphyrin has two different axial ligands, the metal atom will be pulled toward one side, depending on relative ligation strength and steric demands. Various monomeric structures of metalloporphyrins.[201-204] suggest that a double-well potential can be present, as shown schematically in Figure 122. By analogy to the metal oxide compounds,[205-207] the direction of the bulk polarization in such coordination polymers may respond to an external field.

[Figure 120]
[Figure 121]

Suslick and Chen have prepared several one-dimensional coordination polymers of metalloporphyrins with non-symmetric bridging ligands (Figure 123) as candidates for molecular ferroelectric materials.[180,199,200] Metalloporphyrin complexes of Fe(II), Fe(III) and Sn(IV) were examined. Structures determined by single-crystal X-ray diffraction include $[Fe^{II}(TPP)(pyCN)]_\infty$, $[Fe^{III}(TPP)(pyCO_2)]_\infty$, and $[Fe^{III}(TPP)(ImPhO)]_\infty$ (Figure 124). The chain alignment of the bridging ligand is disordered in $[Fe^{II}(TPP)(pyCN)]_\infty$, antiparallel in $[Fe^{III}(TPP)(pyCO_2)]_\infty$, but aligned and polar in $[Fe^{III}(TPP)(ImPhO)]_\infty$. $[Fe^{III}(TPP)(ImPhO)]_\infty$ crystallizes in a non-centrosymmetric space group, $Pna2_1$, with the normal to the metalloporphyrin ring about 20° off the c-axis. Therefore, a net dipole moment or macroscopic polarization parallel to the c-axis can be expected only from $[Fe^{III}(TPP)(ImPhO)]_\infty$. The small size of the doming of the porphyrin in this complex, combined with the large unit cell dimensions, suggests that the spontaneous polarization of $[Fe^{III}(TPP)(ImPhO)]_\infty$ will be much smaller than that of $BaTiO_3$.[208-210] The organic portion of the $Fe^{III}(TPP)(ImPhO)$ polymer does not contribute much to the dipole moment, although it is the major component in the unit cell.

[Figure 122]
[Figure 123]
[Figure 124]

C. Porphyrin-Based Chemical Sensors

Because of their inherent stability, unique optical properties, and synthetic versatility, porphyrins and metalloporphyrins are excellent candidates for a variety of sensing materials applications. Research in this area has

focused on incorporation of synthetic porphyrins and metalloporphyrins into a variety of material matrices, such as polymers, glasses, and Langmuir-Blodgett (LB) films. Substantial work has been done in the areas of solution and gas phase sensing, and highlights of both areas will be discussed. We will also briefly examine molecular recognition and receptor studies, as developments in these areas figure to further the development of porphyrin-based sensing materials.

1. Gas Sensors

Considering the well-understood ability of heme to bind a variety of gases, such as NO, CO_2, and O_2, porphyrins would indeed seem a suitable choice for the detection of gaseous species. During the 1990s, much work has been done involving the porphyrin-based detection of a series of gases, such as oxygen, ammonia, and chlorine. In addition, recent work has entailed utilization of metalloporphyrin arrays for the detection of organic odorants, such as amines, thiols, and phosphines. Many gas sensors take advantage of analyte binding to the porphyrin metal center, which gives a detectable optical change. Other methods, such as the use of piezoelectric substrates coated with porphyrin films, have also been utilized for gas detection.

a. Oxygen

The use of metalloporphyrin-based materials for the detection of molecular oxygen is well developed. One approach that has been employed extensively involves the well known phenomenon of quenching of metalloporphyrin phosphorescence by O_2. Due to their high phosphorescence quantum yields and short triplet lifetimes, platinum and palladium porphyrins were originally suggested as probes for oxygen by Eastwood and Gouterman.[211] The quenching of porphyrin phosphorescence is described by the Stern-Volmer relationship:

$$I_0/I = 1 + K_{sv}(pO_2)$$

where I_0 and I are the phosphorescence intensities in the absence and presence of the quencher, respectively, K_{sv} is the Stern-Volmer constant, and pO_2 is the partial pressure of O_2. Since $1/K_{sv}$ is equal to the pO_2 level at which the phosphorescence intensity is reduced by 50%, it is commonly reported as a characteristic for oxygen detectors. Clearly, K_{sv} will be highly dependent upon the oxygen permeability of the matrix in which the porphyrin is immobilized. Hence, much of the research in this area focuses on these matrices, such as polymers or sol-gel glasses, in addition to the synthesis of new porphyrins.

Okura and coworkers have utilized sol-gels to make optically transparent glasses containing Pt(OEP).[212] This approach is aimed at creating chemically inert, photostable materials which can be used in a variety of environments. As shown in Figure 125, the response is rapid, with a 5 second 90% response time (t_{90}). Reversibility was demonstrated upon exposure to 100% nitrogen followed by 100% oxygen. The sensor shows nearly linear behavior of a range from 0 to 100% oxygen concentration, but no estimate of detection limit was given. One major concern with the use of porphyrins for gas sensing is photo-bleaching. In an effort to enhance porphyrin stability toward photodegradation, Wong and coworkers have used halogenated platinum porphyrins immobilized inside silicone films as materials for oxygen sensing.[213] The porphyrins, Pt(TDCPP), Pt(TFMPP), and Pt(Br_8TMP) (where TDCPP = 5,10,15,20-tetra(2,6-dichlorophenyl)porphyrinate, TFMPP = 5,10,15,20-tetra(3,5-bis(trifluoromethyl)phenyl)porphyrinate, and Br_8TMP = 5,10,15,20-tetramesityl-β-octabromoporphyrinate), were chosen to provide enhanced stability due to their increased oxidation potentials compared to Pt(TPP). The best performance was observed for the Pt(TFMPP) film, with a ($1/K_{sv}$) value of 3.7 torr and a response time of 14 seconds. Stability studies on the porphyrin/rubber films revealed that all of the halogenated porphyrins were indeed more stable than Pt(TPP). After 48 hours of illumination, the Pt(TPP) luminescence intensity was only 43% of its original value, while (Br_8TMP)Pt remained at 93%. Another approach towards enhanced stability is the use of porphyrin ketone complexes. For instance, Hartmann and coworkers have utilized platinum(II) and palladium(II) octaethylporphyrin ketones (Figure 126) in polystyrene matrices for oxygen sensing.[214] Films of Pt(OEPK) have been reported to be ten times more stable than their Pt(OEP) counterparts to photodegradation.[215] The palladium-based sensor gave an excellent ($1/K_{sv}$) value of 0.59 torr.

[Figure 125]
[Figure 126]

Mills and coworkers have recently employed Pt(OEP) and Pd(OEP) in a variety of different encapsulating matrices for the detection of molecular oxygen.[215] Using cellulose acetate butyrate (CAB), poly(methyl methacrylate) (PMMA), and PMMA/CAB polymer blends to encapsulate the porphyrins on glass slide supports, the

researchers studied the K_{sv} and response time variation with polymer composition. They found that amounts of tributyl phosphate (TBP) plasticizer dramatically increased both the sensitivity and response times of the film. As shown in Figure 127, both the pO_2 and the t_{90} response time decrease significantly to give minimum values at about 120 parts per hundred resin (phr) of plasticizer. The $(1/K_{sv})$ value for Pd(OEP) in CAB/plasticizer was 0.24 torr, while the 90% response time was 1.4 seconds.

[Figure 127]

Impressive response times for detection of oxygen via luminescent porphyrins have been demonstrated by Callis, Gouterman, and coworkers.[216] Using special instrumentation designed to characterize coatings for video luminescent barometry (VLB), the researchers demonstrated submillisecond response times upon exposing immobilized Pt(OEP) to ambient air at pressures ranging from 0.1 to 700 torr. This type of system has been studied in an effort to provide aerodynamicists with a method for determining surface pressures during wind-tunnel tests.[217]

Reversible binding of oxygen to cobalt porphyrins forms the basis for another series of oxygen sensors. Systems involving cobalt porphyrins have employed a variety of signal transduction techniques. Work by Oblesby, Leighty, Collman et al. has utilized synthetic cobalt porphyrins for surface acoustic wave (SAW) sensing of oxygen.[218] The SAW sensor, which registers a resonance frequency decrease upon adsorption of an analyte, is coated with the porphyrin, both in the presence and absence of an imidazole or pyridine containing copolymer. Porphyrins used for the study were the cobalt(II) picket-fence porphyrin, Co(PFP),[219] and cobalt(II) picnic basket porphyrins, Co(PBP)[220] (Figure 128). The sensor response to oxygen is reversible, though some hysteresis is noted, which is due to slow diffusion of O_2 out of the polymer matrix. The picnic-basket porphyrins are particularly interesting because they allow easy tailoring of the oxygen binding constant, either by changing the central metal ion or by altering the length of the bridge or "handle". This allows for sensing over a wide range of oxygen concentrations. In related studies, Pretsch and coworkers have utilized picket fence cobalt porphyrins for optical detection of oxygen.[221] Immobilized on poly(octylmethacrylate-*co*-1-vinylimidazole) or poly(2,2,3,3,4,4,5,5-octafluoropentylmethacrylate-*co*-1-vinylimidazole) polymer membranes, the porphyrin gives a readily detectable shift in its visible absorbance spectrum upon binding of molecular oxygen. The useful range of the sensor is 1-1000 kPa oxygen partial pressure, or 0.1-100% of atmospheric pressure. Optimum response is achieved with the fluorinated membrane, at a thickness of 20 μm, which gave a 90% response time range of 5-15 seconds.

[Figure 128]

b. Other Gases

Porphyrin-based sensors have also been used for the detection of gases such as ammonia, hydrazine, and NO. Narayanaswamy and coworkers have developed optical ammonia sensing films based upon immobilized Zn(TPP) in silicone rubber.[222] Upon ligation of the metal center, the well-known phenomena of visible and/or fluorescence spectral shifts can be used to quantify exposure to the analyte. The Zn(TPP)-silicone films gave a linear range of 0-8.5 ppm NH_3 with a detection limit of 0.7 ppm. The equilibration time upon exposure was found to be 4 minutes with good reversibility of the ligation. This approach, of course, could be expanded to other amines, as well as to other ligating vapors. Ammonia detection has also been studied by Valli and coworkers, who have explored Langmuir-Blodgett films grown from a conjugated dimer of nickel(II) octaethylporphyrin.[223] (see Figure 129). The films were created by combining the dimer with arachidic acid, followed by deposition onto hydrophobic quartz substrates. Gold contacts were sputtered onto the film ends to allow for resistivity measurements as a function of vapor exposure. As seen in Figure 130, the sensor demonstrates a series of equilibria as the ammonia concentration is increased in a stepwise fashion, followed by a return to the original resistance value upon exposure to air. At 500 ppm of NH_3, the response time is 200 seconds, with a recovery time of 500 seconds. The authors postulate that the decreased resistivity upon analyte exposure results from electronic holes created in the porphyrin film upon electron transfer to ammonia molecules.

[Figure 129]
[Figure 130]

Detection of nitric oxide has become particularly important in light of its regulatory role in many physiological processes. In an example of NO detection via porphyrin-based sensors, Malinski and coworkers have used microelectrode sensors consisting of layers of a polymeric porphyrin and Nafion deposited on a thermally sharpened carbon fiber.[224] Tetrakis(3-methoxy-4-hydroxyphenyl)porphyrinatonickel(II) was polymerized onto the fiber electrochemically from a solution of 0.1 M NaOH containing the monomer. The resulting sensor operates based on the electrochemical oxidation of NO at the porphyrin-doped electrode. A 10 ms response time and a detection limit of 10 nM have been observed, and the sensor has been applied to NO analysis from single endothelial cells in the pulmonary artery as well as for NO quantitation in the blood.

c. Porphyrin Array Vapor Detectors

Array based sensing has emerged as a powerful approach to vapor detection. Combinations of chemically diverse sensing elements are capable of responding to a variety of analytes. Materials such as polymers, functionalized self-assembled monolayers, metal oxides, and dendrimers have been used in electronic devices via coupling with piezoelectric, SAW, and semiconductor transducers. In notable examples, Lewis and coworkers have utilized composites of carbon black and polymers for electronic sensing,[225] while immobilization of fluorescent dyes in polymer matrices has allowed for optical detection of non-ligating vapors by Walt et al.[226] Much of the work in this area has been driven by a desire to mimic the mammalian sense of smell, which is based upon a large (approximately 1000 members) family of receptor cells.[227] More than half of the receptors respond to any given odorant exposure,[228] and create a temporal response signature that is mapped in the olfactory bulb and interpreted by the brain.

While much work has been done for the detection of non-ligating organic odorants, detection of metal-ligating vapors via array based sensing has been less explored. Included in this class of analytes are noxious ligands such as amines, phosphines, and thiols, as well as more toxic substances, e.g., nerve toxins such as Tabun. Due to their synthetic versatility and excellent chemical and thermal stability, metalloporphyrins are a natural choice for the detection of such species. Natale and coworkers have utilized metalloporphyrin films in piezoelectric sensing arrays, where they have shown some success in detection of ligating vapors and determination of food quality.[229,230] Their approach has been to coat quartz crystalline microbalances with an array of porphyrins, consisting of Ru(TPP)(CO), Rh(TPP)Cl, Mn(TPP)Cl, Co(TPP), Sn(TPP)Cl_2, Co(TpNO_2PP), Co(Tp-OCH_3PP), and Mn-octamethylcorrole. Responses to different ligating species occur upon ligand binding, which induces mass changes detectable by the microbalances. As seen in Figure 131, the array gives high sensitivities for a series of ligating vapors, though the response is limited for alcohols and sulfur-based ligands. This type of array has been applied to the evaluation of quality of several types of foods, such as fish, meats, and wine.

[Figure 131]

Suslick et al. have recently exploited the colorimetric properties of metalloporphyrin arrays for detection of various ligating vapors.[231] Metalloporphyrin visible spectra are known to exhibit shifts in wavelength and intensity upon binding of axial ligands. These shifts produce color changes that are often quite noticeable. The color changes are dependent upon a variety of factors, but vary in large part based upon the degree of polarizability of the analyte.[232,233] Upon exposure to a given analyte, therefore, an array of metalloporphyrins is expected to give a unique color change signature. A series of metalated tetraphenylporphyrins was prepared and spotted onto a reverse phase silica gel plate to give the detector shown in Figure 132. Subtraction of scanned images taken before and after exposure to analytes gives the color change profiles shown in the figure. All of the vapors studied did indeed reveal a unique color change pattern. Particularly notable is the fact that ligands of similar functionality, such as pyridine/hexylamine, or n-tributylphosphine/triethylphosphite, are readily distinguishable. Analyte concentrations of less than 1 ppm can be detected by the array. Ongoing work with this system involves incorporation of functionalized metalloporphyrins, such as dendrimer-metalloporphyrins, which will be discussed later.

[Figure 132]

2. Sensors for Solution Species

Porphyrin-based materials have been widely applied toward the analysis of several types of solution species, including ions and organic analytes. Much of the research in these areas is based upon incorporation of

metalloporphyrins into electrode membranes, where ion-porphyrin interactions can be monitored potentiometrically, or where electrochemical reactions with analyte substrates can be mediated by the porphyrin. As with gas sensors, this is a research area where molecular recognition studies will allow for continued progress.

a. Anion Detection

Detection of anions in solution via potentiometric techniques has been widely studied. If lipophilic electrode membrane materials are employed, the selectivity of the detector is based upon the solubility of the anions in the membrane layer. This gives rise to the Hofmeister pattern, whereby lipophilic anions are preferentially incorporated into the membrane, in the order $ClO_4^- > IO_4^- > I^- > Br^- > Cl^- > HCO_3^-$.[234] Deviation from Hofmeister selectivity can be achieved by incorporating a range of compounds, including porphyrins, metallocorrins, and phthalocyanines, into the membrane. The varying affinities that anions have for the chosen macrocycle metal center can change the ion preference of the material. Porphyrins are also utilized because their synthetic versatility allows for creation of size-selective pockets about the metal center, lending additional selectivity. For instance, Meyerhoff and coworkers have examined various synthetic manganese porphyrins by incorporating them into PVC polymer membranes.[235] The porphyrins, shown in Figure 133, were chosen to give a wide range of steric access and/or hydrophobicity to the metal center anion ligation site. Table 9 lists the anion selectivity coefficients for the membranes containing these porphyrins. The tetraphenylporphyrins, (2 and 3) deviate from the Hofmeister trend due to selectivity imparted by axial binding to the manganese center. The tetrahalonaphthylporphyrins (5,6,7) are even more exclusive of perchlorate and iodate, owing to their more hindered metal centers. Porphyrins 8 and 9, meanwhile, which contain nitrogenous axial ligands, destabilize anion coordination to the metal, restoring the Hofmeister selectivity. Improved affinity for salicylate was subsequently achieved by incorporation of $Sn(TPP)Cl_2$ into the electrode membranes.[236]

[Figure 133]
[Table 9]

Zheng and coworkers have employed a similar methodology and have demonstrated that PVC membranes doped with indium tetraphenylporphyrin show high relative sensitivity to nitrite ions.[237] Manganese and indium porphyrins immobilized in silicone by Paeng et al. have been used for the potentiometric analysis of serum chloride levels.[238]

Studies of synthetic porphyrin-based anion receptors should form the basis for more effective sensors. Metallocene-substituted porphyrins examined by Beer and coworkers have proven successful in the solution phase binding of ions such as chloride, bromide, and nitrate.[239] The cobaltocenium-substituted and ferrocene-substituted porphyrins (Figure 134) bind ions in solution, as shown by ^1H NMR and electrochemical studies. The latter measurements reveal that the porphyrin and ferrocene redox potentials vary with bound ion. Studies of the various atropisomers of the ferrocene-substituted zinc porphyrin have shown interesting isomer-dependent selectivities. For example, the $\alpha,\alpha,\alpha,\beta$ isomer shows a preference for nitrate over chloride, where the other atropisomers show a preference for spherical ions such chloride and bromide. In related work, Sessler and coworkers have shown sapphyrins to be potentially useful receptors for anion sensing. These expanded species are more basic than their porphyrin counterparts, and hence readily form dicationic species in solution.[240] The positively charged dication core forms a site for anion binding. A deca-alkyl sapphyrin was originally shown to bind fluoride ion, as shown by the crystal structure in Figure 135[241] The ion is believed to be stabilized via a combination of electrostatic and hydrogen bonding interactions. In more recent studies, Sessler et al. have found that sapphyrins appended to silica gel show high affinities for phosphate and arsenate, as well as an ability to separate a wide range of anionic species when used as HPLC solid phases.[242] These types of materials may be applicable to more specific anion sensing applications.

[Figure 134]
[Figure 135]

b. Cation Detection

While detection of cations via porphyrin-based materials has been less explored than anion sensing, the ability of a porphyrin to coordinate different metals and the unique spectral signatures that result form the basis for metal ion detection. Use of free base porphyrins in polymer matrices has allowed for the detection of heavy metal ions by Ache et al.[243] Immobilization of 5,10,15,20-tetrakis(4-N-methylpyridyl)porphyrin on Nafion membranes permitted detection of cadmium and mercury in solution with detection limits of 5×10^{-8} M and 2×10^{-7} M, respectively over a 20 minute measuring period. The method is subject to interferences from other metal ions, but the researchers were able to detect several ions simultaneously using pattern recognition techniques, such as principal component analysis. Sol-gel films doped with 5,10,15,20-tetra(p-sulfonatophenyl)porphyrin have also been used by Ache and coworkers for the fluorimetric determination of mercury in solution, with a detection limit of approximately 7×10^{-9} M.[244]

Porphyrin-doped electrodes have been employed for the electrochemical and potentiometric detection of nickel(II) in aqueous solutions. Malinski and coworkers have utilized polymeric tetrakis(3-methoxy-4-hydroxyphenyl)porphyrin, H_2(TMHPP), film electrodes for nickel determination.[245] The films are grown by electrochemical deposition from a solution of 0.1 M NaOH containing 5×10^{-4} M Ni(TMHPP). The film is then demetalated in acid solution, yielding a polymer that the authors postulate to have enhanced selectivity for nickel due to its formation from the nickel monomer. Using differential pulse voltammetry to monitor the Ni(II)/Ni(III) oxidation, a detection limit of 8×10^{-8} M was obtained for a 60 second exposure to a nickel containing solution. The calibration curve shown in Figure 136 shows linear response over a range of 10^{-7} to 2×10^{-6} M. In the presence of interferences (e.g., zinc(II), cadmium(II), or copper(II)), some reduction in signal is seen; however, no ion showed redox activity in the region of detection. Gupta and coworkers have utilized H_2(TPP)and H_2(TTP) in PVC-based membranes for the potentiometric detection of nickel(II).[246] The sensor demonstrated linear response in the range of 5.6×10^{-6}-1.0×10^{-1} M, with a response time of 20 seconds. The primary observed interferences were Co^{2+} and Na^{+} ions. Quantitative determination of Ni^{2+} in chocolate samples using this detector gave good agreement with values obtained from atomic absorption spectroscopy.

[Figure 136]

c. Sensors for Organic Molecules

Many current organic molecular sensors employing metalloporphyrins are based upon the ability of the porphyrin to act as a catalyst for the reduction or oxidation of organic substrates. This concept has been used by Saini and coworkers, who have recently used porphyrin-modified electrodes for the determination of organohalide species in aqueous solution.[247] By precipitating (TPP)Co on a graphite foil working electrode, the researchers were able to induce the reduction of various organohalides, such as carbon tetrachloride, perchloroethylene, and iodobenzene. The sensor is believed to function via a porphyrin-mediated, two electron reduction pathway, shown below:

$$Co^{II}(TPP) + e^{-} \rightarrow Co^{I}(TPP)^{-}$$
$$Co^{I}(TPP)^{-} + RX \rightarrow Co^{I}(TPP)(R) + X^{-}$$
$$Co^{I}(TPP)(R) + e^{-} \rightarrow Co^{II}(TPP) + R^{-}$$

Amperometric studies, with a working potential of –500 mV, gave a detection limit of 0.75 ppm for carbon tetrachloride. The amperometric calibration curves for carbon tetrachloride and perchloroethylene are shown in Figure 137. Greatest sensitivities were seen for haloalkanes, with less sensitivity for haloalkenes or haloarenes. Interference from non-halogenated organics (e.g, ethanol, allyl alcohol, phenol) was not seen, though addition of phosphate ions gave slight decreases in response intensity. In related work, Priyantha and Weerabahu used Fe(TPP)Cl for the amperometric detection of the herbicide propanil.[248] The porphyrin was coated on a glassy carbon working electrode, which was used for the reduction of 3,4-dichloropropionanilide, the main component of the herbicide. The resulting detector provided a detection limit of 80 μM.

[Figure 137]

As alluded to earlier in this section, studies of molecular receptors figure to provide a series of new sensors, particularly for the detection of solution phase species. Towards this end, a series of porphyrin complexes and assemblies have proven successful in assessing the selective binding of organic molecules. Design of shape selective

binding pockets and hydrogen bonding arrangements have proven especially successful using macrocyclic oligosaccharides. By using porphyrins as displaceable substrates of the binding sites, analysis of relative binding of other analytes can be easily monitored through visible spectroscopy: displacement of the porphyrin from within the macrocycle produce observable spectral shifts. For instance, morphine recognition has been probed by Sanders and coworkers via the synthesis of a porphyrin-cyclocholate molecular bowl, shown in Figure 138.[249] Compared to tetrakis(3-methoxyphenyl)porphyrin, which was used as a reference compound, the bowl shows a binding constant for morphine 3.8 x 10^3 times higher, resulting from favorable hydrogen bonding interactions between the bowl and morphine molecule. The bowl also binds other amines such as codeine and pyridine, but with lower binding constants than for morphine. In similar fashion, a cyclodextrin-porphyrin assembly has been demonstrated to have high selectivity for pentachlorophenol (PCP) by Luong and coworkers.[250] Shown in Figure 139, the assembly is organized via hydrogen bonds between the carboxylic acid groups of the tetracarboxy porphyrin and hydroxy groups on the cyclodextrin. PCP is well suited for the cyclodextrin-porphyrin assembly cavity, due to its proper size, sufficient hydrophobicity, and hydroxyl group, which can hydrogen bond to the pyrrole nitrogens of the porphyrin. Visible spectroscopy studies of Soret band shifting upon binding showed that of a range of chlorinated aromatic species, only PCP and 2,3,5,6-tetrachlorophenol exhibited binding.

[Figure 138]
[Figure 139]

Shinkai and coworkers have created a unique sugar sensing system based on the cooperative interactions of two boronic acid receptor moieties.[251] The first is linked to a zinc tetraphenylporphyrin, and the second to a coordinated pyridine. Binding of saccharides to the porphyrin-pyridine complex, as shown in Figure 140, produces spectral shifts. Studies in which solid sugars were extracted into dichloromethane solutions containing the receptor were conducted, and percentage of extracted sugar was determined via circular dichroism spectroscopy. Among a series of sugars, the highest affinities were seen for D and L configurations of fructose and arabinose.

[Figure 140]

Dendrimer-porphyrins are another class of molecular receptors which have been recently demonstrated to have interesting shape-selective ligand binding capabilities by Suslick et al.[252] Linking of first- and second-generation carboxylic acid dendrons to zinc tetrakis(3,5-dihydroxyphenyl)porphyrinate and zinc tetrakis(2,6-dihydroxyphenyl)porphyrinate produced a series of dendrimer-metalloporphyrins (Figure 141). Quantitative determination of the binding constants nitrogenous bases to the zinc were made using visible spectroscopy. The meta-substituted dendrimer-porphyrins interestingly show increased affinity for the bases relative to unhindered Zn(TPP), a phenomenon due to favorable interactions between the amines and the aromatic dendrimer structure. The ortho-substituted dendrimer-porphyrins, however, showed excellent shape-selectivity, as demonstrated by the log(K_{eq}) values (Figure 142). Particularly striking for the ortho-substituted dendrimer porphyrins is the difference in binding affinity between linear and nonlinear amines, such as that between 4-phenylpyridine and quinine (K_{eq} difference > 10^5). This type of selectivity could potentially be exploited in sensors for ligating species in either solution or the gas phase.

[Figure 141]
[Figure 142]

IV. Conclusions

Because of their synthetic versatility and chemical robustness, porphyrins and metalloporphyrins are proving to be a very useful platform on which to tailor field-responsive and chemo-responsive materials. Diverse applications of porphyrins and metalloporphyrins to materials chemistry have been developed over the past decade, both for their optical properties and their applications as sensors.

Notably, porphyrins and metalloporphyrins have found applications as field-responsive materials, particularly for optoelectronic applications, including mesomorphic materials and optical-limiting coatings. Porphyrins show interesting second- and third-order NLO properties, due to their exceptionally large π-electron conjugation length. The primary attention has focused on third-order NLO properties and optical limiting materials. Improvements in the area of nonlinearity versus transparency trade-off should be possible via molecular engineering.

The molecular design of novel porphyrins possessing desired physical, optical and nonlinear optical properties for specific photonic applications remains a difficult, but often rational, challenge. Ingenuous designs and newly developed synthetic methodologies have also led to significant progress in the development of molecular optoelectronic porphyrinic materials. Long term stability against photodegradation remains an important problem to overcome, however, and may preclude effective devices for many molecular electronic applications.

The development of chemo-responsive materials based on porphyrins as highly porous, molecularly-based molecular sieves or shape-selective solid catalysts is currently under development. Porphyrins and metalloporphyrins have also been examined for a variety of sensor applications, which clearly represent an important emerging class of chemo-responsive materials. The unique spectral characteristics and synthetic versatility of porphyrins allow for a variety of sensing applications. In the case of oxygen detection via luminescent porphyrins, the sensing characteristics of the porphyrin are well established, and work on the immobilization matrix is the key to sensor performance. Other areas, such as array-based detection of organic vapors and detection of ionic species in solution, will depend upon continued development of well-designed receptors that exhibit high specificities.

V. Acknowledgments

The contributions from the Suslick research group reported herein have been supported generously by the National Institutes of Health (HL25934), the Department of Energy (DEFG0291ER45439), and the Department of Defense (DAAG55-97-1-0126). We gratefully acknowledge the early efforts by Drs. Chin-Ti Chen, Homer Chou, Christopher L. Hein, Philip A. Gorlin, and Bimal Patel in the development of this work.

VI. References

1) Suslick, K. S. *Comprehensive Supramolecular Chemistry; Bioinorganic Systems*; Elsevier: Oxford, 1996; Vol. 5.
2) Simon, J.; Bassoul, P. *Phthalocyanines: Properties and Applications*; Leznoff, C. C. and Lever, A. B. P., Ed.; VCH: New York, 1989; Vol. 2.
3) van Nostrum, C. F.; Nolte, R. J. M. *J. Chem. Soc., Chem. Commun.* **1996**, 2385.
4) Goodby, J. W.; Robinson, P. S.; Teo, B. K.; Cladis, P. E. *Mol. Cryst. Liq. Cryst.* **1980**, *56*, 303.
5) Gregg, B. A.; Fox, M. A.; Bard, A. J. *J. Amer. Chem. Soc.* **1989**, *111*, 3024.
6) Gregg, B. A.; Fox, M. A.; Bard, A. J. *J. Chem. Soc., Chem. Commun.* **1987**, 1134.
7) Schouten, P. G.; Warman, J. M.; de Haas, M. P.; Fox, M. A.; Pan, H.-L. *Nature* **1991**, *353*, 736.
8) Liu, C. Y.; Pan, H. L.; Tang, H.; Fox, M. A.; Bard, A. J. *J. Phys. Chem.* **1995**, *99*, 7632.
9) Gregg, B. A.; Fox, M. A.; Bard, A. J. *J. Phys. Chem.* **1990**, *94*, 1586.
10) Liu, C.-H.; Pan, H.-I.; Fox, M. A.; Bard, A. J. *Science* **1993**, *231*, 897.
11) Liu, C.-Y.; Pan, H. L.; Fox, M. A.; Bard, A. J. *Chem. Mater.* **1997**, *9*, 1422.
12) Doppelt, P.; Huille, S. *New J. Chem* **1990**, *14*, 607.
13) Shimizu, Y.; Ishikawa, A.; Kusabayashi, S. *Chem. Lett.* **1986**, 1041.
14) Sakaguchi, T.; Shimizu, Y.; Miya, M.; Fukumi, T.; Ohta, K.; Nagata, A. *Chem. Lett.* **1992**, 281.
15) Shimizu, Y.; Miya, M.; Nagata, A.; Ohta, K.; Matsumura, A.; Yamamoto, I.; Kusabayashi, S. *Chem. Lett.* **1991**, 25.
16) Shimizu, Y.; Miya, M.; Nagata, A. *Process for preparing ferromagnetic material*: European Patent #676775, 1995.
17) Kugimiya, S.-I.; Takemura, M. *Tetrahedron Lett.* **1990**, *31*, 3157.
18) Ohta, K.; Yamaguchi, N.; Yamamoto, I. *J. Mater. Chem.* **1998**, *8*, 2637.
19) Neumann, R.; Hugerat, M.; Michaeli, S.; Natt, A.; Bernitz, M.; Levanon, H. *Chem. Phys. Lett.* **1991**, *182*, 249.
20) Michaeli, S.; Hugerat, M.; Levanon, H.; Bernitz, M.; Natt, A.; Neumann, R. *J. Amer. Chem. Soc.* **1992**, *114*, 3612.
21) Griesar, K.; Athanassopoulou, M. A.; Bustamante, E. A. S.; Tomkowicz, Z.; Zaleski, A. J.; Haase, W. *Adv. Mater.* **1997**, *9*, 45.
22) van Nunen, J. L. M.; Folmer, B. F. B.; Nolte, R. J. M. *J. Amer. Chem. Soc.* **1997**, *119*, 283.
23) Patel, B. R.; Suslick, K. S. *J. Amer. Chem. Soc.* **1998**, *120*, 11802.
24) Gaspard, S.; Maillard, P.; Billard, J. *Mol. Cryst. Liq. Cryst.* **1985**, *123*, 369.
25) Bruce, D. W.; Dunmar, D. A.; Santa, L. S.; Wali, M. A. *J. Mater. Chem.* **1992**, *2*, 363.
26) Bruce, D. W.; Wali, M. A.; Wang, Q. M. *J. Chem. Soc., Chem. Commun.* **1994**, 2089.

27) Wang, Q. M.; Bruce, D. W. *J. Chem. Soc., Chem. Commun.* **1996**, 2505.
28) Wang, Q. M.; Bruce, D. W. *Tetrahedron Lett.* **1996**, *37*, 7641.
29) Wang, Q. M.; Bruce, D. W. *Angew. Chem. Int. Ed. Engl.* **1997**, *36*, 150.
30) Nalwa, H. S. *Nonlinear Optics of Organic Molecular and Polymeric Materials*; Nalwa, H. S. and Miyata, S., Ed.; CRC Press: Boca Raton, FL, 1997, pp 611-797.
31) Nalwa, H. S.; Watanabe, T.; Miyata, S. *Nonlinear Optics in Organic Molecular and Polymeric Materials*; Nalwa, H. S. and Miyata, S., Ed.; CRC Press: Boca Raton, FL, 1997, pp 89-350.
32) Nalwa, H. S. *Handbook of Organic Conductive Molecules and Polymers*; Nalwa, H. S., Ed.; John Wiley & Sons: Chichester, 1997, pp 261-363.
33) Nalwa, H. S. *Handbook of Organic Conductive Molecules and Polymers*; John Wiley & Sons: Chichester, 1997; Vol. 1-4.
34) Nalwa, H. S.; Shirk, J. S. *Phthalocyanines: Properties and Aplications*; Leznoff, C. C. and Lever, A. B. P., Ed., 1996; Vol. 4, pp 79-118.
35) Nalwa, H. S. *Adv. Mater.* **1993**, *5*, 341.
36) Nalwa, H. S. *Appl. Organometal. Chem.* **1991**, *5*, 349.
37) Chemla, D. S.; Zyss, J. *Nonlinear Optical Properties of Organic Molecules and Crystals*; Academic Press: Orlando, 1987.
38) Suslick, K. S.; Chen, C. T.; Meredith, G. R.; Cheng, L. T. *J. Am. Chem. Soc.* **1992**, *114*, 6928-30.
39) Chou, H.; Chem, C.-T.; Stork, K. F.; Bohn, P. W.; Suslick, K. S. *J. Phys. Chem.* **1994**, *98*, 383.
40) Sen, A.; Ray, P. C.; Das, P. K.; Krishnan, V. J. *J. Phys. Chem.* **1996**, *100*, 19611.
41) Sen, A.; Krishnan, V. *J. Chem. Soc., Faraday Trans.* **1997**, *93*, 4281.
42) Priyadarshy, S.; Therien, M. J.; Beratan, D. N. *J. Am. Chem. Soc.* **1996**, *118*, 1504.
43) LeCoers, S. M.; Guan, H.-W.; Dimagno, S. G.; Wang, C. H.; Therien, M. J. *J. Am. Chem. Soc.* **1996**, *118*, 1497.
44) Karki, L.; Vance, F. W.; Hupp, J. T.; LeCoers, S. M.; Therien, M. J. *J. Am. Chem. Soc.* **1998**, *120*, 2606.
45) Yeung, M.; Ng, A. C. H.; Drew, M. G. B.; Vorpagel, E.; Breitung, E. M.; McMahon, R. J.; Ng, D. K. P. *J. Org. Chem.* **1998**, *63*, 7143.
46) Albert, I. D. L.; Marks, T. J.; Ratner, M. A. *Chem. Mater.* **1998**, *10*, 753.
47) Peng, Z.; Bao, Z.; Yu, L. *J. Am. Chem. Soc.* **1994**, *116*, 6003.
48) Peng, Z.; Gharavi, A.; Yu, L. *Polym. Preprints* **1995**, *36*, 41.
49) Li, D.; Swanson, B.; Robinson, J. M.; Hoffbauer, M. A. *J. Am. Chem. Soc.* **1993**, *115*, 6975.
50) Meloney, C.; Byrne, H.; Dennis, W. H.; Blau, W.; Kelly, J. M. *Chem. Phys.* **1988**, *121*, 21.
51) Sakaguchi, T.; Shimizu, Y.; Miya, M.; Fukumi, T.; Ohta, K.; Nagata, A. *Chem. Lett.* **1992**, 281.
52) Rao, D. V. G. L. N.; Arando, F. J.; Roach, J. F.; Remy, D. E. *Appl. Phys. Lett.* **1991**, *58*, 1241.
53) Guha, S.; Kang, K.; Porter, P.; Roach, J. E.; Remy, D. E.; Arando, F. J.; Rao, D. V. G. L. N. *Opt. Lett.* **1992**, *17*, 264.
54) Hosada, M.; Wada, T.; Garito, A. F.; Sasabe, H. *Japan. J. Appl. Phys.* **1992**, *31*, L249.
55) Norwood, R. A.; Sounik, J. R. *Appl. Phys. Lett.* **1992**, *60*, 295.
56) Anderson, H. L.; Martin, S. J.; Dradley, D. D. C. *Angnew. Chem. Int. Ed. Engl.* **1994**, *33*, 655.
57) Bao, Z.; Yu, L. *Proc. ACS Mtg. Polym. Mater. Sci. (PMSE)* **1994**, *71*, 781.
58) Kandasamy, K.; Shetty, S. J.; Puntambekar, P. N.; Srivastava, T. S.; Kundu, T.; Singh, B. P. *J. Porph. Phthalocyanines* **1998**, *2*, (In Press).
59) Kumar, G. R.; Ravikanth, M.; Banerjee, S.; Sevian, A. *Opt. Comm.* **1997**, *144*, 245.
60) Kafafi, Z. H.; Flom, S. R.; Sarkas, H. W.; Pong, R. G. S.; Merritt, C. D.; Bartoli, F. J. *SPIE Proc.* **1994**, *2284*, 134.
61) Flom, S. R.; Pong, R. G. S.; Bartoli, F. J.; Kafafi, Z. H. *Nonlin. Opt.* **1995**, *10*, 183.
62) Kajzar, F.; Shudo, Y. O.; Meritt, C.; Kafafi, Z. *Synth. Metals* **1998**, *94*, 91.
63) Sinha, A.; Bihari, B.; Mandal, K.; Chen, L. *Macromolecules* **1995**, *28*, 5681.
64) Tutt, L. W.; Kost, A. *Nature* **1992**, *356*, 225.
65) Perry, J. W. *Nonlinear Optics of Organic Molecules and Polymers*; Nalwa, H. S., Ed.; CRC Press: Boca Raton, FL, 1997, pp 813-840.
66) Blau, W.; Byrne, H.; Dennis, W. M.; Kelly, J. M. *Opt. Comm.* **1985**, *56*, 25.
67) Fei, H. S.; Han, L.; Ai, X. C.; Yin, R.; Shen, J. C. *J. Chin. Sci. Bull.* **1992**, *37*, 298.
68) Shi, J.; Yang, M.; Wang, Y.; Zhang, L.; Li, C. *Appl. Phys. Lett.* **1994**, *64*, 3083.
69) Shi, J.; Yang, M.; Wang, Y.; Zhang, L.; Li, C.; Wang, D.; Dong, S.; Sun, W. *Opt. Comm.* **1994**, *109*, 487.

70) Su, W.; Cooper, T. M. *Chem. Mater.* **1998**, *10*, 1212.
71) Robison, G. W. *Brookhaven Symp. Biol.* **1967**, *19*, 16.
72) Pearlstein, R. H. *New Compr. Biochem.* **1987**, *15*, 299.
73) Fleming, G. R.; Martin, J.-L.; Breton, J. *Nature* **1988**, *333*, 190.
74) Paddock, M. L.; Rongey, S. H.; Feher, G.; Okamura, M. Y. *Proc. Natl. Acad. Sci. U.S.A.* **1989**, *86*.
75) Feher, G.; Allen, J. P.; Okamura, M. Y.; Rees, D. C. *Nature* **1989**, *339*, 111.
76) Holten, D.; Kirmarier, C. *Photosynth.* **1987**, *13*, 225.
77) Girolami, G. S.; Hein, C. L.; Suslick, K. S. *Angew. Chem. Intl. Ed.* **1996**, *35*, 1223-1225.
78) Kong, J. L.; Loach, P. A. *Frontiers Biol. Energ.* **1978**, *I*, 73-82.
79) Kong, J. L.; Loach, P. A. *J. Heterocyclic Chem.* **1980**, *17*, 737.
80) Tabushi, I.; Koga, N.; Yanagita, M. *Tetrahedron Lett.* **1979**, 257.
81) Wasielewski, M. R. *Chem. Rev.* **1992**, *92*, 435.
82) Moore, T. A.; Gust, D.; Mathis, P.; Mialocq, J. C.; Chachaty, C.; Bensasson, R. V.; Land, E. J.; Doisi, D.; Liddell, P. A.; Lehman, W. R.; Nemeth, G. A.; Moore, A. L. *Nature* **1984**, *307*, 630.
83) Gust, D.; Moore, T. A.; Liddell, P. A.; Nemeth, G. A.; Makings, L. R.; Moore, A. L.; Barrett, D.; Pessiki, P. J.; Bensasson, R. V.; Rougee, M.; Chachaty, C.; De Schryver, F. C.; Van der Auweraer, M.; Holzwarth, A. R.; Connolly, J. S. *J. Am. Chem. Soc.* **1987**, *109*, 846.
84) Gust, D.; Moore, T. A.; Moore, A. L.; Barrett, D.; Harding, L. O.; Makings, L. R.; Liddell, P. A.; De Schryver, F. C.; Van der Auweraer, M.; Bensasson, R.; Raugee, M. *J. Am. Chem. Soc.* **1988**, *110*, 321.
85) Gust, D.; Moore, T. A.; Moore, A. L.; Makings, L. R.; Seely, G. R.; Ma, X.; Trier, T. T.; Gao, F. *J. Am. Chem. Soc.* **1988**, *110*, 7567.
86) Gust, D.; Moore, T. A.; Moore, A. L.; Seely, G.; Liddell, P.; Barrett, D.; Harding, L. O.; Ma, X.; Lee, S. J.; Gao, F. *Tetrahedron* **1989**, *45*, 4867.
87) Osuka, A.; Nagata, T.; Maruyama, K. *Chem. Lett.* **1991**, 481.
88) Osuka, A.; Maruyama, K.; Magata, N.; Asahi, T.; Yamazaki, I.; Tamai, N.; Nishimura, Y. *Chem. Phys. Lett.* **1991**, *181*, 413.
89) Osuka, A.; Nakajima, S.; Maruyama, K.; Magata, N.; Asahi, T.; Yamazaki, I.; Y., N.; Ohno, T.; Nozaki, K. *J. Am. Chem. Soc.* **1993**, *115*, 4577.
90) Osuka, A.; Nakajima, S.; Okada, T.; Taniguchi, S.; Nozakl, K.; Ohno, T.; Yamazaki, I.; Nishimura, Y.; Magata, N. *Angew. Chem. Int. Ed. Engl.* **1996**, *35*, 92.
91) Liddell, P. A.; Kuciauskas, D.; Sumida, J. P.; Nash, B.; Nguyen, D.; Moore, A. L.; Moore, T. A.; Gust, D. *J. Am. Chem. Soc.* **1997**, *119*, 1400.
92) Girolami, G. S.; Gorlin, P. A.; Suslick, K. S. *Inorg. Chem.* **1994**, *33*, 626-627.
93) O'Neil, M. P.; Niemczyk, M. P.; Svec, W. A.; Gosztola, D.; Gaines, G. L.; Wasielewski, M. R. *Science* **1992**, *257*, 63.
94) Debreczeny, M. P.; Svec, W. A.; Wasielewski, M. R. *Science* **1996**, *274*, 584.
95) Wagner, R.; Lindsey, J. S. *J. Am. Chem. Soc.* **1994**, *116*, 9759.
96) Crossley, M.; Burn, P. L. *J. Chem. Soc., Chem. Commun.* **1991**, 1569.
97) Wagner, R. W.; Lindsey, J. S.; Seth, J.; Palaniappan, V.; Bocian, D. F. *J. Am. Chem. Soc.* **1996**, *118*, 3996.
98) Segawa, H.; Nakayama, N.; Shimidzu, T. *J. Chem. Soc., Chem. Commun.* **1992**, 784.
99) Segawa, H.; Kunimoto, K.; Susumu, K.; Taniguchi, M.; Shimidzu, T. *J. Am. Chem. Soc.* **1994**, *116*, 11193.
100) Shimidzu, T. *Pure &Appl. Chem.* **1995**, *67*, 2039.
101) Shimidzu, T. ; Jehneke, S. A. W., Kenneth J., Ed.; Am. Chem. Soc.: Washington, D.C., 1997, pp 460-474.
102) Mauzerall, D. C.; Greenbaum, N. L. *Biochim. Biophys. Acta* **1989**, *974*, 119.
103) Hunter, C. N.; Van Grondelle, R.; Olsen, J. D. *Trends Biochim, Sci.* **1989**, *14*, 72.
104) McDermott, G.; Prince, S. M.; Freer, A. A.; Hawethornthwaite-Lawless, A. M.; Papiz, M. Z.; Cogdell, R. J.; Isaacs, N. W. *Nature* **1995**, *374*, 517.
105) Karrasch, S.; Bullough, P. A.; Ghosh, R. *EMBO J.* **1995**, *14*, 631.
106) Nagata, T.; Osuka, A.; Maruyama, K. *J. Am. Chem. Soc.* **1990**, *112*, 3055.
107) Osuka, A.; Tanabe, N.; Nakajima, S.; Maruyama, K. *J. Chem. Soc., Perkin. Trans. 2* **1995**, 199.
108) Osuka, A.; Shimidzu, H. *Angew. Chem. Int. Ed. Engl.* **1997**, *36*, 135.
109) Nakano, A.; Osuka, A.; Yamazaki, I.; Yamazaki, T.; Nishimura, Y. *Angew. Chem. Int. Ed. Engl.* **1998**, *37*, 3023.
110) Prathapan, S.; Johnson, T.; Lindsey, J. *J. Am. Chem. Soc.* **1993**, *115*, 7519.

111) Seth, J.; Palaniappan, V.; Johnson, T.; Prathapan, S.; Lindsey, J. S.; Bocian, D. F. *J. Am. Chem. Soc.* **1994**, *116*, 10578.
112) Li, F.; Yang, S. I.; Ciringh, Y.; Seth, J.; Martin, C. H.; Singh, D. L.; Kim, D.; Birgh, R. R.; Bocian, D. F.; Holten, D.; Lindsey, J. S. *J. Am. Chem. Soc.* **1998**, *120*, 10001.
113) Drain, C. M.; Lehn, J.-M. *J. Chem. Soc., Chem. Commun.* **1994**, 2313.
Drain, C.M.; Nifiatis, F.; Vasenko, A.; Batteas, J.D. *Angew. Chem. Int. Ed.* **1998,** *37*, 2344.
114) Yuan, H.; Thomas, L.; Woo, L. K. *Inorg. Chem.* **1996**, *35*, 2808.
115) Sasaki, Y.; Imamura, T.; Kariya, N. *Inorg. Chem.* **1997**, *36*, 833.
116) Alessio, E.; Macchi, M.; Heath, S.; Marzilli, L. G. *J. Chem. Soc., Chem. Commun.* **1996**, 1411.
117) Funatsu, K.; Kimura, A.; Imamura, T.; Ichimura, A.; Sasaki, Y. *Inorg. Chem.* **1997**, *36*, 1625.
118) Woiaczynski, J.; Latos-Grazynski, K. *Inorg. Chem.* **1996**, *35*, 4812.
119) Chernook, A. V.; Rempel, U.; von Broczyskowski, C.; Shulga, A. M.; Zenkevich, E. I. *Chem. Phys. Lett.* **1996**, *254*, 229.
120) Abrahams, B. F.; Hoskins, B. F.; Michail, D. M.; Robson, R. *Nature* **1994**, *369*, 727.
121) Dagani, D. *Chem & Eng. News* **1998**, 35.
122) Lin, V. S.; DiMagno, S. G.; Therien, M. J. *Science* **1994**, *264*, 1105.
123) Suslick, K. S.; Van Deusen-Jeffries, S. *Biomimetic Shape-Selective Oxidations*; Suslick, K. S., Ed.; Elsevier Science, Ltd.: Oxford, 1996; Vol. 5, pp 733-756.
124) Meunier, B. *Metalloporphyrins Catalyzed Oxidations*; Monanari, F. and Casella, L., Ed.; Kluwer Academic Publishers: Boston, 1994, pp 1-47.
125) Byrn, M. P.; Curtis, C. J.; Khan, S. I.; Sawin, P. A.; Tsurumi, R.; Strouse, C. E. *J. Amer. Chem. Soc.* **1990**, *112*, 1865.
126) Byrn, M. P.; Curtis, C. J.; Goldberg, I.; Hsiou, Y.; Khan, S. I.; Sawin, P. A.; Tendick, S. K.; Strouse, C. E. *J. Amer. Chem. Soc.* **1991**, *113*, 6549.
127) Byrn, M. P.; Curtis, C. J.; Hsiou, Y.; Khan, S. I.; Sawin, P. A.; Tendick, S. K.; Terzis, A.; Strouse, C. E. *J. Amer. Chem. Soc.* **1993**, *115*, 9480.
128) Byrn, M. P.; Curtis, C. J.; Goldberg, I.; Huang, T.; Hsiou, Y.; Khan, S. I.; Sawin, P. A.; Tendick, S. K.; Terzis, A.; Strouse, C. E. *Mol. Cryst. Lig. Cryst.* **1992**, *211*, 135.
129) Krupitsky, H.; Stein, Z.; Goldberg, I. *J. Incl. Phenom. Mol. Recog. Chem.* **1995**, *20*, 211.
130) Goldberg, I.; Krupitsky, H.; Stein, Z.; Hsiou, Y.; Strouse, C. E. *Supramol. Chem.* **1995**, *4*, 203.
131) Dastidar, P.; Krupitsky, H.; Stein, Z.; Goldberg, I. *J. Incl. Phenom. Mol. Recog. Chem.* **1996**, *24*, 241.
132) Philip, D.; Stoddart, J. F. *Angew. Chem., Int. Ed. Engl.* **1996**, *35*, 1154.
133) Kumar, R. K.; Balasubramanian, S.; Goldberg, I. *Inorg. Chem.* **1998**, *37*, 541.
134) Dastidar, P.; Stein, Z.; Goldberg, I.; Strouse, C. E. *Supramol. Chem.* **1996**, *7*, 257.
135) Bhyrappa, P.; Wilson, S. R.; Suslick, K. S. *J. Amer. Chem. Soc.* **1997**, *119*, 8492.
136) Bhyrappa, P.; Suslick, K. S. *Supramolec. Chem.* **1998**, *9*, 169-174.
137) Robson, R. *Infinite Frameworks*; MacNicol, D. D., Toda, F. and Bishop, R., Ed.; Pergamon: New York, 1996; Vol. 6, pp 733-759.
138) Bowes, C. L.; Ozin, G. A. *Adv. Mater.* **1996**, *8*, 13-28.
139) Yaghi, O. M.; Li, H.; Davis, C.; Richardson, D.; Groy, T. L. *Acc. Chem. Res.* **1998**, *1998*, 474.
140) Krupitsky, H.; Stein, Z.; Goldberg, I. *J. Incl. Phenom. Mol. Recog. Chem.* **1994**, *18*, 177.
141) Abrahams, B. F.; Hoskins, B. F.; Robsin, R. *J. Amer. Chem. Soc.* **1991**, *113*, 3606.
142) Abrahams, B. F.; Hoskins, B. F.; Michall, D. M.; Robson, R. *Nature* **1994**, *369*, 727.
143) Patel, B. *Porphyrin Liquid Crystals*; University of Illinois at Urbana-Champaign: Urbana, 1996.
144) Kosal, M. E.; Suslick, K. S. *unpublished results* .
145) Chou, J. H.; Kosal, M. E.; Suslick, K. S. *unpublished results* .
146) Bedioui, F. *Coord. Chem. Rev.* **1995**, *144*, 39.
147) de Vismes, B.; Bedioui, F.; Devynck, J.; Bied-Charreton, C. *J. Electroanal. Chem.* **1985**, *187*, 197.
148) de Vismes, B.; Bedioui, F.; Devynck, J.; Bied-Charreton, C.; Perree-Fauvet, M. *New J. Chem.* **1986**, *10*, 81.
149) Gaillon, L.; Bedioui, F.; Devynck, J. *J. Mater. Chem.* **1994**, *4*, 1215.
150) Li, Z.; Wang, C. M.; Persaud, L.; Mallouk, T. E. *J. Phys. Chem.* **1988**, *92*, 2592.
151) Persad, L.; Bard, A. J.; Canpion, A.; Fox, M. A.; Mallouk, T. E.; Webber, S. E.; White, J. M. *J. Amer. Chem. Soc.* **1987**, *109*, 7309.
152) Le Guern, F.; Bied-Charreton, C.; Faure, J. *Bull. Soc. Chim. Fr.* **1993**, *130*, 753.

153) Chen, S.-M. *J. Mol. Cat. A.* **1996**, *112*, 277.
154) Guerra, S. V.; Xavier, C. R.; Nakagaki, S.; Kubota, L. T. *Electroanal.* **1998**, *10*, 462.
155) Nakamura, M.; Tatsumi, T.; Tominaga, H. *Bull. Chem. Soc. Jpn.* **1990**, *63*, 3334.
156) Li, G. Q.; Govind, R. *Inorg. Chim. Acta.* **1994**, *217*, 135.
157) Liu, C.-J.; Li, S.-G.; Pang, W. Q.; Che, C. M. *Chem. Commun.* **1997**, 65.
158) Sung-Suh, H. M.; Luan, Z.; Kevan, L. *J. Phys. Chem.* **1997**, *101*, 10455.
159) Zhan, B.-Z.; Li, X. Y. *Chem. Comm.* **1998**, 349.
160) Holland, B. T.; Walkup, C.; Stein, A. *J. Phys. Chem. B* **1998**, *102*, 4301.
161) Anson, F. C.; Ni, C.; Saveant, J. *J. Am. Chem. Soc.* **1985**, *107*, 3442.
162) Battioni, P.; Lallier, J. P.; Barloy, L.; Mansuy, D. *J. Chem. Soc., Chem. Commun.* **1989**, 1149.
163) Persaud, L.; Bard, A. J.; Campion, A.; Fox, M. A.; Mallouk, T. E.; Webber, S. E.; White, J. M. *J. Am. Chem. Soc.* **1987**, *109*, 7309.
164) Li, Z.; Wang, C. M.; Persaud, L.; Mallouk, T. E. *J. Phys. Chem.* **1988**, *92*, 2592.
165) DeVismes, B.; Bedioui, F.; Devynck, J.; Bied-Charreton, C.; Peree-Fauvet, M. *Nouv. J. Chim.* **1986**, *10*, 81.
166) Kosiur, D. R. *Clays Clay Minerals* **1977**, 365.
167) Kameyama, H.; Suzuki, H.; Amano, A. *Chem. Lett.* **1988**, 1117.
168) Barloy, L.; Battioni, P.; Mansuy, D. *J. Chem. Soc., Chem. Commun.* **1990**, 1365.
169) Carrado, K. A.; Wasserman, S. R. *Chem. Mater.* **1996**, *8*, 219.
170) Carrado, K. A.; Thiyagarajan, P.; Winans, R. E.; Botto, R. E. *Inorg. Chem.* **1991**, *30*, 794.
171) Park, I. Y.; Kuroda, K.; Kato, C. *Chem. Lett.* **1989**, 2057.
172) Barloy, L.; Lallier, J. P.; Battioni, P.; Mansuy, D.; Piffard, Y.; Tournoux, M.; Vali, J. B.; Jones, W. *New J. Chem.* **1992**, *16*, 71.
173) Bonnet, S.; Forano, C.; De Roy, A.; Besse, J. P. *Chem. Mater.* **1996**, *8*, 1962.
174) Kim, R. M.; Pillion, J. E.; Burwell, D. A.; Groves, J. T.; Thompson, M. E. *Inorg. Chem.* **1993**, *32*, 4509.
175) Borg, R. J.; Diences, G. J. *The Physical Chemistry of Solids*; Academic Press: New York, 1992.
176) Beno, M. A.; Soderholm, D. W.; Capone II, D. W.; Hinks, D. G.; Jorgensen, J. D.; Segre, C. U.; Zhang, K. *Appl. Phys. Lett.* **1987**, *51*, 57.
177) Sleight, A. W. *Science* **1987**, *242*, 1519.
178) Steinflink, H.; Sinnea, J. S.; Sui, T. Z.; Hsu, H. M.; Goodenough, J. B. *J. Am. Chem. Soc.* **1987**, *109*, 3348.
179) Crossley, M. J.; Burn, P. L. *J. Chem. Soc., Chem. Commun.* **1991**, 1569-1571.
180) Chen, C.-T.; Suslick, K. S. *Coord. Chem. Rev.* **1993**, *128*, 293-322.
181) Hanack, M.; Deger, S.; Lange, A. *Coord. Chem. Rev.* **1988**, *83*.
182) Collman, J. P.; McDevitt, J. T.; Yee, G. T.; Leidner, C. R.; McCullough, L. G.; Little, W. A.; Torrance, J. B. *Proc. Natl. Acad. Sci. U.S.A.* **1986**, *83*, 4581.
183) Buchler, J. W. ; Smith, K. M., Ed.; Elsevier: Amsterdam, 1976.
184) Collman, J. P.; McDevitt, J. T.; Yee, G. T.; Zisk, M. B.; Torrance, J. B.; Little, W. A. *Synth. Met.* **1986**, *15*, 129.
185) Collman, J. P.; McDevitt, J. T.; Leidner, C. R.; Yee, G. T.; Torrance, J. B.; Little, W. A. *J. Am. Chem. Soc.* **1987**, *109*, 4606.
186) Kubel, F.; Strahle, J. *A. Naturforsch. Teil B* **1981**, *36*, 441.
187) Bao, Z.; Chen, Y.; Yu, L. *Macromolecules* **1994**, *27*, 4629-4631.
188) Jiang, B.; Szu-Wei, Y.; Jones Jr., W. E. *Chem. Mater.* **1997**, *9*, 2031-2034.
189) Jiang, B.; Yang, S. W.; Bailey, S. L.; Hermans, L. G.; Niver, R. A.; Bolcar, M. A.; Jones, J., W. E. *Coord. Chem. Rev.* **1998**, *171*, 365-386.
190) Segawa, H.; Nakayama, N.; Shimidzu, T. *J. Chem. Soc. , Chem. Commun.* **1992**, 784-786.
191) Segawa, H.; Kunimoto, K.; Susumu, K.; Taniguchi, M.; Shimidzu, T. *J. Am. Chem. Soc.* **1994**, *116*, 11193-11194.
192) Burfoot, J. C. *Ferroelectrics*; Van Nostrand: London, 1967.
193) Mitsui, T.; Tatsuzaki, I.; Nakamura, E. *An Introduction to the Physics of Ferroelectrics*; Gordon and Breach: New York, 1976.
194) West, A. R. *Solid State Chemistry and its Applications*; Wiley: New York, 1984.
195) Goodby, J. W.; Leslie, T. M. *Mol. Cryst. Liq. Cryst.* **1984**, *110*, 175.
196) Walba, D. M.; Slater, S. C.; Thurmes, W. N.; Clark, N. A.; Handschy, M. A.; Supon, F. *J. Am. Chem. Soc.* **1986**, *108*, 5210.

197) Wahl, J.; Matuszcyk, T.; Lagerwall, S. T. *Mol. Cryst. Liq. Cryst.* **1987**, *146*, 143.
198) Walba, D. M.; Razavi, H. A.; Clark, N. A.; Parmar, D. S. *J. Am. Chem. Soc.* **1988**, *110*, 5686.
199) Suslick, K. S.; Chen, C.-T. *Polym. Mater. Sci. Eng.* **1990**, *63*, 272.
200) Chen, C.-T. *Porphyrins and Metalloporphyrins as Field Responsive Materials*; University of Illinois at Urbana-Champaign: Urbana, IL, 1992.
201) Adams, K.; Rasmussen, P. G.; Scheidt, W. R.; Hatono, K. *Inorg. Chem.* **1979**, *18*, 1892.
202) Scheidt, W. R.; Lee, Y. A.; Geiger, D. K.; Taylor, K.; Hatono, K. *J. Am. Chem. Soc.* **1982**, *104*, 3367.
203) Collman, J. P.; Brauman, J. I.; Rose, E.; Suslick, K. S. *Proc. Natl. Acad. Sci. U.S.A.* **1978**, *57*, 1052.
204) Woolery, G. M.; Walter, A.; Suslick, K. S.; Powers, J.; Spiro, T. G. *J. Am. Chem. Soc.* **1985**, *107*, 2370.
205) Caspari, M. E.; Merz, W. J. *Phys. Rev.* **1950**, *80*, 1082.
206) Blinov, L. M.; Kirichenko, N. A. *Sov. Phys. Solid State* **1970**, *12*, 1246.
207) Frauenheim, T.; Hamann, C.; Muller, M. *Phys. Status Solidi A* **1984**, *86*, 736.
208) Kaenzig, W. *Helv. Phys. Acta* **1951**, *24*, 175.
209) Frazer, B. C.; Danner, H. R.; Pepinsk, R. *Phys. Rev.* **1955**, *100*, 745.
210) Wells, A. F. *Structural Inorganic Chemistry*; Clarendon Press: Oxford, 1984.
211) Eastwood, D.; Gouterman, M. *J. Mol. Spec.* **1970**, *35*, 359.
212) Lee, S.; Okura, I. *Analyst* **1997**, *122*, 81-84.
213) Weekey, W.; Kwok-Yin, W.; Xiang-Ming, L.; Yiu-Bong, L.; Chi-Shing, C.; Chan, K. *J. Mater. Chem.* **1993**, *3*, 1031-1035.
214) Hartmann, P.; Wolfgang, T. *Anal. Chem.* **1996**, *68*, 2615-2620.
215) Mills, A.; Lepre, A. *Anal. Chem.* **1997**, *69*, 4653-4659.
216) Baron, A. E.; Danielson, J. D. S.; Gouterman, M.; Wan, J. R.; Callis, J. B. *Rev. Sci. Instrum.* **1993**, *64*, 3394-3402.
217) Kavandi, J.; Callis, J.; Gouterman, M.; Khalil, G.; Wright, D.; Green, E.; Burns, D.; McLachlan, B. *Rev. Sci. Instrum.* **1990**, *61*, 3340-3347.
218) Oglesby, D. M.; Upchurch, B. T.; Leighty, B. D.; Collman, J. P.; Zhang, X.; Herrmann, P. C. *Anal. Chem.* **1994**, *66*, 2745-2751.
219) Collman, J. P.; Gagne, R. R.; Reed, C. A.; Halbert, T. R.; Lang, G.; Robinson, W. T. *J. Am. Chem. Soc.* **1975**, *97*, 1427-1439.
220) Collman, J. P.; Brauman, J. I.; Fitzgerald, J. P.; Hampton, P. D.; Naruta, Y.; Sparapany, J. W.; Ibers, J. A. *J. Am. Chem. Soc.* **1988**, *110*, 3477-3486.
221) Roosli, S.; Presch, E.; Morf, W. E.; Tsuchida, E.; Nishide, H. *Anal. Chim. Acta* **1997**, *338*, 119-125.
222) Vaughan, A. A.; Baron, M. G.; Narayanaswamy, R. *Analytical Communications* **1996**, *33*, 393-396.
223) Arnold, D. P.; Manno, D.; Micocci, G.; Serra, A.; Tepore, A.; Valli, L. *Langmuir* **1997**, *13*, 5951-5956.
224) Malinski, T.; Taha, Z. *Nature* **1992**, *358*, 676-678.
225) Lonergan, M. C.; Severin, E. J.; Doleman, B. J.; Beaber, S. A.; Grubbs, R. H.; Lewis, N. S. *Chem. Mater.* **1996**, *8*, 2298-2312.
226) Dickinson, T. A.; White, J.; Kauer, J. S.; Walt, D. R. *Nature* **1996**, *382*, 697-700.
227) Axel, R. *Scientific American* **1995**, 154-159.
228) Kauer, J. S. *Trends Neurosci.* **1991**, *14*, 79-85.
229) Natale, C. D.; Macagnano, A.; Davide, F.; D'Amico, A.; Paolesse, R.; Boschi, T.; Faccio, M.; Ferri, G. *Sensors and Actuators B* **1997**, *44*, 521-526.
230) Natale, C. D.; Macagnano, A.; Repole, G.; Saggio, G.; D'Amico, A.; Paolesse, R.; Boschi, T. *Materials Science and Engineering C* **1998**, *5*, 209-215.
231) Rakow, N.; Suslick, K. S. *Unpublished Results* **1998**.
232) Gouterman, M.; Schwarz, F. P.; Smith, P. D. *The Journal of Chemical Physics* **1973**, *59*, 676-690.
233) Nappa, M.; Valentine, J. S. *J. Am. Chem. Soc.* **1978**, *100*, 5075-5080.
234) Hofmeister, F. *Arch. Exp. Pathol. Parmakol.* **1888**, *24*, 247-260.
235) Chaniotakis, N. A.; Chasser, A. M.; Meyerhoff, M. E. *Anal. Chem.* **1988**, *60*, 185-188.
236) Chaniotakis, N. A.; Park, S. B.; Meyerhoff, M. E. *Anal. Chem.* **1989**, *61*, 566-570.
237) Gao, D.; Li, J.; Ru-Qin, Y.; Zheng, G. *Anal. Chem.* **1994**, *66*, 2245-2249.
238) Yoon, I. J.; Shin, J. H.; Paeng, I. R.; Nam, H.; Cha, G. S.; Paeng, K. *Anal. Chim. Acta* **1998**, *367*, 175-181.
239) Beer, P. D.; Drew, M. G. B.; Hesek, D.; Jagessar, R. *J. Chem. Soc. Chem. Comm.* **1995**, 1187-1189.
240) Kral, V.; Furuta, H.; Shreder, K.; Lynch, V.; Sessler, J. L. *J. Am. Chem. Soc.* **1996**, *118*, 1595-1607.

241) Sessler, J. L.; Cyr, M. J.; Lynch, V.; McGhee, E.; Ibers, J. A. *J. Am. Chem. Soc.* **1990**, *112*, 2810-2813.
242) Sessler, J. L.; Kral, V.; Genge, J. W.; Thomas, R. E.; Iverson, B. L. *Anal. Chem.* **1998**, *70*, 2516-2522.
243) Morales-Bahnik, A.; Czolk, R.; Reichert, J.; Ache, H. J. *Sensors and Actuators B* **1993**, *13-14*, 424-426.
244) Plaschke, M.; Czolk, R.; Ache, H. J. *Anal. Chim. Acta* **1995**, *304*, 107-113.
245) Malinski, T.; Ciszewski, A.; Fish, J. R.; Czuchajowski, L. *Anal. Chem.* **1990**, *62*, 909-914.
246) Gupta, V. K.; Ajay, K. J.; Singh, L. P.; Khurana, U. *Anal. Chim. Acta* **1997**, *355*, 33-41.
247) Dobson, D. J.; Saini, S. *Anal. Chem.* **1997**, *69*, 3532-3538.
248) Priyantha, N.; Weerabahu, D. *Anal. Chim. Acta* **1996**, *320*, 263-268.
249) Bonar-Law, R. P.; Mackay, L. G.; Sanders, J. K. M. *J. Chem. Soc. Chem. Comm.* **1993**, 456-458.
250) Zhao, S.; Luong, J. H. T. *J. Chem. Soc., Chem. Comm.* **1995**, 663-664.
251) Takeuchi, M.; Kijima, H.; Hamachi, I.; Shinkai, S. *Bull. Chem. Soc. Jpn.* **1997**, *70*, 699-705.
252) Bhyrappa, P.; Vaijayanthimala, G.; Suslick, K. S. *Accepted as Communication to the Editor, J. Am. Chem. Soc.* **1999**.
253) Kandasamy, K.; Shetty, S. J.; Puntambekar, P. N.; Srivastava, T. S. K., T.; Singh, B. P. *J. Chem. Soc., Chem. Commun.* **1997**, 1159.

Table 1. Abbreviations

$(DEtyP)_n$	5,10,15,20-diethylnylporphyrin polymer
$(O_2C_nH_{2n+1})OEP$	2,3,7,8,12,13,17,18-octakis(β-*n*-alkylester)ethylporphyrinate
$(OC_nH_{2n+1})DPP$	5,15-bis(4-*n*-alkoxyphenyl)porphyrinate
$(OC_nH_{2n+1})OECNP$	2,3,7,8,12,13,17,18-octakis(β-*n*-alkoxy)ethyl-5-cyanoporphyrinate
$(OC_nH_{2n+1})OENO_2P$	2,3,7,8,12,13,17,18-octakis(β-*n*-alkoxy)ethyl-5-nitroporphyrinate
$(OC_nH_{2n+1})OEP$	2,3,7,8,12,13,17,18-octakis(β-*n*-alkoxy)ethylporphyrinate
$(C_nH_{2n+1})Cy)_2DPP$	5,15-bis(4'-*n*-alkylcyclohexyl-4-esterphenyl)porphyrinate
$(C_nH_{2n+1})Cy)OHPP$	5-(4'-*n*-alkylcyclohexyl-4-esterphenyl)-15-(4-hydroxyphenyl)porphyrinate
$((OC_nH_{2n+1})_2Ph)_2DPP$	5,15-bis(2',4'-*n*-alkoxyphenyl-4-esterphenyl)porphyrinate
$((OC_nH_{2n+1})_3Ph)_2DPP$	5,15-bis(2',4',6'-*n*-alkoxyphenyl-4-esterphenyl)porphyrinate
$((OC_nH_{2n+1})Ph)_2DPP$	5,15-bis(4'-*n*-alkoxyphenyl-4-esterphenyl)porphyrinate
$((OC_nH_{2n+1})Ph)OHPP$	5-(4'-*n*-alkoxyphenyl-4-esterphenyl)-15-(4-hydroxyphenyl)porphyrinate
APTES	3-aminopropyltriethoxysilane
$B(C_nH_{2n+1}O)_mTP$	5,15-bis(3,4,3",4"-tetra-alkoxy-*o*-terphenyl)porphyrinate
BDPY	boron-dipyrrin
Bpy	Bipyridine
Br_8TPP	2,3,7,8,12,13,17,18-octabromo-5,10,15,20-tetraphenylporphyrinate
D-(DPP)-A	[5-((4'-(dimethylamino)-phenyl)ethynyl)-15((4"-nitrophenyl)ethynyl)-10,20-diphenylporphyrinate
D–A	donor-acceptor pair
dabco	1,4-Diazabicyclooctane
DEtyP	5,10,15,20-diethylnylporphyrinate
DFWM	degenerate four-wave mixing
dmg	Dimethylglyoximato
DMTBP	5,10,15,20-tetrakis((dimethyl)tetrabenzo)porphyrinate
DP	diporphyrinate
DPP	5,20-diphenylporhyrinate
DSC	differential scanning calorimetry
EFISH	electric field induced second harmonic generation
EPR	electron pair resonance
G1A	3,5-di(4'-*tert*-butylphenylamido)benzoyl
G1	3,5-bis(3',5'-di(*tert*-butyl)phenylester)benzoyl
G2	3,5-bis(3',5'-bis(3",5"-di(*tert*-butyl)phenylester)phenylester)benzoyl
GPC	Gel Permeation Chromatography

HRS	hyper-Rayleigh scattering
ITO	indium-tin-oxide
$(Me_4OEP)^{+2}$	N,N',N'',N'''-tetramethyl-octaethylporphyrin(+2)
MV^{2+}	methylviologen
NLO	nonlinear optical
OEP	2,3,7,8,12,13,17,18-octaethylporphyrinate
OEPK	2,3,7,8,12,13,17,17-octaethyl-18-oxo-porphyrinate ketone
OPTAP	2,3,7,8,12,13,17,18-octaphenyltetrazaporphyrinate
PBDCI	N,N'-diphenyl-3,4,9,10-perylenebis(dicarboximide)
Pc	phthalocyaninato
pim	dianion of pimelic acid
pm	pyromellitimide
PMMA	poly(methyl methacrylate)
PSI	5,15,10,20-bis{2,2'-[3,3'-(*p*-phenylene)-dimethoxy]diphenyl}porphyrinate
pyz	pyrazine
RSA	reverse saturable absorption
SHG	second harmonic generator
STM	scanning tunneling microscope
suc	dianion of succinic acid
T(2',6'-G1AP)P	5,10,15,20-tetrakis(2',6'-octa-G1A-phenyl)porphyrinate
T(2',6'-DHP)P	5,10,15,20-octakis(2,6-hydroxyphenyl)porphyrinate
T(3,5-CO_2H)PP	5,10,15,20-tetrakis(3,5-dicarboxyphenyl)porphyrinate
T(3,5-CO_2R)PP	5,10,15,20-tetrakis(3,5-dicarboxyalkylphenyl)porphyrinate
T(3',5'-DHP)P	5,10,15,20-octakis(3,5-hydroxyphenyl)porphyrinate
T(3´,5´-G1P)P	5,10,15,20-tetrakis(2',6'-octa-G1-phenyl)porphyrinate
T(3´,5´-G2P)P	5,10,15,20-tetrakis(2',6'-octa-G2-phenyl)porphyrinate
T(4-*n*-$C_{12}H_{25}$)PP	5,10,15,20-tetrakis(4-*n*-dodecylphenyl)porphyrinate
T(4-*n*-$C_{15}H_{31}$)PP	5,10,15,20-tetrakis(4-n-pentadecylphenyl)porphyrinate
T(4-*n*-$C_{15}H_{31}$)PP	5,10,15,20-tetrakis(4-*n*-pentadecylphenyl)porphyrinate
T($C_{12}H_{25}O)_{16}$TP	5,10,15,20-tetrakis(3,4,3",4"-tetradodecyloxy-*o*-terphenyl)porphyrinate
T(*o*-NH_2)PP	5,10,15,20-tetrakis(2-aminophenyl)porphyrinate
T(*o*-$OCH_2CO_2C_2H_5$)PP	5,10,15,20-tetrakis(2-$OCH_2CO_2C_2H_5$phenyl)porphyrinate
T(*p*-Br)PP	5,10,15,20-tetrakis(4-bromophenyl)porphyrinate
T(*p*-Cl)PP	5,10,15,20-tetrakis(4-chlorophenyl)porphyrinate
T(*p*-CN)PP	5,10,15,20-tetra(4-cyanophenyl)porphyrinate

T(*p*-CO_2H)PP	5,10,15,20-tetra(4-carboxy)phenylporphyrinate
T(*p*-F)PP	5,10,15,20-tetrakis(4-fluorophenyl)porphyrinate
T(*p*-NO_2)PP	5,10,15,20-tetrakis(4-nitrophenyl)porphyrinate
T(*p*-*n*-$OC_{10}H_{21}$)PP	5,10,15,20-tetrakis(4-*n*-decyloxyphenol)porphyrinate
T(*p*-*n*-$OC_{12}H_{25}$)PP	5,10,15,20-tetrakis(4-*n*-dodecyloxyphenol)porphyrinate
T(*p*-OCH_3)PP	5,10,15,20-tetrakis(4-methoxyphenyl)porphyrinate
T(*p*-OH)PP	5,10,15,20-tetra(4-hydroxyphenyl)porphyrinate
TCEMPP	5,10,15,20-tetrakis((4-carboethoxymethyleneoxy)phenyl]porphyrinate
TCNE	tetracyanoethylene
TFPTBP	5,10,15,20-tetrakis(3-fluorophenyl)tetrabenzoporphyrinate
TFTBP	2, 3, 4, 5-tetrakis(fluoro)tetrabenzoporphyrinate
T_g	glass transition temperature
THF	tetrahydrofuran
THG	third harmonic generation
TMAP	5,10,15,20-tetra(5-trimethylaminopentyl)porphyrinate
TMAPTBP	5,10,15,20-tetrakis(4-dimethylaminophenyl)tetrabenzoporphyrinate
TMOPTBP	5,10,15,20-tetrakis(4-dimethoxyphenyl)tetrabenzoporphyrinate
TMP	5,10,15,20-tetramethylporphyrinate
TMPTBP	5,10,15,20-tetrakis(p-methylphenyl)tetrabenzoporphyrinate
TMPyP	5,10,15,20-tetrakis(4-N-methylpyridinium)porphyrinate
TMTBP	5,10,15,20-(tetramethyl)tetrabenzoporphyrinate
TPN	5,10,15,20-tetraphenylnaphthacene
TPP	5,10,15,20-tetraphenylporphyrinate
TPTBP	5,10,15,20-(tetraphenyl)tetrabenzoporphyrinate
TPyP	5,10,15,20-tetra-para-pyridylporphyrinate

Table 2. Mesomorphism of the octa-substituted porphyrins.

compound	transition*	T/ °C	reference
$H_2((OC_4H_9)OEP)$	K- I	154	5
$Zn((OC_4H_9)OEP)$	K-D D-I	159 164	5
$H_2((OC_6H_{13})OEP)$	K-D	111	5
$Zn((OC_6H_{13})OEP)$	K-D D-I	114 181	5
$H_2((OC_8H_{17})OEP)$	K-D D-I	84 89	5
$Zn((OC_8H_{17})OEP)$	K-D D-I	107 162	5
$Cu((OC_8H_{17})OEP)$	K-D D-I	84 132	5
$Pd((OC_8H_{17})OEP)$	K-D D-I	89 123	5
$Cd((OC_8H_{17})OEP)$	K-D D-I	103 136	5
$Zn((OC_{10}H_{21})OEP)$	K-D D-I	86 142	5
$Zn((OC_8H_{17})OECNP)$	K-D D-I	61 147	5
$Zn((OC_8H_{17})OENO_2P)$	K-D D-I	85 140	5
$Zn((OC_8H_{17})OEP)$ / $Zn((OC_{10}H_{21})OEP)$ (1:1)	K-D D-I	93 118	5
$H_2((O_2C_4H_9)OEP)$	K-D D-I	178 222	6
$Zn((O_2C_4H_9)OEP)$	K-D D-I	184 273	6
$H_2((O_2C_6H_{13})OEP)$	K-D D-D’ D’-I	59 132 220	6
$Zn((O_2C_6H_{13})OEP)$	K-D D-D’ D’-I	61 136 232	6
$H_2((O_2C_8H_{17})OEP)$	K-D D-D’ D’-I	96 99 166	6
$Zn((O_2C_8H_{17})OEP)$	K-D D-D’ D’-I	91 101 208	6

* Abbreviations: K = Crystalline phase, D = discotic columnar phase, I = isotropic fluid.

Table 3. Mesomorphism of the di-substituted zinc porphyrins.

compound	transition*	T/ °C	reference
Zn((OC_8H_{17})DPP)	K-K' K'-S_b S_b-I	233 243 270	25
Zn(($OC_{10}H_{21}$)DPP)	K-K' K'-S_b S_b-I	181 235 249	25
Zn(($OC_{12}H_{25}$)DPP)	K-$S_{e'}$ $S_{e'}$-S_e S_e-S_b S_b-I	140 207 224 234	25
Zn(($OC_{14}H_{29}$)DPP)	K-$S_{e'}$ $S_{e'}$-S_e S_e-S_b S_b-I	144 176 181 213	25
Zn(($OC_{16}H_{31}$)DPP)	K-$S_{e'}$ $S_{e'}$-S_e S_e-S_b S_b-I	156 162 181 200	25
Zn((C_7H_{15})Cy)OHPP)	K-N N-I	330 353	26
Zn(((OC_7H_{15})Ph)OHPP)	K-N N-I	298 320	26
Zn((C_7H_{15})Cy)$_2$DPP)	K-S_a S_a-I	330 384	26
Zn(((OC_7H_{15})Ph)$_2$DPP)	K-N N-I	309 433	26
Zn(((OC_8H_{17})$_2$Ph)$_2$DPP)	K-I	177	27
Zn((($OC_{14}H_{29}$)$_2$Ph)$_2$DPP)	K-K' K'-I	37 143	27
Zn(((OC_8H_{17})$_3$Ph)$_2$DPP)	K-K' K'-I	126 130	27
Zn(((OC_7H_{15})Ph)$_2$DPP) with single ortho-OC_8H_{17} chain on 5-phenyl group	K-N N-I	212 244	27
Zn(((C_7H_{15})Cy)$_2$DPP) with two ortho-OC_8H_{17} chains on 5,15-phenyl groups	$K_{\alpha\alpha}$-$K_{\alpha\beta}$ ($K_{\alpha\alpha}$+$K_{\alpha\beta}$)-I	129 178	27
Zn(((OC_7H_{15})Ph)$_2$DPP) with two ortho-OC_8H_{17} chains on 5,15-phenyl groups	$K_{\alpha\beta}$-N N-I $K_{\alpha\alpha}$-I	141 177 192	27
Zn(((OC_8H_{17})Ph)$_2$DPP) with two ortho-OC_8H_{17} chains on 5,15-phenyl groups	$K_{\alpha\beta}$-N N-I $K_{\alpha\alpha}$-I	122 160 176	27
Zn(((OC_7H_{15})Ph)$_2$DPP) with two ortho-OSO_2-p-$C_6H_5NO_2$ chains on 5,15-phenyl groups	K-N N-T_d	310 338	28
Zn(((C_7H_{15})Cy)$_2$DPP) with two ortho-OSO_2-p-$C_6H_5NO_2$ chains on 5,15-phenyl groups	K-T_d	323	28

Zn(((OC$_7$H$_{15}$)Ph)$_2$DPP) with ortho-xylyl "strap" between 5,15-phenyl groups	K-K' K'-I	213 317	28
Zn(((OC$_{10}$H$_{21}$)$_2$Ph)$_2$DPP)	K-I	251	29
Zn(((OC$_{12}$H$_{25}$)$_2$Ph)$_2$DPP) with an additional phenyl ester spacer	K-K' K'-S$_c$ S$_c$-N N-I	138 276 287 321	29
Zn(((OC$_{12}$H$_{25}$)$_3$Ph)$_2$DPP) with two additional phenyl ester spacers	K-K' K-D D-I	107 188 288	29
Zn(((OC$_{12}$H$_{25}$)$_2$Ph)$_2$DPP) with additional phenyl ester spacer and with two *o*-OC$_8$H$_{17}$ chains on 5,15-phenyl groups	K-N N-I	133 169	29
Zn(((OC$_{12}$H$_{25}$)$_3$Ph)$_2$DPP) with two additional phenyl ester spacers and with two *o*-OC$_8$H$_{17}$ chains on 5,15-phenyl groups	K-N N-I	50 153	29

* Abbreviations: K = Crystalline phase, D = columnar phase, S_b = smectic B phase, S_E = smectic E phase, S_c = smectic C phase, S_a = smectic A phase, N = nematic phase, I = isotropic fluid, T_d = thermal decomposition.; $\alpha\alpha$ and $\alpha\beta$ refer to isomers of porphyrin.

Table 4. Structure and first hyperpolarizability of Sen's β-pyrrole substituted "push-pull" fluoroarylporphyrins.[40,41]

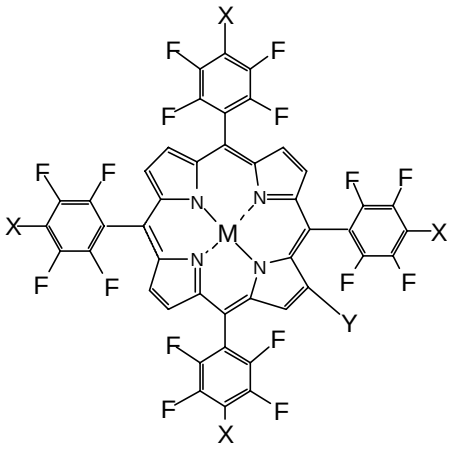

X	**Y**	**M**	**β_{HRS} (10^{-30} esu)**
F	H	2H	1.90 (Calc. 1.20)
$N(CH_3)_2$	H	2H	7.20 (Calc. 3.20)
F	NO_2	2H	10.1 (Calc. 4.60)
$N(CH_3)_2$	NO_2	2H	54.0 (Calc. 32.0)
F	H	Zn	2.80
$N(CH_3)_2$	H	Zn	11.2
F	NO_2	Zn	11.8
$N(CH_3)_2$	NO_2	Zn	92.0
F	H	Cu	3.90
$N(CH_3)_2$	H	Cu	19.2
F	NO_2	Cu	19.6
$N(CH_3)_2$	NO_2	Cu	118

Table 5. INDO/SCI-SOS calculated β values at 1064 nm for porphyrin-bridged donor-acceptor molecules.[42]

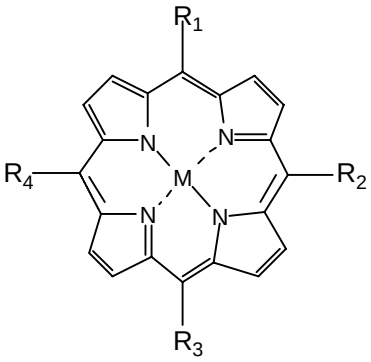

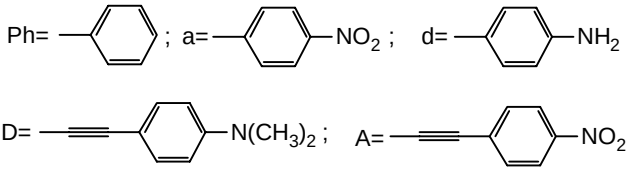

No.	**Porphyrins**	**R^1**	**R^2**	**R^3**	**R^4**	**M**	**β (10^{-30} esu)**
1	Zn(DPP)	Ph	H	Ph	H	Zn	-
2	D-Zn(DPP)	Ph	D	Ph	H	Zn	106.7
3	Zn(DPP)-A	Ph	H	Ph	A	Zn	147.5
4	D-Zn(DPP)-A	Ph	D	Ph	A	Zn	477.3
5	d-H_2(DPP)-A	Ph	d	Ph	a	H_2	50.9
6	d_2-H_2(P)-a_2	d	d	a	a	H_2	95.3
7	d_3-H_2(P)-a	d	d	d	a	H_2	53.6
8	d-H_2(P)-a_3	d	a	a	a	H_2	65.2

Table 6. INDO/S Hamiltonian and singles-only CI calculated b values for pyrrole substituted triphenyl porphyrins.[46]

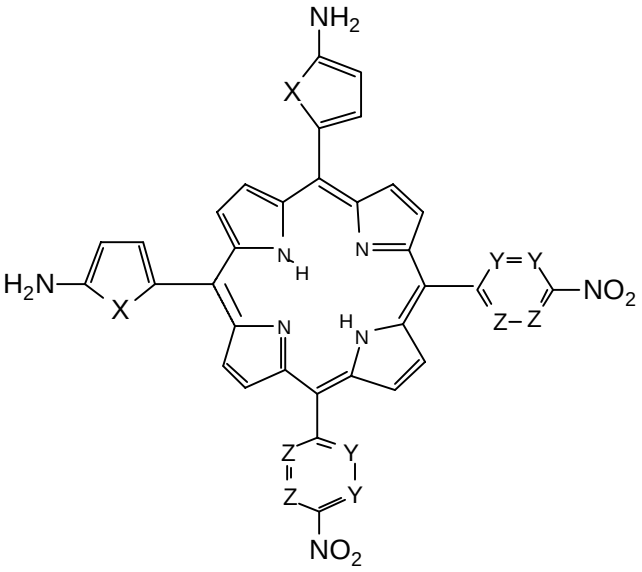

No.	X	Y	Z	β_x (10^{-30} esu)	$\mu\beta_x$ (10^{-48} esu)
1a	CH=CH	N	CH	64.02	687.76
1b	CH=CH	N	N	78.98	1349.74
1c	O	CH	CH	75.55	908.32
1d	O	N	CH	87.68	942.84
1e	O	N	N	85.02	1222.98
1f	S	CH	CH	46.42	838.73
1g	S	N	CH	59.44	1042.33
1h	S	N	N	69.35	1352.37
1i	NH	CH	CH	80.43	839.91
1j	NH	N	CH	89.19	742.33
1k	NH	N	N	93.14	1071.33

Table 6 (cont.)

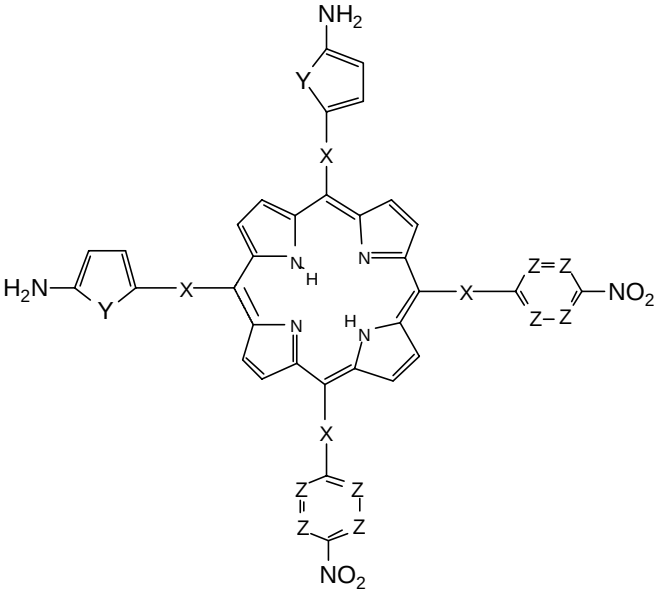

No.	**X**	**Y**	**Z**	**β_x (10^{-30} esu)**	**$\mu\beta_x$ (10^{-48} esu)**
2a	C=C	CH=CH	CH	146.75	2633.8
2b	N=N	CH=CH	CH	193.96	5454.7
2c	N=N	NH	N	245.49	5892.8

Table 6 cont.

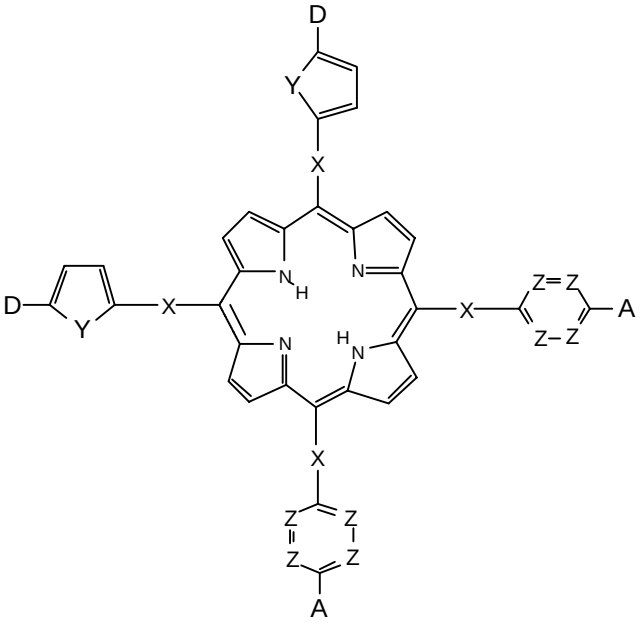

No.	**D**	**A**	**X**	**Y**	**Z**	**β_x (10^{-30} esu)***	**$\mu\beta_x$ (10^{-48} esu)**
3a	NH_2	NO_2	C=C	CH=CH	CH	157.22	2492.4
3b	NH_2	NO_2	N=N	CH=CH	CH	218.76	4625.4
3c	NH_2	NO_2	N=N	NH	N	345.75	3616.78
3d	NO_2	NH_2	C=C	CH=CH	CH	98.86	2390.65
3e	NO_2	NH_2	N=N	CH=CH	CH	352.69	6435.4
3f	NO_2	NH_2	N=N	NH	N	305.22	8897.73

Table 7. Third-order nonlinear optical susceptibility data of metalloporphyrins compounds measured by different techniques.[30]

Porphyrin	**γ (10^{-30} esu)**	**$\chi^{(3)}$ (10^{-12} esu)**	**Wave-length (μm)**	**Measure-ment Technique**	**Reference**
H_2(TPP)	-	28.6	0.532	DFWM	50
	-10.2	-	0.802	Z-Scan	58
Zn(TPP)		14.3	0.532	DFWM	50
	-16.6	-	0.802	Z-Scan	58
Co(TPP)		7.16	0.532	DFWM	50
H_2(TC_{15}PP)		40.0	0.532	DFWM	51
Co(T(4-n-C15H31)PP)		56.0	0.532	DFWM	51
Ni(T(4-n-C15H31)PP)		69.0	0.532	DFWM	51
Cu(T(4-n-C15H31)PP)		50.0	0.32	DFWM	51
Zn(T(4-n-C15H31)PP)		15.0	0.532	DFWM	51
V(T(4-n-C15H31)PP)(O)		32.0	0.532	DFWM	51
Zn(TMAPTBP)	10	28000	0.532	DFWM	52
Zn(TMTBP)	3.3	15000	0.532	DFWM	52
Zn(TFPTBP)	3.8	13000	0.532	DFWM	52
Zn(TMOPTBP)	4.8	14000	0.532	DFWM	52
	0.0010	0.078	1.064	OKE	53
Zn(TMPTBP)	4.0	12000	0.532	DFWM	52
Mg(OMTBP)	1.6	8000	0.532	DFWM	52
Zn(TPTBP)	0.90	3000	0.532	DFWM	52
	0.0018	0.091	1.064	OKE	53
Zn(TFTBP)	0.70	2000	0.532	DFWM	52
H_2(TBP)	0.50	3000	0.532	DFWM	52

H_2OEP	0.00049	1.9	1.907	THG	54
Mn(OEP)Cl	0.0006	2.6	1.907	THG	54
$Me_4(OEP)^{+2}$	0.0024	10	1.907	THG	54
Mg(OPTAP)	-	11.7	0.598	DFWM	55
Porphyrin Polymer		73000	-	-	56
H_2DEtyP monomer		0.6	0.532	DFWM	57
Zn(DEtyP) monomer		1.2	0.532	DFWM	57
$(H_2(DEtyP))_n$ polymer		510	0.532	DFWM	57
$(Zn(DEtyP))_n$ polymer		128	0.532	DFWM	57
(TPP)-1	-8.5	-	0.784	Z-Scan	253
(TPP)-2	-48.2	-	0.784	Z-Scan	253
(TPP)-3	-6.5	-	0.784	Z-Scan	253
(TPP)-4	-6.7	-	0.784	Z-Scan	253
(TPP)-5	-6.3	-	0.784	Z-Scan	253
(TPP)-6	-6.2	-	0.784	Z-Scan	253
Cu(TPP)	-26.7	-	0.802	Z-Scan	58
Ni(TPP)	-52.8	-	0.802	Z-Scan	58
$Sn(TCEMPP)I_2$	-109.7	-	0.802	Z-Scan	58
$Sn(TCEMPP)(N_3)_2$	-9.7	-	0.802	Z-Scan	58
$Sn(TCEMPP)Br_2$	-7.5	-	0.802	Z-Scan	58
$Sn(TCEMPP)Cl_2$	-4.7	-	0.802	Z-Scan	58
$Sn(TCEMPP)(OH)_2$	-3.9	-	0.802	Z-Scan	58
Cu(PSI)	-	0.88	0.532	DFWM	59
$Cu(PSIBr_8)$	-	0.50	0.532	DFWM	59
$Cu(PSIBr_9)$	-	0.47	0.532	DFWM	59

Cu($PSIBr_{12}$)	-	0.40	0.532	DFWM	59
Cu($MSICl_8$)	-	0.35	0.532	DFWM	59
Cu(TPP)	-	1.03	0.532	DFWM	59
C_{60}:(TPP) (film)	5720		0.590	DFWM	60
C_{60}:(TPP) (multilayer)		7.74	1.907	THG	62
C_{60}:(TPP) (composite)		11.5	1.907	THG	62

Table 8. Channel Volumes for Various Porphyrin Complexes.[135]

Porphyrin Complex	**Z**	**Unit Cell Volume (Å^3)**	**Porphyrin Volume/ unit cell[a] (Å^3)**	**Solvate Volume/ unit cell[a] (Å^3)**	**Void Volume/ unit cell[a] (Å^3)**	**Total Channel Volume/ unit cell[b] (Å^3)**
H_2(TPP)	1	801.9	590.8	0	211	211 [26.3%]
H_2(T(3´,5´-DHP)P) • 5 EtOAc	1	1581	620.8	412.5	547.7	960.2 [60.7%]
H_2(T(2´,6´-DHP)P) • 4 EtOAc	2	2770.9	1233.0	660	877.9	1537.9 [55.5%]
H_2(T(3´,5´-DHP)P) • 7 C_6H_5CN	2	3811	1241.6	1547	1022	2569.4 [67.4%]
Zn(T(2´,6´-DHP)P)$(EtOAc)_2$ • 2 EtOAc	1	1387.2	804.1	168	415.2	583.2 [42.0%]
Zn(T(3´,5´-DHP)P)$(THF)_2$ • 3 CH_2Cl_2 • 2 THF	1	1597.6	755.8	326.9	514.8	841.7 [52.7%]
Mn(T(3´,5´-DHP)P)$(THF)_2$ • Cl^- • 2 THF • 5 $C_6H_5CH_3$	2	4289	1612.2	1355	1321.8	2676.7 [62.4%]

[a]Porphyrin and solvate van der Waals volumes were calculated from Quanta for each unit cell. Void volume is defined as the unit cell volume minus the sum of the porphyrin volume and the solvate volume. For the metalloporphyrins, the volumes of the coordinated ligands were counted as part of the porphyrin volume.

[b]Total channel volume is defined as the sum of void and solvate volume, in Å^3. Values in brackets refer to the percentage of total channel volume in the unit cell.

Table 9: Logarithm of Anion Selectivity Coefficients for Mn(III) Porphyrin Based Membranes

Anion	Por 1	Por 2	Por 3	Por 4	Por 5	Por 6	Por 7	Por 8	Por 9
Cl^-	0.0	0.0	0.0	0.0	0.0	0.0	0.0	0.0	0.0
Br^-	0.6	0.3	0.5	0.2	0.2	0.4	0.3	0.4	0.6
I^-	2.8	1.5	1.5	1.5	1.6	1.5	1.7	2.1	2.5
Sal	2.7	2.1	2.4	3.2	2.0	2.4	2.4	2.4	2.3
SCN^-	3.0	1.3	1.6	2.5	3.5	3.0	3.2	2.0	2.0
IO_4^-	4.0	1.8	2.1	1.7	0.6	1.5	1.0	3.0	2.6
ClO_4^-	4.6	1.5	1.7	1.5	0.4	1.2	0.8	3.5	3.3

VIII. Figure Captions

Figure 1. Structure of *uro*-porphyrin I octa-*n*-dodecyl ester (R = $CH_2CO_2C_{12}H_{25}$, M = H_2) and other octylether and octylester porphyrins (R = $CH_2OC_nH_{2n+1,}$ *n* = 4, 6, 8, 10 or R = $CH_2O_2C_nH_{2n+1}$, *n* = 4, 6, 8; M = H_2, Zn, Cu, Pd, Cd).

Figure 2. Schematic representation of the tilted columnar stacking.[7]

Figure 3. Schematic representation of the columnar arrangement of discotic zinc *n*-decyl ether octa-substituted porphyrin stacks.[8]

Figure 4. Readout current pulses with the same writing conditions: (a) initial readout and (b) after 1.5 billion write/erase cycles.[11]

Figure 5. Structure of sulfur-substituted azaporphyrin.

Figure 6. Structure of *n*-pentadecylphenyl porphyrin.

Figure 7. Temperature dependence of the dark-current under 4000 V/cm.[13]

Figure 8. Temperature dependence of the photocurrent at 620 nm under 4000 V/cm.[13]

Figure 9. Structure of substituted 5,10,15,20-tetrakis(3,4,3",4"-tetradecyloxy-*o*-terphenyl)porphyrins (R^1 = R^2 = *n*-$C_{12}H_{25}O$; M = H_2 or Cu; or R^1 = *n*-$C_{12}H_{25}O$, R^2 = H; M = H_2).

Figure 10. Orientation of H_2(TPP)and Neumann's mesogenic *o*-amino-substituted tetraphenylporphyrin in nematic liquid crystal phase.[20]

Figure 11. Structure of Nolte's mesomorphic inducing "clipper" molecule.[22] and schematic representation of a tetra-substituted porphyrin guest being held by the "clipper" molecule.[22]

Figure 12. Histogram of DSC results for T(3,5-COOR)PP materials: black = solid phase, white = mesophase, gray = isotropic.

Figure 13. Structure of 3,5-di-carboxyphenyl porphyrin.

Figure 14. Structure of ether-substituted di-phenyl porphyrins (R = $C_nH_{2n+1,}$ *n* = 8, 10, 12, 14, 16)[25,26]

Figure 15. Structure of ester substituted diphenyl porphyrins (R = CO-C_6H_{10}-OC_7H_{15}, R' = H; or R = CO-C_6H_4-OC_7H_{15}, R' = H; or R = R' = CO-C_6H_{10}-OC_7H_{15}; or R = R' = CO-C_6H_4-OC_7H_{15}; or R = R' = (2',4'-OC_8H_{16})C_6H_4 or R = R' = (2',4'-$OC_{14}H_{29}$)C_6H_4 or R = R' = (2',4',6'-OC_8H_{16})C_6H_4).

Figure 16. Structure of ester substituted di-phenyl porphyrin with single lateral chain.

Figure 17. Structure of ester substituted di-phenyl porphyrins with two lateral chains (R = C_6H_{10}-*n*-C_7H_{15}; or R = C_6H_4-O-*n*-C_mH_{2m+1}, *m* = 7,8.).

Figure 18. Structure of *o*-(*p*-nitrophenylsulfonyl)oxy substituted Zn^{II} di-phenyl porphyrin (R = C_6H_4-O-*n*C_7H_{15} or R = C_6H_{10}-*n*C_7H_{15}).Wang, 1996 #104]

Figure 19. Structure of "strapped" Zn^{II} di-phenyl porphyrin (R = -C_6H_4-O-*n*C_7H_{15}).[28]

Figure 20. Structure of catenane substituted di-phenyl porphyrin systems (Y = H; *n* = 10, *m* = 0; or Y = H; *n* = 12, *m* = 1; Y = $OC_{12}H_{25}$; *n* = 12, *m* = 2).[29]

Figure 21. Structure of catenane substituted di-phenyl porphyrin systems with lateral chains (Y = H; *m* = 1; or Y = $OC_{12}H_{25}$; *m* = 2)[29]

Figure 22. Structure of 5,15-bis(3,4,3",4"-tetradodecyloxy-*o*-terphenyl)porphyrin derivatives (R^1 = R^2 =$C_{12}H_{25}O$; or R^1 = R^2 =$C_{16}H_{33}O$; or R^1 =$C_{12}H_{25}O$, R^2 = H).

Figure 23. Structure of 5,15-bis(3,4-didodecyloxyphenyl)porphyrin.

Figure 24. Structure of 5,15-bis(4-didodecyloxybiphenyl)porphyrin.

Figure 25. Structure of Suslick's donor-acceptor "push-pull" tetraphenylporphyrin, R=NO_2 or NH_2.

Figure 26. Effects of environment on second-order NLO behavior.

Figure 27. Langmuir-Blodgett isotherms or amphiphilic derivatives of push-pull porphyrins.

Figure 28. Structure of LeCoer's zinc porphyrin dimer.

Figure 29. Structure of Peng's porphyrin polyimide.

Figure 30. Structure of Peng's zinc porphyrin polyimide system with pendant organic NLO chromophore.

Figure 31. Structure of Rao's tetrabenzoporphyrin derivatives Zn(TMAPTBP): M = Zn, X = H, R = *p*- C_6H_4-$N(CH_3)_2$; Zn(TMTBP): M = Zn, X = H, R = CH_3; Zn(TFPTBP): M = Zn, X = H, R = *m*-FC_6H_4; Zn(TMOPTBP): M = Zn, X = H, R = *p*-CH_3O-C_6H_4; Zn(TMPTBP): M = Zn, X = H, R = *p*-

Figure 96. Crystal structure of Zn(TPyP)•CH_3OH•$2H_2O$. The marked hexagons indicate hydrogen-bonding interactions between six water molecules and pyridyl groups of porphyrins in adjacent unit cells.[140]

Figure 97. Interporphyrin coordination in Zn(T(p-CN)PP)•2 $C_6H_5NO_2$ to form two-dimensional network. Guest molecules removed for clarity.[133]

Figure 98. Crystal structure of Zn(T(p-CN)PP)•2 $C_6H_5NO_2$showing arrangement of guest molecules.[133]

Figure 99. Schematic illustration of three-dimensional porphyrin network in Pd(TPyP)•$Cd(NO_3)_2$•$8.6H_2O$ in which porphyrins are represented as squares and cadmium ions as circles. Solvent molecules are omitted for clarity.[141]

Figure 100. Packing arrangement in $[Cu(TPyP)•Cu]_n^{n+}$ framework. Larger circles represent copper ions. Solvent and non-coordinating anions omitted for clarity.[142]

Figure 101. (a) Packing arrangement in $[Cu(TCNPP)•Cu]_n^{n+}$ framework. Separate frameworks are indicated by light and dark shading. Large circles represent copper ions. (b) Schematic representation of extended framework. Cu(II) ions in center of porphyrin macrocycle represented by small circles. Cu(I) ions coordinating between porphyrin molecules indicated by large circles. Solvate and non-coordinating anions omitted for clarity.[142]

Figure 102. Parallel polymeric porphyrin bands showing coordinate bonding between tetrabidentate porphyrin carboxylate and calcium ions both as space filling and schematic models (top). In this schematic model, intersection of cylinders represents center of porphyrin macrocycle and corners represent calcium ions. Extended three-dimensional structure showing interpenetration of porphyrin bands (bottom). Guest pyridine molecules and coordinated water molecules have been omitted for clarity.[144]

Figure 103. Crystal packing in cobalt coordinative network of Co(III) derivative of H_2(TpCPP).[145]

Figure 104. Crystal packing in Mn(II) coordinative network of Mn(III) derivative of H_2(TpCPP).[145]

Figure 105. Crystal packing in H_2(DiCarPP) molecular species showing channels between porphyrin columns. Solvent molecules omitted for clarity.[143]

Figure 106. (Top) Schematic of zeolite L main channel and (bottom) idealized Zn($TMPyP^{4+}$) methylviologen $(MV^{2+})_n$ complex.[151]

Figure 107. Cyclic voltammograms obtained for Cu(TPP)/zeolite Y modified carbon paste electrode in absence (A), presence of 1.0 x 10^{-5} mol L^{-1} hydrazine (B) and 1.0 x 10^{-3} mol L^{-1} cysteine (C). Supporting electrolyte of 0.5 mol L^{-1} $NaClO_4$ at pH 7 and a scan rate o 20 m V s^{-1}[157]

Figure 108. Diffuse reflectance spectra of zeolite Y with (top) encapsulated Mn(TMP) showing porphyrin Soret band and (bottom) Mn(II) ions.[155]

Figure 109. Comparison of dioxygen and argon absorption isotherms of Co(TMP)/zeolite Y material at 25°C.[156]

Figure 110. XRD patterns of (a) Ru(T(p-Cl)PP)(CO)(EtOH), (b) a physical mixture of Ru(T(p-Cl)PP)(CO)(EtOH) and APTES surfaced modified MCM-41 in a mass ratio of 8:92, (c) 8.3 mass % APTES surface modified Ru/M-41 and (d) MCM-41 and APTES surface modified MCM-41.[157]

Figure 111. EPR spectra of photoinduced $H_2(TPP^{•+})$ in TiMCM-41, MCM-41 and AlMCM-41 after 30 minutes irradiation with $\lambda > 350$ nm at room temperature.[158]

Figure 112. Structure of M(TMAP) species.[160]

Figure 113. Postulated arrangement of the intercalated H_2(TSPP)inside the LDH.

Figure 114. Schematic representation of the $(TpCPP)^{4-}$ (a) and $(ToCPP)^{4-}$ (b) oriented in the interlayers of LDH.

Figure 115. Various “shish kebab” one-dimensional coordination polymers.

Figure 116. A linearly conjugated porphyrin tetramer.

Figure 117. Synthesis of a porphyrin polymer via the Heck reaction.

Figure 118. Synthesis of conjugated porphyrin polymers via the Wittig reaction.

Figure 119. Synthesis of one-dimensional porphyrin-oligothiophene polymers.

Figure 120. Schematic representation of a ferroelectric coordination polymer and dipole moment switching in response to an external field.
Figure 121. The dipole moment of metalloporphyrins.
Figure 122. The double-well potential of the position of the metal atom relative to the porphyrin core.
Figure 123. Three classes of the non-symmetrical bridging ligands.
Figure 124. Three alignments of bridging ligands in metalloporphyrin polymers and ORTEP plots of the packing diagrams.
Figure 125. Response of Pt(OEP)-doped sol-gel glass on switching between (a) 100% Nitrogen and (b) 100% oxygen.
Figure 126. A metalloporphyrin ketone, M(OEPK), R = C_2H_5.
Figure 127. Variation of (a) pO_2 and (b) t_{90} with TBP plasticizer content.
Figure 128. Collman's "picnic basket" porphyrins.
Figure 129. Structure of a conjugated Ni(OEP) dimer.
Figure 130. Langmuir-Blodgett Film Sensor Response at varying NH_3 concentrations.
Figure 131. Response of porphyrin array towards 14 chemical species.
Figure 132. Black and white projection of color change fingerprints for a series of ligating vapors. In color, the differences among analytes are considerably more distinct.
Figure 133. Structures of quaternary ammonium and manganese metalloporphyrin species used for membrane preparation.
Figure 134. Metallocene containing porphyrins for anion recognition.
Figure 135. Molecular structure of deca-alkyl sapphyrin binding fluoride ion.
Figure 136. Response of TMHPP film based nickel sensor at varying concentration.
Figure 137. Response of Co(TPP)/graphite electrode to carbon tetrachloride (CT) and perchloroethylene (PCE).
Figure 138. A Porphyrin-cyclocholate Bowl.
Figure 139. Cyclodextrin-porphyrin assembly for recognition of pentachlorophenol.
Figure 140. Binding of saccharides to a boronic-acid containing receptor.
Figure 141. Molecular models showing a side view of the binding sites of dendrimer porphyrins. Upper: *meta*-substituted H_2(T(3′,5′-G1P)P). Lower: *ortho*-substituted dendrimer-porphyrin H_2(T(2′,6′-G1AP)P. Note the open cavity of ≈10Å versus a narrow slit of ≈5, respectively; in both cases, top access to the porphyrin is completely blocked.
Figure 142. Binding of axial ligands to dendrimer porphyrins; log(K_{eq}) values for a series of nitrogenous bases with various shapes.